Shun Hing Institute of Advanced Engineering
信興高等工程研究所

Report and Research Highlights
2013 - 2014

June 2014

香 港 中 文 大 學
The Chinese University of Hong Kong

Printed in July 2014, this report contains information know as June 2014.

Every effort has been made to ensure that the information contained in this report is correct at the time of printing. Shun Hing Institute of Advanced Engineering (SHIAE) – CUHK, reserves the right to make appropriate changes to the materials presented in this report without prior notice.

For further information, please visit our website: http://www.shiae.cuhk.edu.hk


蒙民偉工程學大樓
William M. W. Mong
Engineering Building

Contents

Introduction of SHIAE

Mission of SHIAE

The MISSION of the Institute is to spearhead, conduct, promote and co-ordinate research in advanced engineering. There is no end to the list of areas to be explored and the plan is to give priority to research topics that are both exciting and innovative. The Institute also aspires to transferring its research results to industry for practical application and to put across to the community at large the role of engineering as a driving force for human development through educational activities.

As a pioneering institute exploring the forefront of the engineering science, The Shun Hing Institute of Advanced Engineering will

- spearhead state-of-the-art advanced engineering research
- create and sustain synergy with world-class researchers
- develop with and transfer to industries cutting edge technologies
- promote appreciation of engineering in society through educational programmes

The Shun Hing Education and Charity Fund was founded by Dr. William Mong Man Wai with the aim of enhancing educational opportunities for the younger generations. The Fund has already sponsored numerous educational and research programmes in Hong Kong, the Mainland, and overseas educational institutions. Himself an engineer and a firm believer in advancing the quality of life through the development of science and technology, Dr. Mong had been there to support the establishment and growth of this Institute from the beginning.

Centre of Excellence at CUHK

The Chinese University of Hong Kong is an internationally renowned institution of higher learning devoted to quality teaching and both academic and applied research. The University has established 29 research institutes and a number of research centres with a view to pursuing up-front research endeavours with focused goals and objectives. The Shun Hing Institute of Advanced Engineering plays a crucial part in the research infrastructure of the Chinese University which is committed to exciting research programmes in advanced engineering areas.

As a strategic centre of excellence at The Chinese University of Hong Kong, the Institute supports greater regional and international research collaborations, and strives to attract talent from the world over to achieve greater internationalization, a vision strongly advocated by every member of the University.

Commitment of the Faculty of Engineering

The Faculty of Engineering was founded in 1991 and was built upon existing strengths with added talent from all over the world. The Faculty has been able to attract some of the best minds. Many received their training in leading universities in North America, Great Britain and Australia. Most of them have extensive experience in industry and many are leaders in their fields. This team of top-notch talent is gathered to nurture local talent through educational programmes, and break new frontiers in research through innovative and exciting research endeavours.

The positioning of The Shun Hing Institute of Advanced Engineering in the William M.W. Mong Engineering Building is deliberate as a key nucleating point to integrate research endeavours in the Engineering Faculty and its neighbours. Our members join hands with their counterparts from the Faculties of Science and Medicine in many interesting research collaborations. It is the ambitious goal of the Faculty of Engineering that the Institute should become a lighthouse for the local technology landscape to herald the migration towards high value-added technology and an information economy.

The mission of the Institute is to spearhead, conduct, promote and co-ordinate research in advanced engineering. There is no end to the list of areas to be explored and the plan is to give priority to research topics that are both exciting and innovative. The Institute also aspires to transferring its research results to industry for practical application and to put across to the community at large the role of engineering as a driving force for human development through educational activities.

Building on Strength and The Way Ahead

Many of the Institute's research projects are built upon areas in which the Faculty has already achieved outstanding performance. These are areas that have great potential for further technological advancement and in line with industrial development in Hong Kong. The Institute provides a vibrant R&D environment to spur new discoveries and speed up their translation into applications. Since 2012, we have expanded our scope to cover new frontiers in Renewable Energy striving to answer tomorrow's energy challenges.

Technology Transfer

Synergy with industry is the ultimate goal of research and development in Hong Kong. External experts have been brought in to the Institute to lead research projects that could benefit the industrial sector.

The technology transfer arm of the Faculty of Engineering plays an important role in the traffic between the Institute and industry. The Institute houses an array of top-notch research and development activities encompassing contract research, spin-off companies, and consultancies.

Contribution to Society

The Institute has been making contributions to the progress of Hong Kong through a wide range of educational activities like training courses, seminars, symposiums which disseminate the latest technologies to promote appreciation of engineering in society and arouse interest of the younger generations in engineering.

Organization of SHIAE

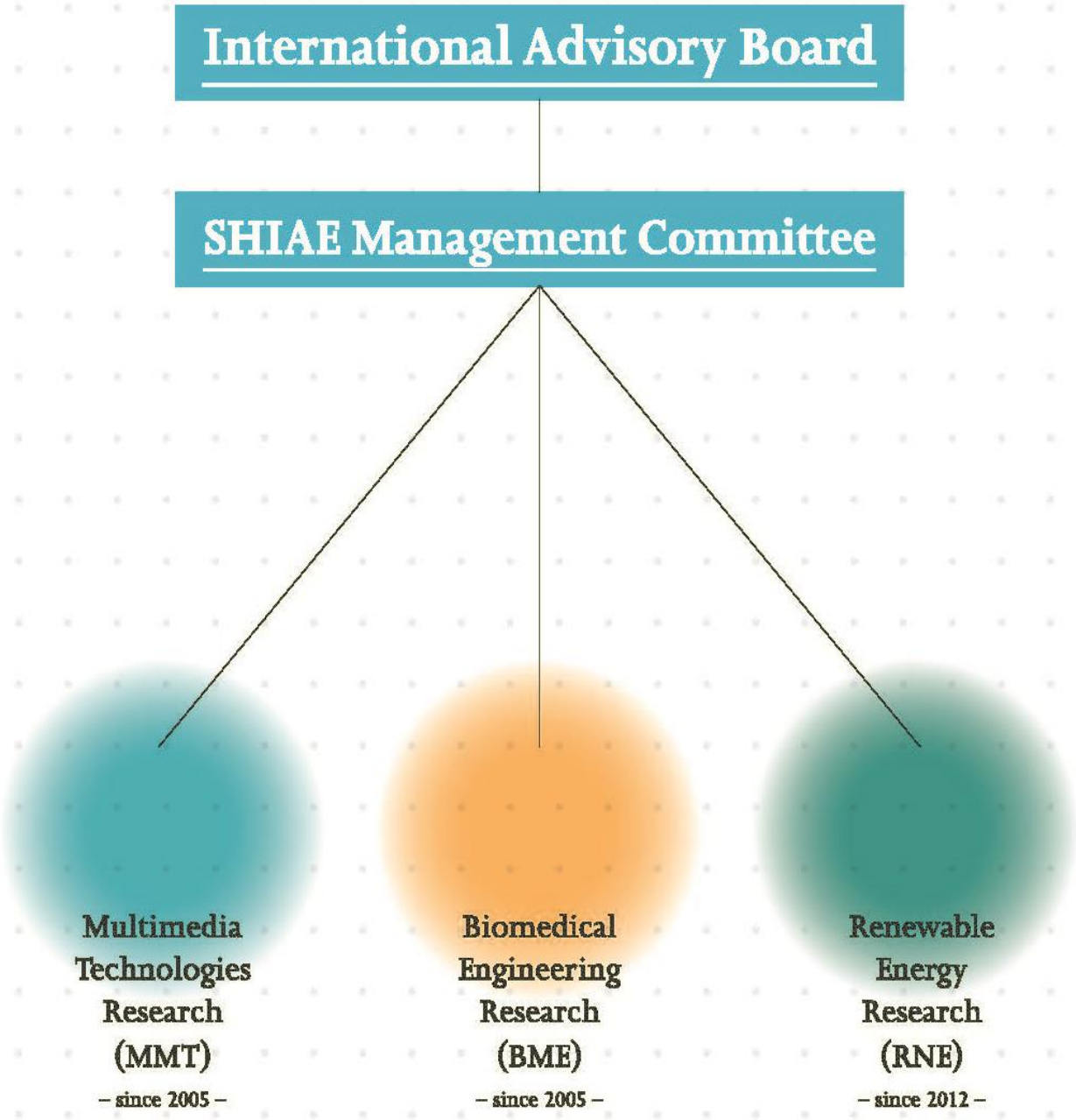

We also provide support and sponsorship to the Faculty of Engineering in organizing prestigious academic conference in Hong Kong so as to raise our international profile.

Composition of International Advisory Board

Chairman:

Mr. David T.Y. MONG 蒙德揚先生

Managing Director
Shun Hing Electronic Trading Co., Ltd.,
Hong Kong

Members:

Professor Victor ZUE

Professor of Electrical Engineering and Computer Science
Massachusetts Institute of Technology,
U.S.A

Dr. Harry SHUM 沈向洋博士

Corporate Vice President
Microsoft Corporation,
U.S.A.

Professor Yongmin KIM

Hunter and Dorothy Simspon Endowed Chair in Bioengineering
Department of Bioengineering, University of Washington,
U.S.A.

Professor Chih-Ming HO 何志明教授

Ben Rich-Lockheed Martin Professor in School of Engineering
University of California, Los Angeles,
U.S.A.

Professor C.C. Jay KUO

Professor of Electrical Engineering and Computer Science
University of Southern California,
U.S.A.

Professor Tai Fai FOK 霍泰輝教授

Pro-Vice-Chancellor
The Chinese University of Hong Kong
Hong Kong

Professor Wing-shing WONG 黃永成教授

Dean of the Graduate School
The Chinese University of Hong Kong
Hong Kong

Professor Ching Ping WONG 汪正平教授

Dean of Engineering
The Chinese University of Hong Kong
Hong Kong

Professor Pak Chung CHING 程伯中教授

Director of Shun Hing Institute of Advanced Engineering
Pro-Vice-Chancellor and Professor of Electronic Engineering
The Chinese University of Hong Kong
Hong Kong

Composition of Management Committee

Director:

Professor Pak Chung CHING
Pro-Vice-Chancellor
Professor of Electronic Engineering

Secretary:

Professor John C.S. LUI
Department of Computer Science and Engineering

Members:

Professor Ching Ping WONG *(ex-officio)*
Dean of Faculty of Engineering

Mr. Terrence CHAN
Managing Director of Shun Hing Technology Co., Ltd
Hong Kong

Professor HENG Pheng Ann
Department of Computer Science and Engineering
(until July 31, 2014)

Professor LEUNG Kwong-sak
Department of Computer Science and Engineering
(from August 1, 2014)

Professor Dennis Y.M. LO
Associate Dean (Research) of Faculty of Medicine
Department of Chemical Pathology

Professor Helen M.L. MENG
Professor of Systems Engineering & Engineering Management

Professor Max Qing Hu MENG
Department of Electronic Engineering

Professor WANG Yu, Michael
Department of Mechanical and Automation Engineering
(until July 31, 2014)

Professor LIAO Wei-Hsin
Department of Mechanical and Automation Engineering
(from August 1, 2014)

Professor WONG King-lap
Department of Mechanical and Automation Engineering

Professor WONG Wing-shing
Department of Information Engineering

Shun Hing Visiting Scholars/ Fellows

The Institute has launched a Shun Hing Distinguished Scholar Program with an aim to attract distinguished scholars to pursue research collaboration with our faculty and to strengthen our research profile. The following scholars visited to work either on a short term or on a longer term engagement with the Institute between 2013 and 2014.

Shun Hing Fellows and Research Associate:
(in alphabetical order)

Dr CHENG Hui *The Sun Yat-sen University, China*	2011-2013
Dr LI Jinming *Nanyang Technological University, Singapore*	2014-2015
Dr LOU Yishan *The Chinese University of Hong Kong*	2014-2015
Dr Lu LIU *The Chinese University of Hong Kong*	2008, 2012-2013
Dr LUO Yangjun *Northwestern Polytechnical University, China*	2013
Dr WANG Feng *The Chinese University of Hong Kong*	2013
Dr WANG Xiaoming *Dalian University of Technology, China*	2012-2013
Dr XU Huihua *Chinese Academy of Science, China*	2012-2013
Dr YANG Juekuan *Southeast University, China*	2012-2013
Dr YANG Shih-Mo *National Chiao Tung University, Taiwan*	2013-2014
Dr YAO Hong *The Chinese University of Hong Kong*	2013-2014
Dr ZHOU Aijun *University of Electronic Science and Technology of China, China*	2013-2014

Financial Status of SHIAE

		As at 30 June 2014 HK$
INCOME		
Start Up Seed Fund		34,500,000
Interest and investment income (May 2014)		6,547,742
Sub-total:		41,047,742
EXPENDITURE		
Research funding granted since 2005-2014	(1)	32,991,200
Committed Research Budget in 2015	(2)	1,002,000
Unspent remaining fund from completed projects		-2,734,471
Operating cost		3,228,185
Sub-total:		34,486,914
BALANCE as at 30 June 2014		**6,560,828**

(1) Annualized Research Funding to each research areas granted since 2005

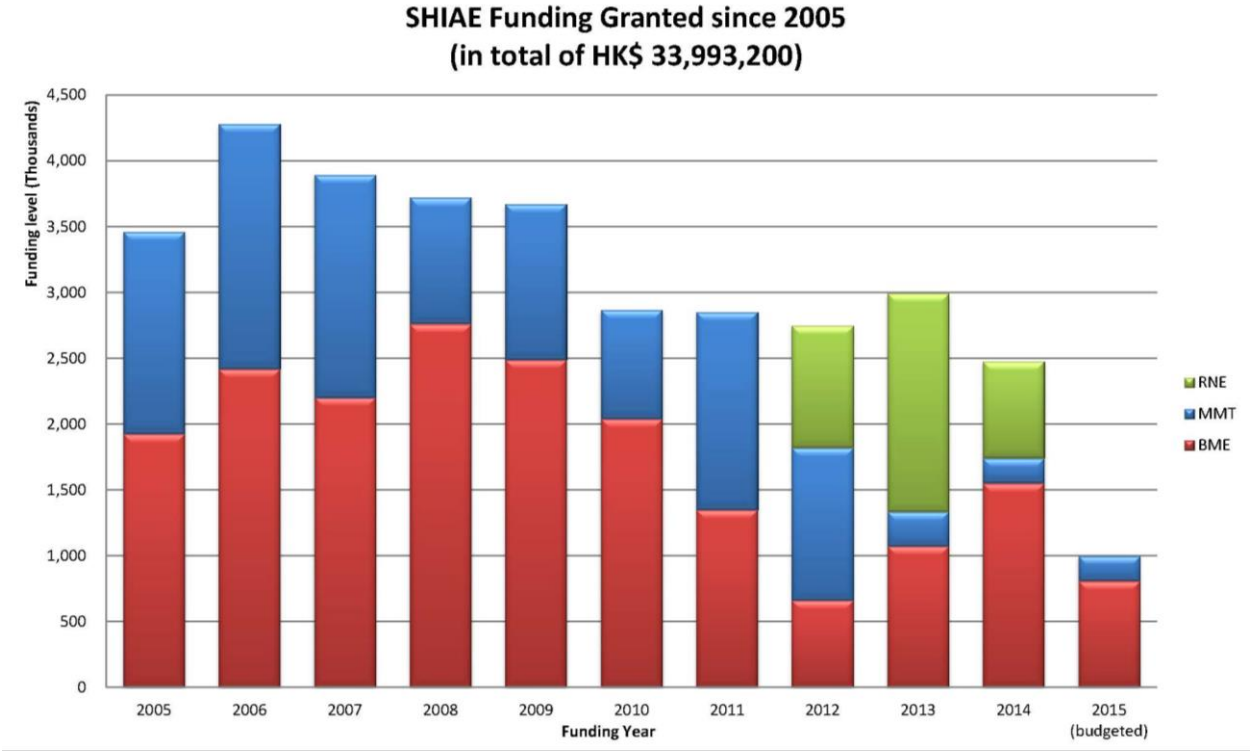

This figure shows the distribution of the SHIAE funding granted to each track of research projects, namely Biomedical Engineering (BME), Multimedia Technology (MMT) and Renewable Energy (RNE) annually.

(2) Detail funding level on each batch of projects (in HK$ '000)

Funding Year/ No. of projects	**2015** (budgeted)	2014	*2013*	*2012*	2011	2010	2009	2008	2007	2006	2005
Year 2005 Batch (6 Projects)	-	-	-	-	-	-	-	-	60	2,586	3,462
Year 2006 Batch (5 Projects)	-	-	-	-	-	-	-	-	1,480	1,695	-
Year 2007 Batch (7 Projects)	-	-	-	-	-	-	200	1,792	2,354	-	-
Year 2008 Batch (4 Projects)	-	-	-	-	-	-	1,848	1,928	-	-	-
Year 2009 Batch (5 Projects)	-	-	-	-	268	1,414	1,624	-	-	-	-
Year 2010 Batch (5 Projects)	-	-	-	-	1,334.6	1454.6	-	-	-	-	-
Year 2011 Batch (4 Projects)	-	-	-	*1,228*	1,248	-	-	-	-	-	-
Year 2012 Batch (5 Projects)	-	-	*1,520*	*1,520*	-	-	-	-	-	-	-
Year 2013 Batch (4 Projects)	-	*1,474*	*1,474*	-	-	-	-	-	-	-	-
Year 2014 Batch (3 Projects)	***1,002***	*1,002*	-	-	-	-	-	-	-	-	-
WOSP2007 Workshop	-	-	-	-	-	-	-	-	25	-	-
Annualized total:	***1,002***	*2,476*	*2,994*	*2,768*	2,850.6	2,868.6	3,672	3,720	3,919	4,281	3,462
Accumulated Total	**HK$33,993.200**										

This table shows the detail amount of SHIAE funding granted to each batch of research projects. The subtotal amount of 1.002million budgeted for 2015 is committed to support research projects in July 2015.

Research - *Outstanding Research Highlights*

"SEMANTIC ANALYSIS FOR IMAGE RESIZING"

(Project funded in Year 2011)

by Professor WONG Tien Tsin
Department of Computer Science & Engineering, CUHK

「中大研新 3D 技術提升畫質」，香港新聞台, 香港寬頻電視, 2013 年 4 月 9 日

"Man with a Vision," South China Morning Post, 10 April 2013.


南華早報 2013 年 4 月 10 日
South China Morning Post 10 April 2013

Man with a vision

Iron Man looks dark, the clouds behind him blending with the sky, but suddenly the scene changes, the clouds and the superhero's armour pop. Now let's introduce the man behind the marvel – a talented engineer, just like the movie's hero – Professor Wong Tien-tsin of Chinese University's computer science and engineering department. Wong, pictured above, and his two graduate students developed the "Binocular Tone Mapping" technology to enhance 3-D movies. It may lack a catchy title but they still hope to wow Hollywood with their work. Wong said: "Currently, what you see on screen has a lot less detail than in real life. In reality, when you look at a dark patch you can see more detail; technology loses that detail." He and his team manipulate tone and detail to create a more realistic scene by allowing our eyes to decide what to bring into focus, and what to blur, much like in real life. The new technology is on show at the International ICT Expo at the Hong Kong Convention and Exhibition Centre in Wan Chai this week. Photo: Felix Wong

「中大研新3D 畫面技術」, 明報, 2013 年 4 月 10 日


明報 2013 年 4 月 10 日
Ming Pao Daily News 10 April 2013

中大研新 3D 畫面技術

近年3D電影大受歡迎，但一般電視、手機屏幕無法同時顯示3D電影的光暗對比以及紋理細節，令電影像真度大減。中大計算機科學與工程學系教授黃田津（右）及其研究團隊成功開發「雙目立體影調融合」技術，提供低成本、高質素的3D畫面。有關技術透過一個畫面產生的兩幅圖像，分別展示光暗對比及紋理細節，再利用人類雙眼視覺的自然融合能力及3D立體設備，令影像更具層次感，預料技術日後可應用於3D電影和遊戲等。（中大提供）

「中大學者開發低成本 3D 技術 研雙眼視覺融合能力」，星島日報, 2013 年 4 月 10 日


星島日報 2013 年 4 月 10 日
Sing Tao Daily 10 April 2013

研雙眼視覺融合能力

中大學者開發低成本3D技術

三維（3D）電影近年大行其道，觀眾對畫質的要求亦相對提高。中文大學工程學院最近開發了低成本「雙目立體影調融合」技術，首次利用人類雙眼視覺的自然融合能力及日漸普及的3D立體設備，用家可清楚看到3D畫面中強烈的光暗對比和豐富的圖像紋理細節。負責研究的學者表示，新技術已取得美國專利，下一步將研究由靜態圖像拓展至動態影像，又不排除日後與電影商合作。

記者 曾雯芳

■中大計算機科技與工程學系教授黃田津，首次利用人類雙眼視覺的自然融合能力及日漸普及的3D立體設備，開發「雙目立體影調融合」技術。 圖像華盛

中大將於本周六起，一連四日在會展舉行「國際資訊科技博覽」，展出十二項科研項目，當中包括「雙目立體影調融合」技術。中大計算機科技與工程學系教授黃田津及其研究團隊，兩年前開始構思和進行研究，由於傳統顯示屏受最大亮度和灰階級別所限，不能全面展現畫面中最暗暗至最光亮的所有亮度，即使是現時發展迅速的高動態範圍（HDR）技術，仍須面對發烈光時對比與暗富紋理細節的兩難取捨之處。

集中開發軟件

黃田津表示，人類的雙眼看到影像時，能容許左眼和右眼有一定程度的差異，如由距離產生的位移、顏色、對比度，甚至內容等，而大腦會自然地將兩個存在差異的影像合併，「雙目立體影調融合技術主要利用人眼這個特點，將一個畫面產生兩幅圖像，一幅顯示光暗變化產生的對比，另一幅顯示紋理細節，當用家戴上3D眼鏡，可感受到更具層次感的圖像。」

曾參考醫學文獻

被問到研究最困難的地方，黃田津回言，現時市面上已有3D顯示屏，故研究集中在軟件開發方面，「最難是如何量度和調校人眼可接受影像的程度，因為兩幅影像的差異愈大，用家看到的細節會愈多，但如果差異過大，用家便會感到視覺上的不適。」他又稱，研究過程中參考過醫學和心理學文獻，今次是跨學科的研究。

冀與電影公司合作

至於新技術的應用，黃田津表示，已為技術成功取得美國專利，預料可廣泛應用於3D電影、3D遊戲及其他數碼影像等，並有望用家可利用家居電視機及手機收看3D節目。「下一步會研究將技術應用於動態影像，要克服當中圖像運算的技術問題，希望日後與電影公司合作。」

Academic Publications

So far 36 projects have been successfully completed and 282 articles arising from the results of these research projects have been published in international conference proceedings and journals. The other 11 on-going projects are also progressing well with encouraging results produced. All publications generated by each individual projects are kept in the archive of SHIAE office. The chart below shows the number of academic publications produced each year.

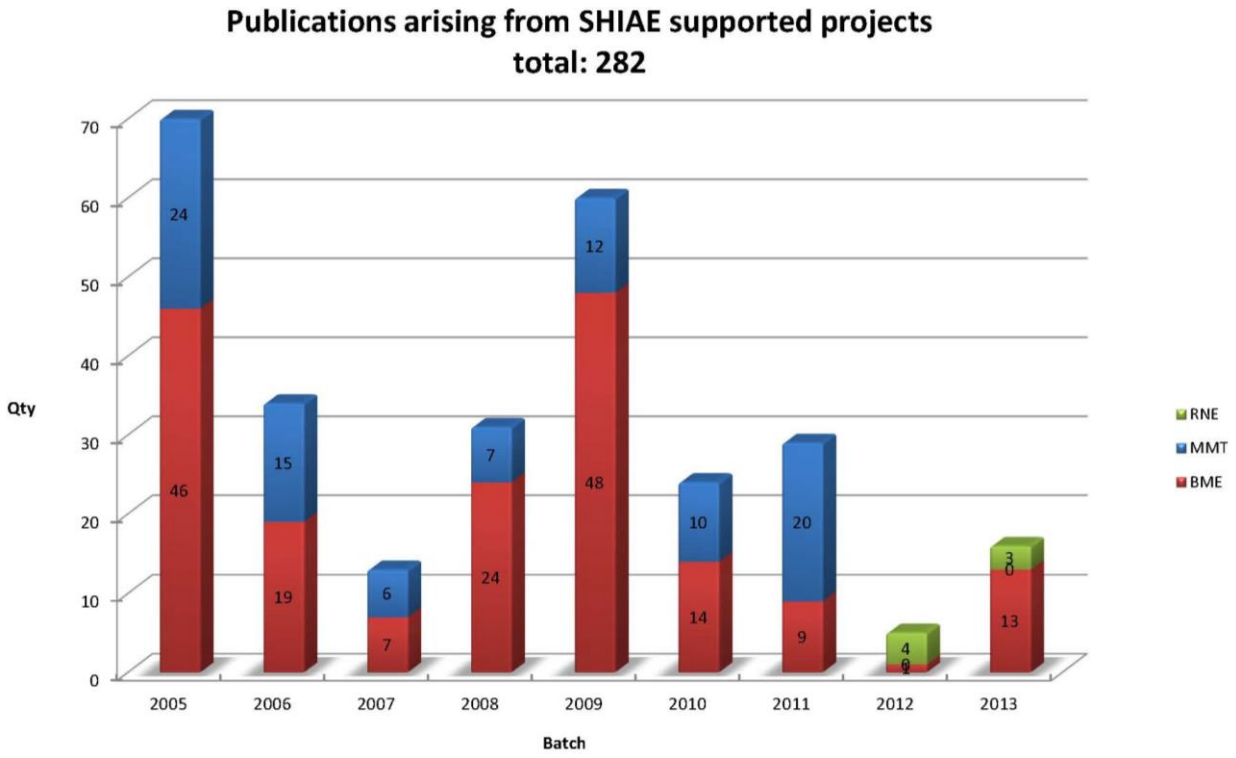

The list of publications can also be downloaded from the webpage of SHIAE at www.shiae.cuhk.edu.hk/research.htm

Renewable Energy Track

Research Reports
In Renewable Energy

Continuing Projects	
(2013-2015)	* Earth-Abundant Metal/Metal Oxide Nanostructures for Rechargeable Li-Air Batteries: Catalyst Design and Mechanistic Investigation
	* Graphene-based asymmetric supercapacitors with high energy density for clean energy storage systems
(2012-2014)	* Vibration Energy Harvesting Utilizing Multifunctional Phononic Meta-Materials and Structures
	* Understanding Electron and Phonon Transport in Boron Carbide Nanowires for Thermoelectric Energy Conversion
	* Ternary Hybrid Polymer/Nanocrystal Bulk Heterojunction Solar Cells with Cascade Energy-Level Alignmen

EARTH-ABUNDANT METAL/METAL OXIDE NANOSTRUCTURES FOR RECHARGEABLE LI-AIR BATTERIES: CATALYST DESIGN AND MECHANISTIC INVESTIGATION

Principal Investigator: Professor Yi-Chun LU
Department of Mechanical & Automation Engineering
CUHK
Research Team Members: Yulin CAO, Research Assistant [(1)]
Zhuojian LIANG, Junior Research Assistant [(1)]

[(1)] Dept. of Mechanical and Automation Engineering of CUHK

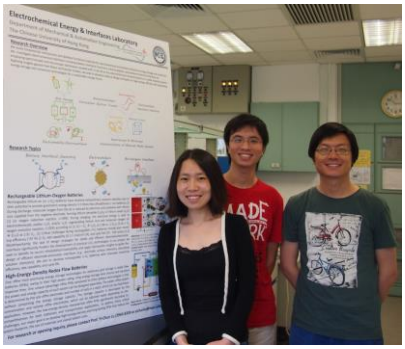

Progress Reporting Period: 01 August 2013 – 30 April 2014

ABSTRACT
Electrical storage technologies are of vital importance to enable effective utilization of intermittent renewable energy sources and the creation of sustainable electric transportation. Lithium-air (or Li-O_2) batteries have received extraordinary research attention owing to their potential to provide gravimetric energy density 3-5 times that of the conventional Li-ion batteries. However, the lack of fundamental understanding of the reaction mechanisms and materials design strategies has led to numerous critical challenges including poor round-trip efficiency, low rate capability, and poor cycle life. Here, we propose to develop earth-abundant metal/metal oxide nanostructures including nanoporous metal foams and mesoporous metal oxides as electrode materials to promote the rate capability, round-trip efficiency and cycle life of rechargeable Li-O_2 batteries. In addition, we will investigate the Li-O_2 interfacial chemistry and electrode reactivity via spectroscopic characterization techniques coupled with in situ and ex situ electrochemical characterizations. We seek to identify the source of instability/irreversibility and apply mechanistic insights to guide the design of efficient electrode-electrolyte interfaces (e.g., electrode surface chemistry, electrolyte solution chemistry). We intend to demonstrate rechargeable Li-O_2 batteries with improved round-trip efficiency, rate capability, and cycle life with minimum capacity loss.

1. OBJECTIVES AND SIGNIFICANCE
We aim to (1) develop earth-abundant nanostructured metal/metal oxide electrode materials to promote the rate capability and round-trip efficiency of rechargeable Li-O_2 batteries; (2) develop stable electrode-electrolyte interfaces to improve the cycle life of rechargeable Li-O_2 batteries; (3) unravel Li-O_2 reaction mechanisms, identify key processes that limit battery performance and develop design guidelines for stable and efficient electrode-electrolyte interfaces. These objectives will directly address the most critical challenges of rechargeable Li-O_2 batteries and are expected to enable transformative advances in rechargeable Li-air technology

2. RESEARCH METHODOLOGY
To improve the round-trip efficiency, rate capability and cycle life of rechargeable Li-O_2 batteries, we propose to (1) develop earth-abundant nanostructured metal/metal oxide electrode materials and (2) investigate Li-O_2 interfacial chemistry and identify battery degradation mechanism to guide the design of stable electrode-electrolyte interfaces. The overview of the proposed research plans is summarized in Fig.1.

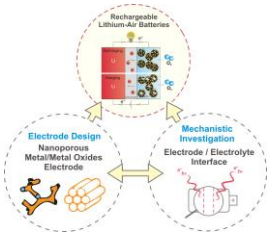

Fig.1. Overview of the research plans

2.1. Synthesis of nanostructured indium tin oxide/chromium oxide nano-composite
Indium tin oxide (ITO) is one of the most promising conducting oxides for electrochemical application and has been shown stable during Li-O_2 cycling environment by Li et al.[1] However, noble metal ruthenium (Ru)

was used in the work of Li et al.[1] as a catalyst to facilitate the Li-O_2 reactions due to the low catalytic activity of ITO. A recent work of the PI has revealed that chromium-containing oxide exhibit superior charging activity compared to carbon and exhibit similar catalytic activity as noble metals. Therefore, we here exploit chromium oxide (Cr_2O_3)/ITO nano-composite as cathode materials for rechargeable Li-O_2 batteries. Here we use a surfactant assisting method followed by a low-temperature heat treatment. 50 mg ITO is firstly dispersed in 50 ml distilled water by ultrasonication for 15 min. Then 250 mg triblock copolymer ($HO(CH_2CH_2O)_{106}(CH_2CH(CH_3)O)_{70}(CH_2CH_2O)_{106}H$) Pluronic® F127 is added under vigorous stirring for 24 h. Then 2 ml of K_2CrO_4 (10 mg/ml H_2O) is added to the above suspension under vigorous stirring for another 24 h. The resulting mixture is aged in air at 50 ℃ for 48 h in a Petri dish and then calcinated by heat treated at 500 ℃ for 1.5 h under H_2/Ar atmosphere.

2.2. Synthesis of nanostructured titanium carbide

Titanium carbide (TiC) has been recently reported to demonstrate superior cycling stability in rechargeable Li-O_2 batteries.[2] However, the TiC used in the reported literature only exhibits limited specific surface area (~15 m^2/g),[2] which significantly limit the specific capacity of the Li-O_2 batteries. Here we aim to synthesize high surface area TiC using C_3N_4 as carbon source.[3] Bulk C_3N_4 can be synthesized using melamine as precursor.[4] We design a solid-state reaction assisted by carbothermal reduction process to synthesize fine TiC nanoparticles. The C_3N_4 acts as a precursor to react with another oxide TiO_2 at 1100-1200 ℃. The C_3N_4 was firstly prepared by reaction of melamine under air at 500-600 ℃ according to the literature.[4] For the fabrication of TiC, the as-synthesized C_3N_4 and oxide TiO_2 are mixed together. The mixed powder are then put on an alumina boat and inserted into a tube furnace. The furnace is evacuated to 10^{-2} mbar. And then the furnace is heated to 1100-1200 ℃ at the rate of 5 ℃/min and kept at high temperature for 1-2 hours. Finally, black powder sample is obtained and cooled down naturally to room temperature.

2.3 Synthesis of porous silicon nanowires

Porous materials have been used as supports for catalysts because of their large number of pores, large surface area, and ease of recycling compared with other nanomaterials. Porous Si nanowires (Si NWs) have high surface areas, good electrical conductivity and fine chemical stability, which make Si NWs interesting candidate as cathode materials for rechargeable Li-O_2 batteries. We synthesize Si NWs via a method involving the deposition of silver particles on the surface of bare Si substrates followed by wet chemical etching.[5] Briefly, pieces of commercially available highly doped p-type Si(100) wafers are used as starting materials. The Si wafers are cleaned by sonication in DI water, acetone and isopropanol and dried by nitrogen blowing. The cleaned Si wafers are immersed on a buffered oxide etchant (BOE) for 2 minutes to remove the native oxide layer and then immersed in a solution containing 0.01-0.04 M $AgNO_3$ and 5 M HF for 1 minute at room temperature. The colorful surface of Si wafer indicates that Ag nanoparticles have been formed on Si surface. The Ag-deposited Si wafers are cleaned with DI water to remove the extra Ag^+ ions and then immersed on the solution containing 4.8 M HF and 0.3 M H_2O_2 for different time. Finally the Ag particles are removed by immersing the Si wafers in the concentrated H_3NO_3 for one hour. The as-etched products are inspected with a scanning electron microscope (SEM) at 10 kV of electron acceleration voltage.

2.4. Lithium-air cell design and assembly

We have designed and fabricated an electrochemical Li-O_2 testing apparatus or Li-O_2 cells, as shown in Fig. 2. The cell design is modified upon on a model proposed by the PI in a previous work.[6] Basic function of the cell is to enclose battery components and active material and protect them from exposing to the ambient environment. The cell composes mainly of stainless steel and polytetrafluoroethylene (PTFE). The cell is assembled by placing a lithium metal foil, a polymer separator (Celgard 2325), a cathode and a current collector in the center of the bottom plate, between two of which 100uL of electrolyte (0.1 M lithium perchlorate ($LiClO_4$) in dimethyl sulfoxide (DMSO)) is added, followed by installing bolts that hold the top plate, spacer and bottom plate together. Gas (i.e., pure O_2) is then purged through the valves and the gauge will

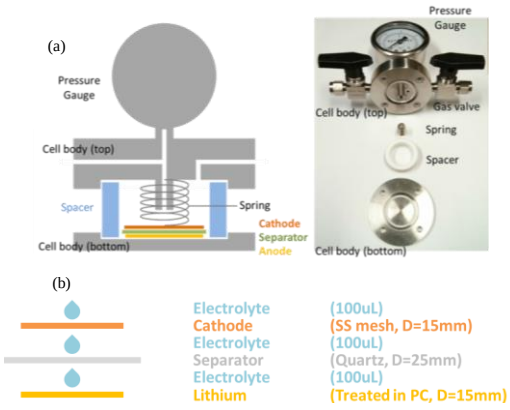

Fig. 2. (a) Illustration of the Li-O_2 cell; (b) Assembling of Li-O_2 cells

be used to indicate quality of the hermetic sealing. We have conducted a leakage test that successfully proved that the cell can be well-sealed. Therefore the fabricated cell is suitable for our future work on battery materials.

3. RESULTS ACHIEVED SO FAR

3.1. Materials characterization of as-synthesized Cr_2O_3/ITO cathode material.

Cathode materials consisting Cr_2O_3 nanoparticles supported on ITO were synthesized by a soft template method followed by low temperature heat treatment. Fig. 3 shows the schematic of the synthesis process, SEM and energy-dispersive X-ray spectroscopy (EDS) of the as-synthesized Cr_2O_3/ITO. It is interesting to note that the original color of ITO was yellow and after the coating of Cr_2O_3, the final Cr_2O_3/ITO product is dark color, which might indicate improved electronic conductivity. The EDS result shows the major composition consists of In, Sn, and Cr. The atomic ratios of Cr and In elements are 19.08% and 54.12%, respectively.

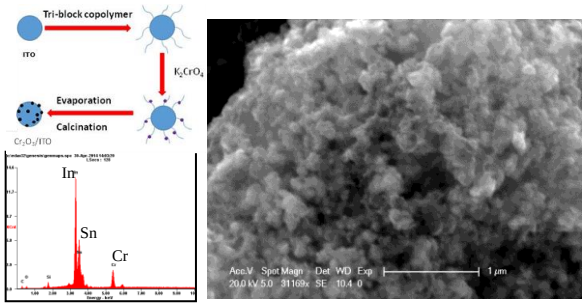

Fig. 3. Synthesis process of Cr_2O_3/ITO; SEM and EDS spectrum of the as-synthesized Cr_2O_3/ITO

3.2. Materials characterization of as-synthesized TiC cathode material.

Fig. 4 shows the SEM images and the XRD pattern of as-synthesized black product by the solid-state reaction assisted by carbothermal reduction method described earlier. SEM images show that the obtained product composed of irregular nanoparticles. The EDS spectrum (not shown here) shows that the as-synthesized product contains the Ti, O, and C elements. And the atomic ratios of Ti and C elements are 17.07% and 14.93%, respectively. The atomic ratio of Ti/C is close to 1:1. The XRD pattern demonstrate that the as-synthesized product was crystalline TiC. The index pattern basically agrees with JCPDS card no.32-1383. The XRD pattern of oxide precursor TiO_2 was also shown for comparison. It means that the TiO_2 precursor can be transformed into TiC after reaction with C_3N_4 by present method in this case. The results suggest that this route is effective in converting TiO_2 to TiC. The reaction mechanism can be expected to include two steps: Firstly, C_3N_4 decomposes into different carbon nitride species, such as $C_2N_2^+$, $C_3N_2^+$, and $C_3N_3^+$, at temperature higher than 550 ℃. These species are highly reactive and easily bonded to oxygen atoms and reduce the titanium oxide into titanium metal. The subsequent carbonizing process between the titanium metal and the carbon-rich species will occur and finally lead to the formation of nanoparticles of TiC. We will evaluate the specific surface area of the as-synthesized TiC via the Brunauer, Emmett and Teller (BET) method.

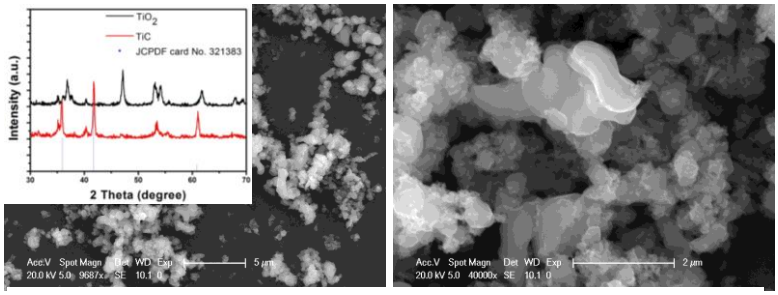

Fig. 4. SEM images and XRD pattern of as-synthesized TiC.

3.3. Materials characterization of as-synthesized porous Si NWs cathode material.

Fig. 5 shows the photograph (top left) and top view SEM image (top right) of the as-synthesized Si nanowires on highly doped Si substrate. In order to clearly reveal the Si NWs morphologies, the cross-section view of the Si substrate is shown in Fig. 5 (bottom). It is observed that surface of Si substrate is etched and morphology of these etched Si is nanowire arrays. The Si nanowire arrays have length of 10 μm and width of 80-120 nm. The Si nanowire arrays have been successfully fabricated. The Si nanowires have crystalline crystal structures and large length-diameter aspect ratio and porous properties.[7] The as-synthesized porous Si nanowires have large surface areas

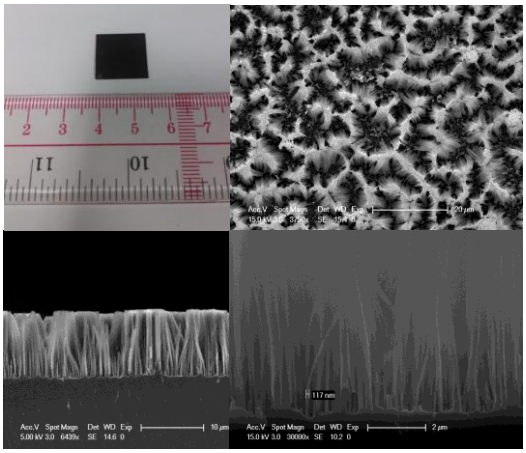

Fig. 5. Photograph and SEM images of Si NWs.

which may be a good candidate as catalyst supporter. We will evaluate the specific surface area of the as-synthesized Si NWs via the BET method.

3.4. O_2-cathode fabrication and electrochemical characterization of select cathode materials

Oxygen-cathodes are fabricated by first mixing the cathode powder with PTFE binder in the ratio 95:5 (m/m) in isopropanol (Fig. 6a). The slurry is then drop casted onto a stainless steel mesh (0.6 mg/cm^2). The coated mesh is dried in vacuum for over 12 hours at 150 ^{o}C. After this the electrodes are transfer to the glove box without exposure to air. As shown in Fig. 6b, the resulted electrode that the cathode material is evenly distributed across the mesh, both on and between the mesh wires. To establish our testing apparatus and methodology, we first select commercial available conducting metal carbide as cathode model systems due to its superior reaction stability reported recently.[2] We systematically select five metal carbides including TiC, vanadium carbide (VC), chromium (Cr_3C_2), molybdenum carbide (Mo_2C), and tungsten carbide (WC). The galvanostatic electrochemical characterizations of the five carbide nanoparticles are shown in Fig. 7. The rates for discharge and charge were 50mA/$g_{cathode}$ and 10mA/$g_{cathode}$, respectively. We also limited the discharge process to a capacity of 100mAh/$g_{cathode}$ to examine the discharge and charge behavior of Li-O_2 batteries without forming large/thick insulating Li_2O_2 particles. As shown in Fig. 7, the VC exhibits low discharge (i.e., poor discharge activity) but exceptionally low charge voltage (i.e., high charge activity). The low discharge voltage may be explained by its relatively small specific surface area, which further suggests that the VC exhibits the best catalytic activity for charging of the Li-O_2 batteries among the five carbides. In addition, TiC shows the highest charge potential, suggest that TiC exhibit lower charging activity compared with other four carbides. To quantitatively evaluate and compare the intrinsic catalytic activity of the five select cathode materials for discharge and charge reactions, we will perform comprehensive electrochemical characterizations including cyclic voltammetry (CV), Potentiostatic Intermittent Titration Technique (PITT) and Galvanostatic Intermittent Titration Technique (GITT) tests on these materials. Activity obtained from these measurements will be normalized by the true surface area of each material to be measured by the BET method.

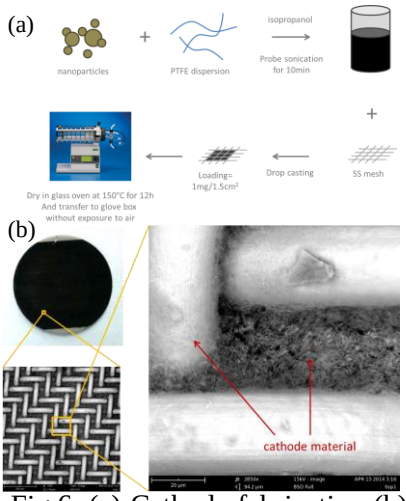

Fig.6. (a) Cathode fabrication (b) SEM image of O_2-cathodes on stainless steel.

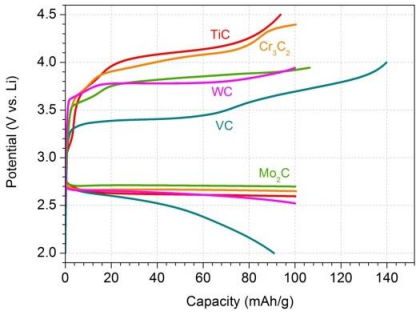

Fig. 7. First charge/discharge profile of Li-O_2 cells with cathode materials including TiC, Cr_3C_2, WC, VC and Mo_2C.

3.5. Design and setting up on-line electrochemical mass spectrometer

We designed and are developing an on-line electrochemical mass spectrometer (OEMS, Fig. 8)[8] to identify and quantify the gas or volatile species formed in the cell during charge. It consists of an electrochemical cell, a sampling system and a mass spectrometer. A pressure transducer will be connected to the cell and measures during discharge the change of oxygen pressure, from which the amount of oxygen consumed can be determined. During charging, the gas and volatile species yield during charge will be sent to the vacuum chamber by the sampling system. The mass spectrometer can be used to analyze the composition of the gas.

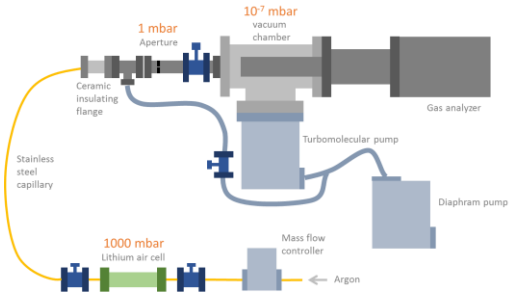

Fig. 8. Schematic of the OEMS design.

References: (1) Li et al., *Nano Lett.* 2013, 13, 4702. (2) Ottakam Thotiyl et al., *Nat. Mater.* 2013, 12, 1050. (3) Li et al., *J. Alloys Compd.* 2007, 430, 237. (4) Zhang et al., *J. Am. Chem. Soc.* 2013, 135, 18. (5) Qu et al., *Nanoscale* 2011, 3, 4060. (6) Lu et al., *Electrochem. Solid State Lett.* 2010, 13, A69. (7) Qu et al., *J. Mater. Chem.* 2010, 20, 3590. (8) Tsiouvaras et al., *J. Electrochem. Soc.* 2013, 160, A471.

4. PUBLICATION AND AWARDS

To date, there is no publication arising from this funded project, but we expect 1-2 journal articles to be

published upon the completion of the second year project period.

GRAPHENE-BASED ASYMMETRIC SUPERCAPACITORS WITH HIGH ENERGY DENSITY FOR CLEAN ENERGY STORAGE SYSTEMS

Principal Investigator: Professor ZHANG Li[1, 2]
Department of Mechanical & Automation Engineering, CUHK

Research Team Members:
HAN Lijuan, Shun Hing Research Assistant [1, 2]
WANG Feng, Shun Hing Research Assistant [1, 2]

[1] Dept. of Mechanical and Automation Engineering
[2] Shun Hing Institute of Advanced Engineering

Progress Reporting Period: 1 July 2013 – 30 April 2014

ABSTRACT

The objective of the proposed research is to fabricate, characterize and optimize graphene-based supercapacitors with high performance for clean energy storage systems.

Supercapacitors have attractive properties such as high charge-discharge efficiency at high power densities, long cycling life, and pollution-free for clean energy storage; however, to date, their potential applications are hurdled by the low energy density. Graphene is recently considered as an ideal electrode material for supercapacitors due to their 2-D single-atom-layer structure and excellent intrinsic physical properties such as ultra-high specific surface area (SSA), outstanding electrical conductivity and excellent mechanical and chemical stability. Though graphene-based supercapacitors are promising for practical applications, their energy and power densities are still need to be adequately improved to reach their best performance.

Taking advantage of novel synergistic effect of graphene nanosheets (GNS) and active nanostructured components, the PI proposes to design and prepare asymmetric supercapacitors using GNS-based nanocomposites as electrodes, and to characterize and optimize the microstructural and electrochemical properties of prototype supercapacitor devices having high energy and power densities. The ultimate goal is to develop high-performance and low-cost supercapacitors which can be scaled-up for future commercial applications.

This proposed research will result in fundamental understanding on the synergistic effect of the nanocomposites consisting of GNS and metal oxide/hydroxide nanostructures for the enhanced performance of the supercapacitors, thus, to pave the way for the development of next-generation energy storage devices and systems.

1. OBJECTIVES AND SIGNIFICANCE

1. To synthesize graphene oxide (GO) from expanded graphite using Hummers method. Since the surface of GO containing rich oxygen functional groups, it is an advantage to dispersively anchor metal ions for the nucleation of nanoscale metal oxides or hydroxides for the preparation of graphene-based nanocomposites.

2. To fabricate metal-oxide/reduced-graphene-oxide nanocomposites (MO/RGO, such as nanocomposite consisting of Mn_3O_4 and RGO) and metal hydroxide/graphene (MOH/RGO) nanocomposites using a one-step solution method, a facile and low-cost process. Their microstructural aspects will be

investigated by SEM, high resolution electron microscopy (HRTEM), X-ray diffraction (XRD), infrared spectrometer and thermogravimetric analysis (TG) to understand the formation mechanism of the nanocomposites.

3. To design and prepare prototype asymmetric supercapacitors using MO/RGO or MOH/RGO as positive electrodes and activated carbon as negative electrodes. These kinds of asymmetric supercapacitors are expected to have much higher working voltage and energy density than other type of supercapacitors.

4. To investigate the electrochemical properties of the as-fabricated supercapacitors using cycle voltammetry (CV), galvanostatic charge–discharge and electrochemical impedance spectroscopy (EIS) to determine their capacitance properties.

5. To conduct systematic optimization from both the composition of the hybrid materials and the design of the asymmetric electrodes to enhance the capacitor performance.

Long-term impact: Graphene-based nanocomposites are considered as one of the most suitable candidates for preparing supercapacitors, however, several crucial problems remain challenging: i.e., how to fabricate massive and high-quality graphene-based nanocomposites in low-cost for the high-performance supercapacitors, and how to effectively enhance their energy and power densities for future commercial applications. In this research, a facile one-step method will be developed, where the reduction of graphene oxide and formation of nanocomposites can be realized simultaneously. Based on this strategy, the high specific surface area of graphene will be effectively utilized through the sandwiched nanostructures and the chemical structure of metal-oxides/hydroxide nanostructures would be significantly stabilized upon their rooting on the graphene substrate. Thus, both the double layer capacitance of graphene and pseudocapacitance of metal-oxide/hydroxide can be gained to significantly enhance the performance of supercapacitors owing to the synergy of the hybrid materials. Moreover, asymmetric prototype supercapacitors will be designed, assembled, tested and then optimized, in order to reach the best working voltage and the energy density of the devices. The proposed study will impact scientific and technological development through providing high-performance supercapacitors for future low-cost and environmental-friendly commercial energy storage systems.

2. RESEARCH METHODOLOGY

Supercapacitor is promising for energy storage applications, in particular for the systems which require high power density, such as energy back-up systems and electrical/hybrid vehicles [1]. According to the different energy storage mechanism there are two types of supercapacitors: electrochemical double-layer capacitors (EDLC) and Faradic pseudocapacitors. Their performance can be quantified by the energy and power density respectively, i.e. $E=1/2(C_sU^2)$ and $P=E/t$, where C_s is the specific capacitance, U is the working voltage window and t is the time to discharge. Apparently, to enhance the E and P, large specific capacitance and voltage window with high electrical conductivity are required. Graphene is a single layered carbon material with ultra-large SSA (2675 m2/g), high electrical conductivity and mechanical strength (~1 TPa), showing great potential applications in EDLC, however, it remains a great challenge to fully utilize its SSA due to the re-stacking and agglomeration of the graphene nanosheets. By contrast, metal-oxides/hydroxides such as RuO_2 and $Ni(OH)_2$ show much higher pseudocapacitance than EDLCs, but their low electrical conductivity and power density, poor structural stability are still the drawback for practical applications. Therefore, to improve the performance of supercapacitors, an effective strategy is to design, synthesize and optimize advanced nanocomposites using the synergy between graphene and other active nanoscale structures.

Work done by us before the project: The PI was engaged in electrochemical capacitor researches from 2006 (Tao *et al*., Carbon, Vol. 44, 1425-1428, 2006), and he has noticed that hybrid/nanocomposite materials have great potential for high-performance supercapacitors and other green energy systems.

The research was started from the fabrication of supercapacitors using carbon-based nanocomposites as electrode materials. Initially, nanocomposites of goethite nanorods and reduced graphene oxide (RGO) was synthesized and investigated, which showed an electrochemical capacitance of 165.5 Fg^{-1}, promising for

electrochemical capacitors [7]; the electrode material we prepared from *in situ* construction of potato-starch-based carbon nanofiber/AC hybrid structure also exhibited good performance for EDLC [8]. Recently, the PI conducted some experiments of synthesizing graphene-based nanocomposites, such as Co_3O_4/RGO (inserted figure, upper one) and $CoAl(OH)_2$/RGO, as electrode materials of supercapacitors, and the preliminary results are striking [9, 10]. The prototype asymmetric electrochemical capacitors we assembled using $CoAl(OH)_2$/RGO nanocomposite as positive electrode and activated carbon as negative electrode showing an improved electrochemical properties with higher energy density and working voltage (1.75 V in 6 M KOH aqueous electrolyte) in comparison to the traditional ones, which are capable of lighting a red LED with 1.5 V on-voltage (inserted figure, below one). As the PI proposed in this proposal, to further develop the graphene-based supercapacitors with higher performance for the new clean energy storage systems, great efforts on systematic investigation and optimization of the nanocomposites are still required.

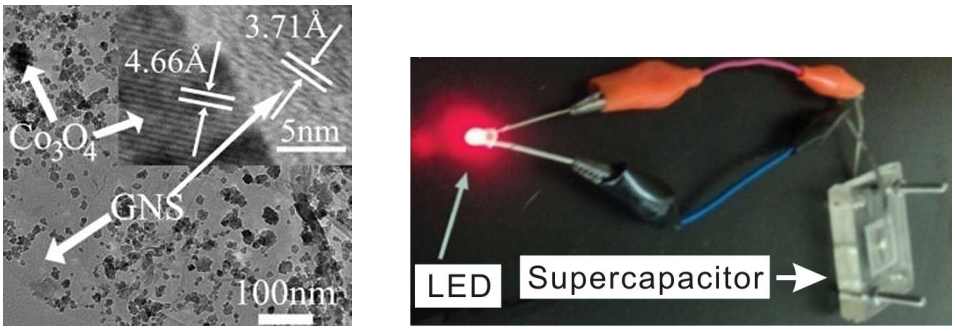

Fig. 1: The left image shows the microstructural properties of the nanocomposite consisting of GNS and Co_3O_4. The right photograph shows a LED connected with a supercapacitor.

3. RESULTS ACHIEVED SO FAR

In order to design and prepare asymmetric supercapacitors with optimized performance, nanocomposites with varied materials and architectures as well as thin graphene paper are investigated in parallel.

Hierarchical core-shell-shell nanowire arrays based on metal oxide-conductive polymer-metal oxide were successfully developed using hydrothermal synthesis and electrode position (Fig. 2). The key to fabricate one-dimensional hierarchical architecture, Co_3O_4@PPy@MnO_2 "core–shell–shell" nanowires, was to introduce a PPy intermediate layer on the surface of Co_3O_4 nanowire, which could enhance the conductivity of nanowire arrays and act as a reactive template to induce a coating of amorphous MnO_2. The device based on the ternary composite Co_3O_4@PPy@MnO_2 nanowire arrays exhibited prominent electrochemical performance with a high energy density of 34.3 Wh kg^{-1} at a power density of 80.0 W kg^{-1} and it is notable that the device exhibits a superior cycling behavior with 100.4% retentions of initial capacitance after 11,000 charge/discharge cycles because the elastic thin PPy shell can provide facile strain relaxation during long cycling, enhancing structural stability.

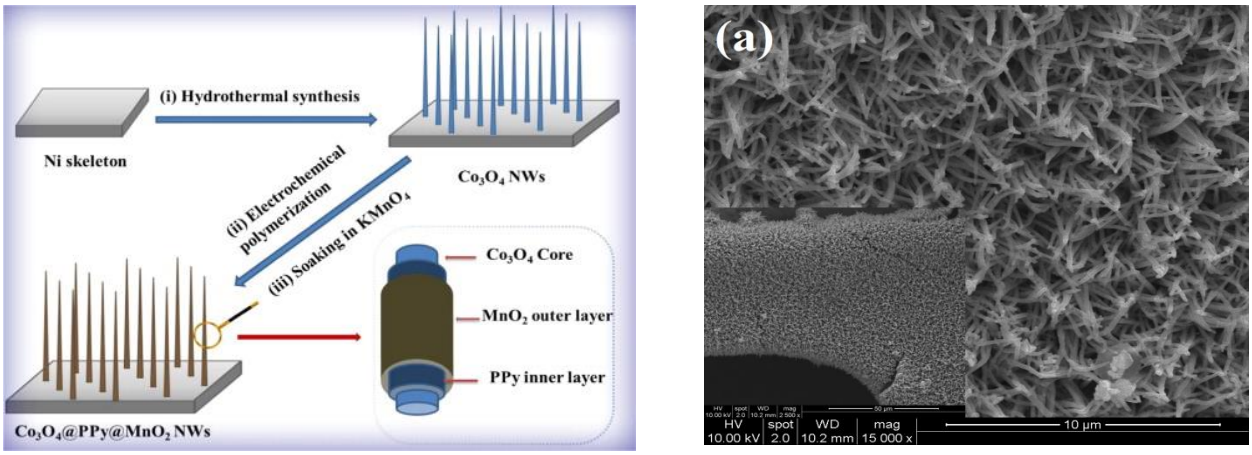

Fig. 2: (left) Schematic illustration of the fabrication process for Co_3O_4@PPy@MnO_2 core-shell-shell

nanowire arrays. (right). SEM micrograph of ternary Co_3O_4@PPy@MnO_2 hybrid nanowire arrays.

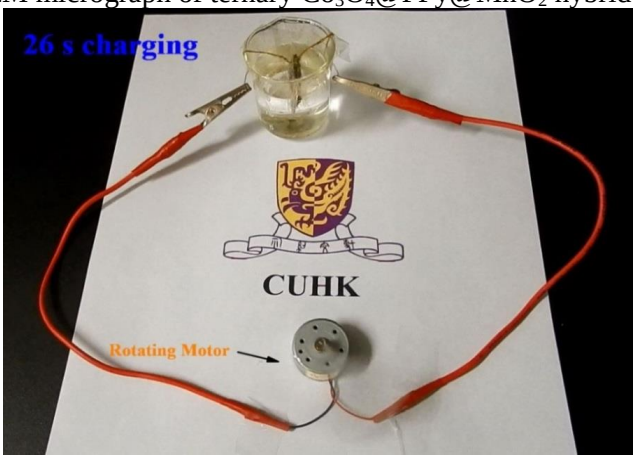

Fig. 3: A DC motor is powered by an AC//Co_3O_4@PPy@MnO_2 aqueous supercapacitor device in 1.0 M NaOH solution which was charged for 26 s. The mini-motor was able to rotate approximate 30 seconds by the charged supercapacitor. The length and the width of the device is ca. 1cm × 1 cm.

The performance of as-assembled asymmetrical supercapacitor was demonstrated using a DC motor (Fig. 3), in which the device can drive a mini-motor rotating robustly for approximately 30 s after charging at 17.4 mA cm^{-2} for 26 s. The results were published in *Nano Energy* in 2014 (see Section 4). In the second year of this project, we plan to replace the conductive polymer layer, i.e. PPy, with graphene using chemical vapor deposition (CVD) or chemical solution methods. The goal is to achieve freestanding 3D networked structures based on graphene materials as the electrode of high-performance supercapacitors. It is also notable that, inspired by the paper published by Ajayan *et al*., (*Nano Letters*, Vol. 11, 1423-27, 2011), we are also developing planar graphene-paper-based supercapacitors for ultrathin flexible electronic devices. In the first year, r-GO papers were successfully prepared with a varied thickness from nano- to micro-scale.

In addition, nanocomposites of carbon nanotubes (CNTs) coated with Ni-Co oxide nanoparticles were also synthesized using electroless plating in the first year with the collaboration with Zhejiang University, which were then applied as the conductive agents of activated carbon (AC) electrode for supercapacitors. Our results showed the specific surface, porosity, electrical conductivity, as well as electrochemical activity can be tuned by adjusting the molar ratio of nickel and cobalt in the electroless plating process. More importantly, the modification of the conductive agent for the electrode can improve the electrochemical performance of supercapacitors. The results indicate that the nanocomposite of carbon-based material/metal oxide have potential to act as additive materials in AC for the improvement of performance of supercapacitors. This part of results was published in *IEEE Transactions on Nanotechnology* in 2014 (see Section 4), and was presented in the conference IEEE NANO 2013.

4. PUBLICATION AND AWARDS

[1] Q. Li, J. Cheng, and **L. Zhang**, "Nickel-cobalt Oxide Coated CNTs as Additives of Activated Carbon Electrode for High-performance Supercapacitors", *Proc. of the 13th IEEE International Conference on Nanotechnology (IEEE NANO 2013)*, Beijing, China, pp. 348-351, 2013.

[2] L. J. Han, P. Y. Tang, and **L. Zhang**, "Ternary Hierarchical Co_3O_4@PPy@MnO_2 Core-Shell-Shell Nanowire Arrays for Enhanced Electrochemical Energy Storage", *Nano Energy*, Vol. 7, pp. 42-51, 2014.

[3] Q. Li, J. Cheng, B. Wang, and **L. Zhang**, "Activated Carbon Modified by CNTs/Ni-Co Oxide as Hybrid Electrode Materials for High Performance Supercapacitors", *IEEE Transactions on Nanotechnology*, Vol. 13, 3, pp. 557-562, 2014.

VIBRATION ENERGY HARVESTING UTILIZING MULTIFUNCTIONAL PHONONIC META-MATERIALS

Principal Investigator: Professor Michael Yu WANG
Department of Mechanical & Automation Engineering, CUHK

Research Team Member:
Xiaoming WANG, Shun Hing Research Fellow [(1)]

[(1)] Dept. of Mechanical and Automation Engineering

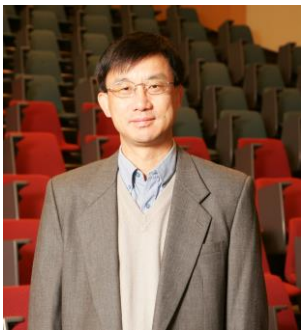

Progress Reporting Period: 1 July 2012 – 30 April 2013

ABSTRACT

Our project focuses on a class of multifunctional, microstructured materials (meta-materials) and structures for vibration energy harvesting. The meta-materials have superior mechanical wave handling properties and energy conversion capabilities. These abilities of meta-materials can inhibit elastic waves from propagating within specific frequency ranges known as phononic bandgaps. By utilizing the multi-functional meta-materials and structures, vibration energy can be localized (or trapped); the vibration wave can be guided (or channeled) to a specific location; and multi-frequency waves can be separated (or filtered) into single-frequency parts. Consequently, the vibration energy can be collected, filtered, and finally channeled to and accumulated at converting locations, where it is converted into electrical power by piezoelectric harvesters with tuned resonances.

1. OBJECTIVES AND SIGNIFICANCE

Energy harvesting has become the talk of the engineering world. Generating electrical energy from natural or environmental sources, such as ambient vibrations and heat, would give self-powered capability to a sea of portable electronic devices, wireless sensors and MEMS systems. Vibration energy harvesting holds a great potential, as vibrations are omnipresent in machines and structures, scattering energy over wide space and in a wide frequency range. The challenge is to collect vibrations effectively and convert them efficiently into electricity, allowing energy harvesting on a continuous basis and employed in hostile and inaccessible environment.

The aim of this research project is to develop the multifunctional structures whereby meta-materials with desired bandgap functions are integrated as building blocks to form the structures for efficient energy harvesting. The proposed approach is hierarchical and is physically driven. The overall goal of the project is to develop the hierarchical design method and to demonstrate the applicability of the proposed vibration energy harvesting system. The proposed system is also scalable for microscale applications. It is expected that this investigation would yield a novel vibration energy harvesting technique that would significant advance the state-of-the-art.

The objectives of the project include:

1. Development of an optimization-based approach that employs level set methods to provide complex designs of bandgap meta-materials of multiple frequency-dependent dispersive dynamic characteristics;

2. Systematic explorations of unit cell optimization of meta-materials to optimize the three desired functional materials crucial to the proposed vibration energy harvesting structure: (1) trapping, to localize elastic waves of a specified frequency range, (2) channeling, to guide vibration waves to a specific location, and (3) filtering, to separate or select multi-frequency waves into single-frequency parts;

3. Hierarchical design for energy harvesting structures: (1) synthesizing the topology of bandgap structure with a layout of regions of the required multifunction meta-materials, and (2) employing the

designed materials to form a bounded structure with bandgap functions that correlate with those of the materials in the structure;

4. Demonstration of the proposed approach with design cases where ambient vibration energy of a structure is filtered, accumulated and channeled for harvesting, showing the feasibility of the concept and the efficiency of the proposed phononic structure.

2. RESEARCH METHODOLOGY

A key contribution of our approach stems from a complete understanding of the dynamics of periodic bandgap materials and structures. We embark upon the difficulties of ambient vibration sources characterized by their spatial distribution (location) and time distribution (frequency), as they are often generated from multiple sources, propagated throughout the structure and distributed over a large surface area. Their energy might be scattered over a range of frequency spectrum. Fortunately, phononic bandgaps can have multiple functions. A phononic material can disperse different wavelengths, stopping or letting pass a selected frequency and, thus, acting as a wave trap. We intend to utilize these fundamental dynamical properties and to construct bounded structures from bandgap materials such that they are to be used as basic functional building blocks for our novel multiscale multifunctional system for vibration energy harvesting.

3. RESULTS ACHIEVED SO FAR

During this period of the project, we focus on vibration energy harvesting with phononic bandgap structures. First, we study benchmark problems of bandgap materials and optimization. The problems include bandgap mechanisms for broadband frequency wave attenuation in low frequency range. We studied flexural beams with multi-DOF resonators attached, which generate locally resonant wave trapping. With the innovative use of different configurations of 2-DOF resonators, we have found very interesting properties of wave dispersion. Particularly, our preliminary results indicate that we can achieve super-wide frequency bandgaps at low frequency range. This is a scenario suited for harvesting the energy of the vibration wave with two piezoelectric harvesters with tuned resonance frequency. We will continue to investigate the properties to the full extend.

4. PUBLICATION AND AWARDS

Our research findings arising from the funded project are to be published in the following publications. All these publications have directly acknowledged the SHIAE funding support.

[1] Xiaoming Wang and Michael Y. Wang, “Band Gaps in Periodic Flexural Beams With Multi-DOF/Continuum Local Resonators,” PHONONICS 2013: 2nd International Conference on Phononic Crystals/Metamaterials, Phonon Transport and Optomechanics, June 2-7, 2013. http://phononics2013.org

[2] Michael Y. Wang and Xiaoming Wang, “Wide-Band Low Frequency Gaps in Periodic Flexural Beams With Nonlinear Local Resonators,” PHONONICS 2013: 2nd International Conference on Phononic Crystals/Metamaterials, Phonon Transport and Optomechanics, June 2-7, 2013. http://phononics2013.org

[3] Michael Y. Wang and Xiaoming Wang, “Broadband Wave Attenuation in Locally Resonant Periodic Flexural Beams With Force-Moment Resonators,” 25th Conference on Mechanical Vibration and Noise, ASME IDETC/CIE 2013, August 5-8, 2013. http://www.asmeconferences.org/idetc2013

UNDERSTANDING ELECTRON AND PHONON TRANSPORT IN BORON CARBIDE NANOWIRES FOR THERMOELECTRIC ENERGY CONVERSION

PI: Professor Dongyan XU
Department of Electronic Engineering, CUHK

Research Team Members:
Juekuan YANG, Visiting Scholar, Shun Hing Fellow [(1)]
Xiaomeng WANG, Postgraduate Student [(1)]
Qiang FU, Postgraduate Student [(1)]

[(1)] Dept. of Mechanical and Automation Engineering

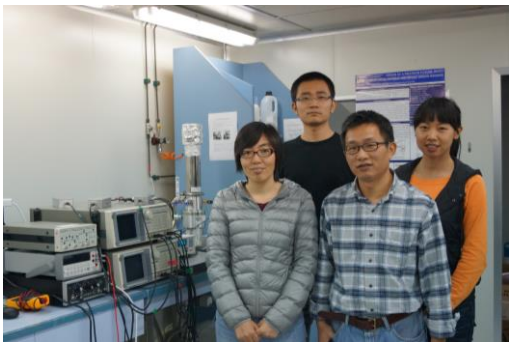

Progress Reporting Period: 1 July 2012 – 30 April 2013

ABSTRACT

The objective of the proposed research is to study the structure and transport property relation of boron carbide nanowires for thermoelectric energy conversion applications. Thermoelectric devices show a great potential for waste heat recovery by directly converting heat into electricity; however, to date their practical applications have been limited by their low efficiencies. Recently, several reports demonstrated significantly improved thermoelectric efficiencies by engineering thermoelectric materials into nanostructures, such as nanowires, primarily through thermal conductivity reduction. Despite boron carbides have been projected as a promising class of high-temperature thermoelectric materials, so far, no one has studied thermoelectric transport properties of one-dimensional boron carbide nanowires yet. The PI proposes to study transport properties of boron carbide nanowires for high-temperature thermoelectric applications. The approach is to integrate systematic transport property measurement on individual boron carbide nanowires and detailed structure and composition characterization for each measured wire. The ultimate goal is to develop the structure-transport property relations for boron carbide nanowires.

1. OBJECTIVES AND SIGNIFICANCE

The objectives of the proposed research are

- To measure thermoelectric properties (thermal conductivity, electrical conductivity, and Seebeck coefficient) of individual boron carbide nanowires in a wide temperature range (10 – 800 K). Since these properties are determined on the same nanowire sample, we can construct thermoelectric figure-of-merit for each boron carbide nanowire.
- To thoroughly characterize the structure and composition of each measured nanowire.
- To construct the relations between composition, structure, and transport properties of boron carbide nanowires upon the completion of the first two objectives.
- To clarify the effects of many important factors, including nanowire diameter, carbon concentration, planar defect, and doping level, on thermoelectric properties of boron carbide nanowires.

Significance: Boron carbides are promising high-temperature thermoelectric materials whose transport properties are not well understood yet especially for one-dimensional nanostructures. The proposed research will provide previously unavailable data to answer the following two fundamental scientific questions: (1) Can we correlate the structure-transport property relation of boron carbide nanowires? (2) To what extent boron carbide nanowires can enhance the thermoelectric performance compared to bulk materials? Answering these questions will not only enhance our understanding on electron and phonon

transport in boron carbide nanowires but also lead to materials design rules to achieve better thermoelectric performance. The proposed study will impact technology development through providing better materials for high-temperature thermoelectric energy conversion applications.

2. RESEARCH METHODOLOGY

2.1. Microdevices for Properties Characterization

To characterize thermoelectric properties of an individual nanowire, we designed and fabricated a unique microdevice as shown in Figure 1. The device consists of two suspended 25 μm×15 μm silicon nitride (SiN_x) membranes separated by 2 to 6 μm. A 30 nm thick Platinum (Pt) coil and two separate Pt electrodes are patterned on each membrane. Each coil is electrically connected to four contact pads via metal lines on suspended beams, enabling four-probe measurement of electrical resistance of the coil. The Pt coils serve as a heater to increase the temperature of the suspended membrane, as well as a resistance thermometer to measure the temperature of each suspended membrane. An individual boron carbide nanowire can be placed bridging two membranes using a micromanipulator. The design of the microdevice enables us to determine thermal conductivity, electrical conductivity, and Seebeck coefficient of an individual nanowire in one measurement. Thus, thermoelectric figure-of-merit of individual boron carbide nanowires can be calculated.

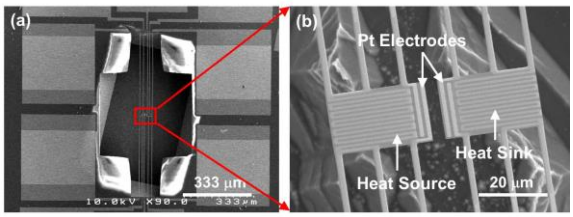

Figure 1 SEM images of the microdevice used to characterize thermoelectric properties of an individual nanowire.

2.2. Thermal Conductivity Measurement

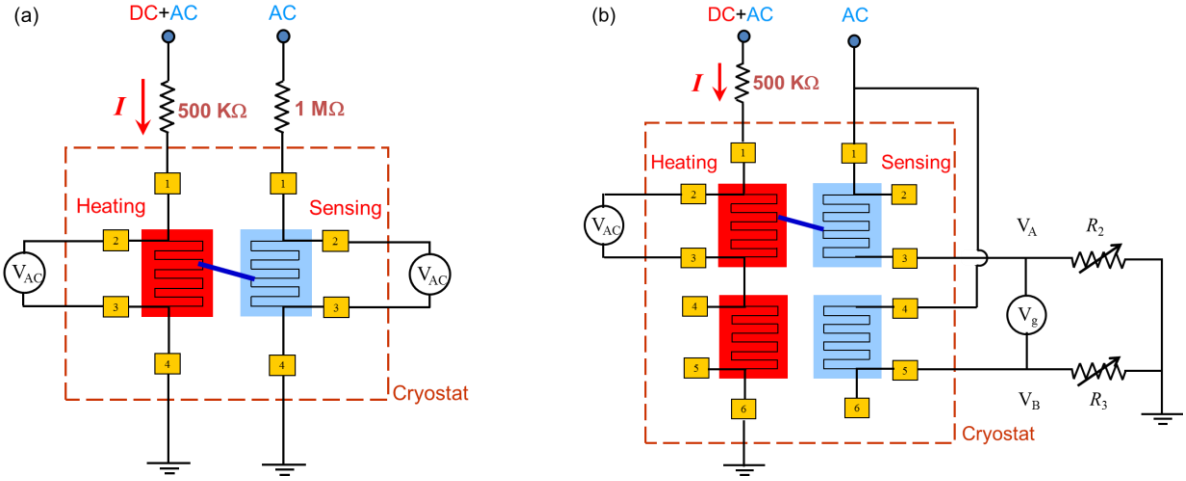

Figure 2 Schematics of traditional measurement method (a) and cancelling bridge method (b).

The measurement technique we used in this project was invented by Kim et al in 2001, and has been widely used to characterize thermal properties of various nanowires, nanoribbons, carbon nanotubes, and graphene sheets. The schematic of traditional measurement method is shown in Figure 2(a). During the measurement, a DC current is applied to one Pt coil and generates Joule heating, and accordingly increases the temperature of the heating membrane. Part of the generated heat will flow through the nanowire to the sensing membrane and raise its temperature. A small AC current will be applied to the Pt coil on each membrane to measure the coil resistance using a four-probe method and then the temperature rise of each membrane can be calculated from the coil resistance change. The thermal conductance of the nanowire can be determined by solving the heat transfer equation for the whole system. Then thermal conductivity of the nanowire can be extracted after its length and cross sectional information are obtained.

The traditional method has a sensitivity of approximately 1 nW/K. Therefore it is applicable for samples with a thermal conductance much higher than 1 nW/K. On the other hand, in the traditional method, radiation between the heating membrane and the sensing membrane also contribute to the total thermal conductance, which may result in an overestimation on thermal conductivity of the nanowire. The radiation

conductance is also on the order of 1 nW/K at room temperature. In order to measure thermal properties of one-dimensional nanostructures with thermal conductance less than 1 nW/K, recently, Wingert et al introduced a Wheatstone bridge into the sensing side circuit to improve the sensitivity (cancelling bridge method), as shown in Figure 2(b). In this method, a reference device without the nanostructure is used to cancel the contribution of radiation to the total thermal conductance. Their experiments show that the cancelling bridge method can achieve a measurement sensitivity of 10 pW/K. In this project, we implemented both traditional measurement method and cancelling bridge method to measure thermal properties of boron nanoribbons and the contribution of radiation to the measurement is evaluated by comparing the measurement results from both methods.

3. RESULTS ACHIEVED SO FAR

In the past year, we have mainly accomplished the following three parts:

3.1. Design and Fabrication of Microdevices

So far, we have designed and fabricated a series of suspended microdevices on silicon wafers through standard microfabrication processes. Devices with different spacing between two suspended membranes are obtained for different applications. To prepare samples, a micromanipulator with a sharp probe tip is used to place individual nanowires or nanoribbons bridging two membranes under an optical microscope.

3.2. Implementation of Traditional Measurement Method and Cancelling Bridge Method

We have built an experimental system for thermal conductivity measurement of one-dimensional nanostructures as shown in Figure 3. Both traditional measurement method and cancelling bridge method have been implemented and calibrated and experimental results are given in next section. In order to determine the temperature dependence of thermal conductivity, the sample is mounted in a cryostat system, which is capable to change the environmental temperature rapidly from 10 K to 800 K. Before the measurement, the cryostat chamber will be pumped down to a pressure lower than 10^{-6} torr to minimize the convective heat loss.

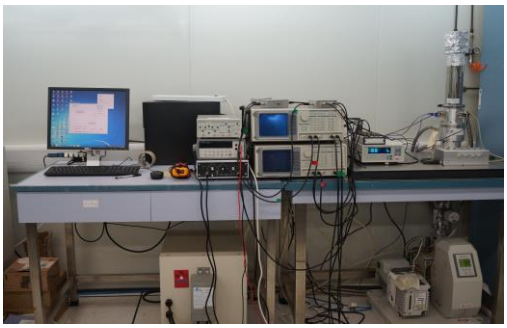

Figure 3 Experimental setup

3.3. Thermal Conductivity Measurements of Boron Nanoribbons

Before characterizing boron carbide nanowires, we first calibrated our experimental system by measuring thermal conductivities of boron nanoribbons. Boron nanoribbons are chosen for calibration mainly for two reasons: 1) Thickness of our boron nanoribbon samples is very uniform, normally within 20±2 nm, and their thermal conductivities are found very repeatable; 2) Prof. Deyu Li's group at Vanderbilt University has measured boron nanoribbon samples with traditional measurement method. Their results can serve as a reference for our measurements. Moreover, one-dimensional boron nanostructures are promising materials for nanoscale electronic devices due to their superior physical properties. However, thermal transport in this complex material has not been well understood yet. On the other hand, thermal conductivity of boron nanoribbons at high temperature (>500 K) has not been studied so far, which will be one of our research focuses in this project.

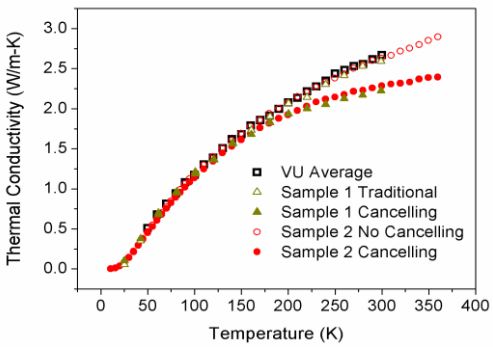

Figure 4 Thermal conductivity of boron nanoribbons.

Two boron nanoribbon samples have been measured and thermal conductivity results are shown in Figure 4. Sample 1 has been measured by using both traditional measurement method and cancelling bridge method. The thermal conductivity result of traditional measurement method (open triangles) agrees well with the average data (open squares) obtained by Prof. Deyu Li's group at Vanderbilt University, which indicates that our traditional measurement system works properly. In order to calibrate the cancelling bridge setup, a DC current is applied only to the heating coil

on the device with a nanoribbon but not to the counterpart on the reference device. Since the reference device is not heated up, the radiation conductance cannot be cancelled in this case and the cancelling bridge method is essentially degraded to the traditional measurement method. As seen in Figure 4, thermal conductivity result of sample 2 measured with degraded cancelling bridge method (Sample 2 No Cancelling) agrees well with the results of traditional measurement method, confirming that our cancelling bridge setup also works well.

Thermal conductivity results of these two boron nanoribbon samples measured with cancelling bridge method are also shown in Figure 4. As we can see in this Figure, thermal conductivity results obtained by cancelling bridge method overlap with the results of traditional measurement method when temperature is below 100 K, and are lower than the results of traditional method above 100 K due to the contribution of radiation conductance. As temperature increases, the difference between two methods also increases, indicating that the contribution of radiation to the measurement error will be significant at high temperature, especially for samples with a low thermal conductance. Since we will characterize thermal properties of boron carbide nanowires from 10 K to 800 K in this project, we will adopt cancelling bridge method for thermal conductivity measurements.

In order to study the temperature dependence of radiation conductance, we also measured a bare device with no nanoribbon bridging two membranes by using the degraded cancelling bridge method (no cancelling mode) and the result is shown in Figure 5. We also calculated radiation conductance by subtracting thermal conductance results of sample 2 measured with no cancelling and cancelling modes and the result is also given in Figure 5. As seen in Figure 5, two results agree well with each other, further confirming that our cancelling bridge setup works properly. The radiation conductance approximately changes with temperature as a function of T^2.

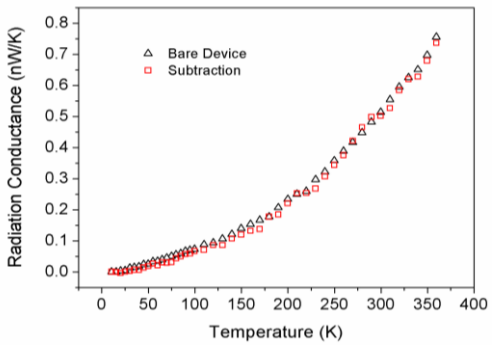

Figure 5 Radiation conductance obtained by measuring a bare device with degraded cancelling bridge method (open triangle) and by subtracting thermal conductance results of sample 2 measured with no cancelling and cancelling modes (open squares).

In the second year, we will mainly focus on high temperature measurement (up to 800 K), which has not been achieved for one-dimensional nanostructures yet. In addition, boron carbide nanowire will be extensively measured over a wide temperature range.

4. PUBLICATION AND AWARDS

To date, we have submitted two conference abstracts based on the research outcomes from this project:

Conference Presentations

1. J. Yang, X. Wang, Y. Yang, Y. Chen, Z. Ni, T. Xu, D. Li, and D. Xu, "Intrinsic Thermal Conductivity Characterization of 20-nm-thick Boron Nanoribbons at Low Temperature," *ASME 2013 4th Micro/Nanoscale Heat & Mass Transfer International Conference*, Hong Kong, China, December 2013. (Abstract accepted)
2. J. Yang, X. Wang, Y. Yang, Y. Chen, Z. Ni, T. Xu, D. Li, and D. Xu, "Thermal Conductivity Characterization of Individual Boron Nanoribbons at High Temperature," *2013 ASME International Mechanical Engineering Congress and Exposition*, San Diego, CA, USA, November 2013. (Abstract accepted)

Ternary Hybrid Polymer/Nanocrystal Bulk Heterojunction Solar Cells with Cascade Energy-Level Alignment

Principal Investigator: Professor Ni ZHAO
Department of Electronic Engineering, CUHK

Research Team Members:
Feng WANG (postdoc)[(1)], Haihua XU (research associate)[(1)], Ting XIAO (PhD student)[(1)], Mengyu CHEN (PhD student)[(1)]

(1) Dept. of Electronic Engineering, CUHK
(2) Institute of Functional Nano & Soft Materials, Soochow University

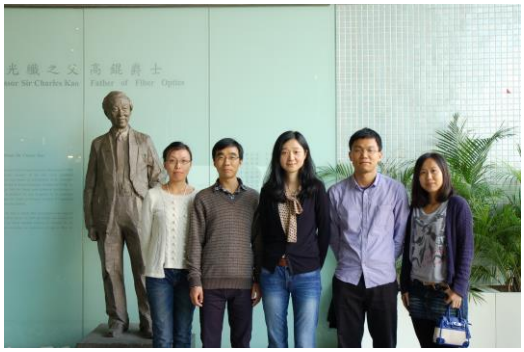

Progress Reporting Period: 1 July 2012 – 1 May 2013

ABSTRACT

This proposal aims to develop ternary polymer/nanocrystal bulk heterojunction (BHJ) solar cells with cascade energy-level alignment. Semiconductor nanocrystals and polymers are attractive photoactive materials due to their solution processability, high absorption coefficient and wide spectral tunability. Hybrid solar cells combine the mechanical flexibility of polymers with the morphological stability of nanocrystals and therefore have the potential to offer superior solar cell properties. In this project we propose to create a cascade of energy levels in the photoactive layer of hybrid solar cells by utilizing a ternary BHJ structure. We will develop solution-based methods to fabricate two ternary BHJ structures, polymer/quantum dot/nanorod and polymer/nanoshell/nanorod. Their properties will be investigated via morphological, electrical and spectroscopic characterizations. The technological know-how and the fundamental understanding gained from this project will greatly benefit efforts to realize the next generation of solar cell technology.

1. OBJECTIVES AND SIGNIFICANCE

1. To develop solution-based processes for scalable fabrication of ternary polymer/quantum-dot/ nanorod and polymer/nanoshell/nanorod bulk heterojunction solar cells with cascade energy- level alignment.

2. To establish a versatile testing platform, consisting of spectroscopic, optoelectronic and microscopic characterization methods, with which the optimal condition for producing photovoltaic effects can be identified for various cascade hybrid systems.

3. To demonstrate high-efficiency ternary hybrid polymer/nanocrystal solar cells via a multi-pronged approach consisting of material selection, processing optimization and device design.

The technological know-how and the fundamental understanding gained from this project will greatly benefit efforts to realize the next generation of solar cell technology.

2. RESEARCH METHODOLOGY

Materials: Polymer materials were purchased from Lumtec Corp. ZnO nanorods were prepared according to the method reported in Refs [1, 2]. In brief, potassium hydroxide solution (in methanol) was added drop by drop into zinc acetate solution (in methanol mixed with water)under constant magnetic stirring. The reaction was then held at 60 ^{o}C for several hours until nanorods with desired dimension were produced. Before use, the nanorods were washed with ethanol for three times. The nanoshell/nanorod structures were fabricated via a surface ion-exchange method we developed. The reactions involved are briefly described below:

$$ZnO + S^{2-} \text{ (supplied by controlled amount of } Na_2S) \longrightarrow ZnO/ZnS$$

$$ZnO/ZnS + Bi^{3+} \text{ (supplied by controlled amount of } Bi(NO_3)_3\text{)} \longrightarrow ZnO/Bi_2S_3$$

Importantly, we placed the reaction apparatus in ice-water bath to achieve a slow reaction rate. In this way the shell thickness can be well controlled. The QD/nanorod structure can be made by anchoring as-prepared QDs through molecular linkers on the nanorod surface.

Device fabrication: Solar cells were fabricated on patterned ITO substrates. The BHJ layer was fabricated via spin-coating; other interlayers and top electrodes were deposited via spin-coating and thermal evaporation.

Characterization: The nanoshell/nanorod structures were examined using transmission electron microscopy (TEM). In the next stage, the morphology of the BHJ structures will be studied using atomic force microscopy and TEM. The current-voltage characteristics of the solar cells were measured using an I-V source meter. To achieve a fundamental understanding of the device performance, spectroscopic methods, such as steady-state and time-resolved photoluminescence spectroscopy, charge modulation spectroscopy (CMS) and photoinduced absorption (PIA) spectroscopy, will be used to probe the charge- and energy-transfer processes in the cascade structure. Transient photovoltage and photocurrent measurement will be used to probe the charge carrier lifetime in the hybrid solar cells.

3. RESULTS ACHIEVED SO FAR

(1) Achievements towards Objective 1: Material preparation (ZnO, ZnO/Bi_2S_3 and Bi_2S_3 nanocrystals)

We have synthesized ZnO nanorods with controllable aspect ratio. The relatively uniform size distribution of the nanorods was confirmed by TEM, as shown in Figure 1a. Furthermore, we have developed a two-step ion-exchange process to grow ZnO/Bi_2S_3 and ZnO/PbS core-shell nanorods. This reaction process is simple and well controlled; furthermore, the whole process is held in aqueous based solution, thus minimizing the use of toxic solvents.

During synthesis of ZnO/Bi_2S_3 core-shell nanorods we discovered that by introducing excess amount of Bi^{3+} and S^{2-} ions we can completely transfer ZnO nanorods to Bi_2S_3 nanoparticles (as confirmed by the Energy-dispersive X-ray (EDX) spectrum shown in Figure 1b). This new synthesis process via sequential cation and anion exchange reaction offers a very simple way of producing colloidal nanoparticles without ligands. TEM images show that Bi_2S_3 nanoparticles have a diameter of around 5 nm and can self-assemble to form nanowires (Figure 1c), which may serve as the charge transport pathways in the hybrid solar cell structures.

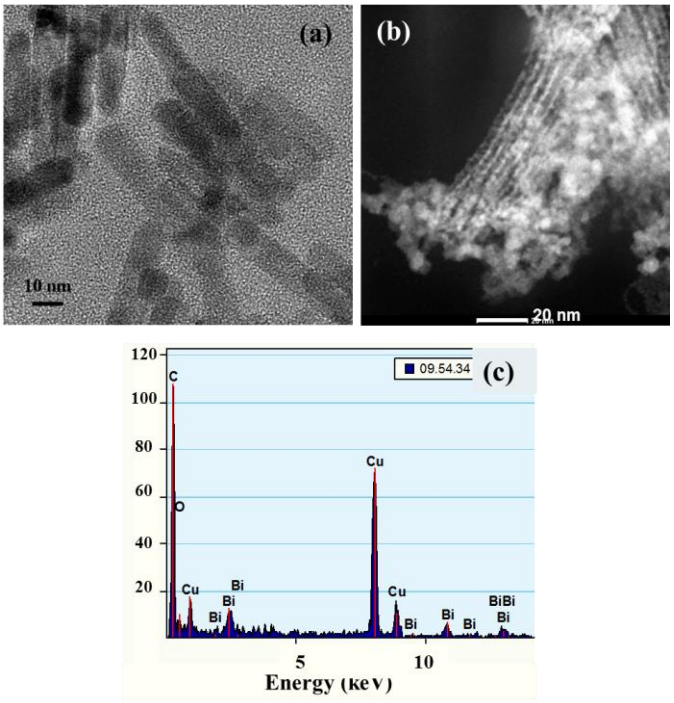

Figure 1 (a) TEM images of ZnO nanorods. (b) TEM image of assembled Bi_2S_3 nanoparticles. (c) EDX spectrum taken at region (b) confirms the complete transfer of ZnO to Bi_2S_3. The Cu and C signal comes from the TEM grids.

(2) Achievements towards Objective 2: Construction of the spectroscopic characterization platform.

We have set up the CMS and PIA spectroscopy to study the charge separation and transport processes in the ternary BHJ system. To test our setup, we first characterized the properties of charge carriers in a pure donor-acceptor polymer system. Based on the spectroscopic data we were able to identify the correlation between charge localization and molecular configuration (Figure 2a). The results, which have recently been published on *Journal of Physical*

Chemistry C [3], provide the fundamental knowledge that is required to understand the more complicated polymer/nanocrystal hybrid systems.

Photoluminescence spectroscopy was used to investigate the impact of the shell passivation on the optical properties of ZnO nanorods. It is shown that the defect emission of ZnO at ~530 nm is greatly decreased after the growth of Bi_2S_3 nanoshell (Figure 2b), suggesting that we have successfully passivated the surface defect states on ZnO nanorods by Bi_2S_3. This is an important step towards reducing the charge recombination loss in the BHJ solar cells. We also note that the intrinsic emission of ZnO at ~440 nm is reduced after shell growth, due to the photogenerated holes partially transferred from ZnO to Bi_2S_3. The charge transfer properties between a donor polymer, P3HT, and the ZnO nanorods are also investigated by photoluminescence spectroscopy. As shown in Figure 2c, the fluorescence intensity of P3HT drops 34% after mixing with ZnO and 70% after mixing with ZnO/Bi_2S_3. This result proves that our proposed cascade energy level alignment (P3HT/Bi_2S_3/ZnO) indeed benefits the charge separation between P3HT and ZnO. Since the photogenerated electrons are funneled from P3HT to ZnO via Bi_2S_3, the chance of charge recombination is greatly reduced. This has been confirmed by the low charge recombination rated constant measured via

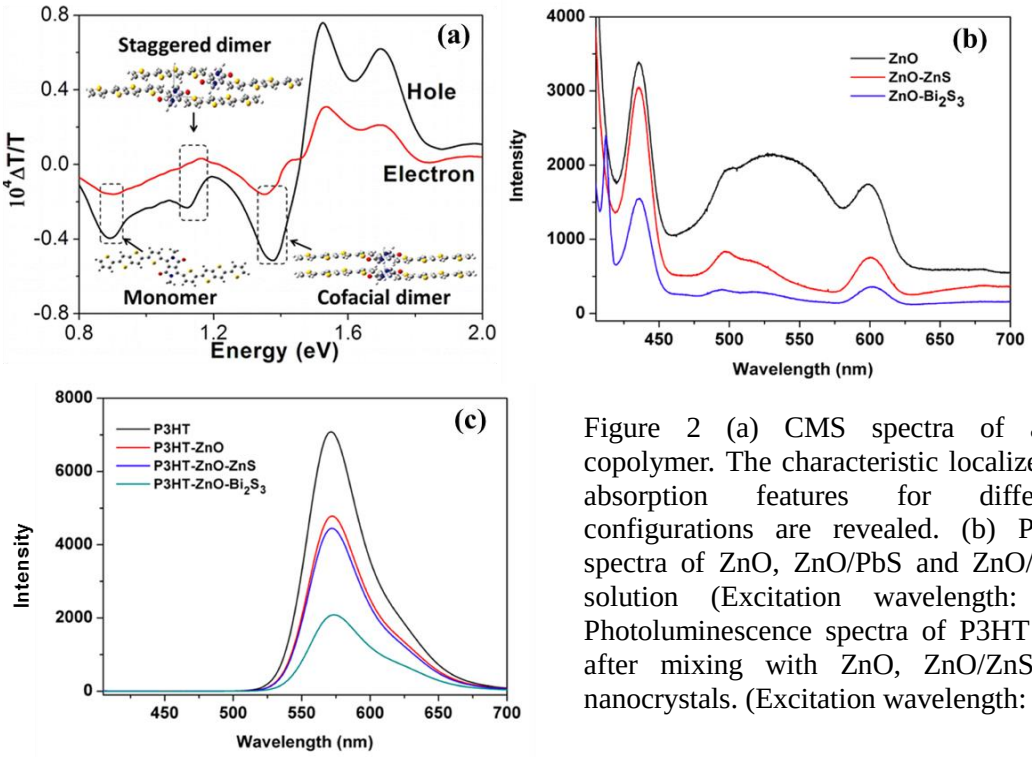

Figure 2 (a) CMS spectra of a donor-acceptor copolymer. The characteristic localized charge-induced absorption features for different molecular configurations are revealed. (b) Photoluminescence spectra of ZnO, ZnO/PbS and ZnO/Bi_2S_3 nanocrystal solution (Excitation wavelength: 380 nm). (c) Photoluminescence spectra of P3HT films before and after mixing with ZnO, ZnO/ZnS and ZnO/Bi_2S_3 nanocrystals. (Excitation wavelength: 380 nm).

transient photovoltage measurement (Data not shown here).

(3) Achievements towards Objective 3: Fabrication and characterization of hybrid solar cells

We have fabricated solar cell devices to evaluate the performance of the material systems we developed. The structure of the devices and the corresponding energy level alignment are shown in Figure 3a and 3b. Our initial testing results (Table 1) show that the open-circuit voltage (V_{oc}) of the ternary P3HT/Bi_2S_3/ZnO solar cells is up to 0.6 V, significantly higher than 0.47 V for the binary P3HT/ZnO solar cells. The short-circuit current density (J_{sc}) and fill factor (*FF*) are still low, mainly due to the low loading ratio of the nanorods. This problem will be solved in the next stage when optimization of the fabrication process is carried out. Also, the morphological and electronic properties of the binary and ternary systems will be studied and correlated with the device parameters.

We also implemented a Bi_2S_3 nanocrystal/P3HT BHJ into the testing solar cell structure. Our preliminary results show that the cells (Figure 3c) exhibit a high short-circuit current density (J_{sc}) up to 2.2 mA/cm^2. This value is about 7 times higher than those reported for the same material system [4, 5]; Moreover, we expect further improvement in the device performance through optimization of the fabrication parameters. The

origin of the high photogenerated current could be related to the ligand-free process during the synthesis of Bi_2S_3 nanocrystals. To confirm this hypothesis, we will perform PIA spectroscopy on the Bi_2S_3 nanocrystal/P3HT blend system. In summary, our device characterization results suggest that Bi_2S_3 could act as an n-type semiconductor with suitable electronic properties for hybrid BHJ solar cells. Using ion-exchange method we can control the loading ratio of Bi_2S_3 in the BHJs. The follow-up work will be focused on the optimization of solar cell performance, as well as understanding of the charge separation and transport processes in the solar cell systems.

Table 1 Device parameters of hybrid P3HT/nanorod solar cells (Tested using an 18 mW/cm^2 white light source)

Material combination	Jsc (mA/cm^2)	Voc (V)	FF
P3HT/ZnO	0.54	0.39	0.34
P3HT/filtered ZnO	3.6*10^{-4}	0.47	0.28
P3HT/Bi_2S_3/ZnO (3% Bi_2S_3)	0.06	0.6	0.23
P3HT/Bi_2S_3/ZnO (3% Bi_2S_3, filtered)	0.05	0.55	0.31

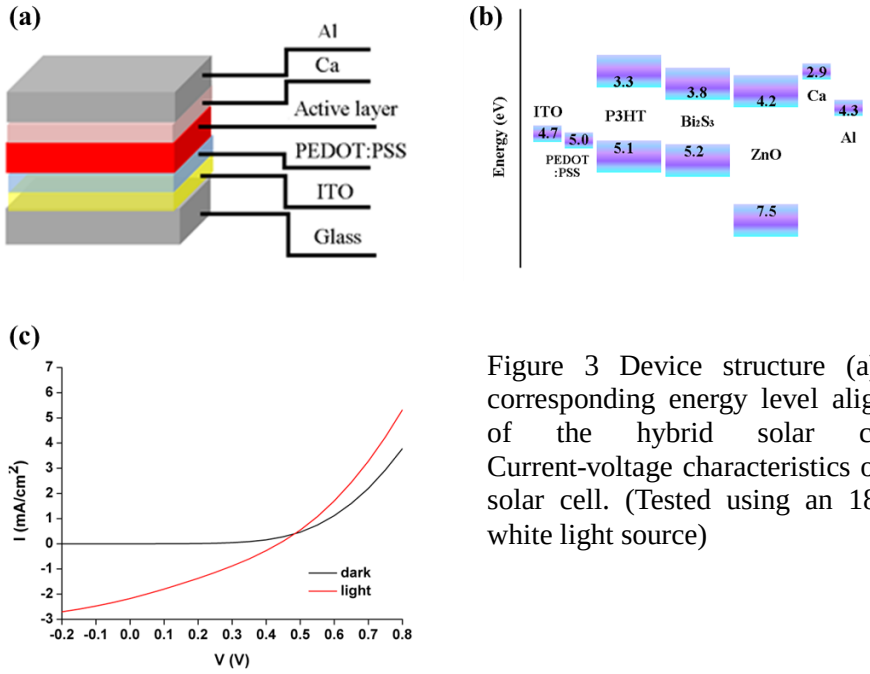

Figure 3 Device structure (a) and the corresponding energy level alignment (b) of the hybrid solar cells. (c) Current-voltage characteristics of a typical solar cell. (Tested using an 18 mW/cm^2 white light source)

References

[1] C. Pacholski, A. Kornowski, H. Weller, *Angew. Chem., Int. Ed.* **2002**, 41, 1188-1191.

[2] B.Q. Sun, H. Sirringhaus, *Nano Lett*. **2005**, 5, 2408-2413.

[3] H.H. Xu, Y.Q. Jiang, J. Li, B.S. Ong, Z.G. Shuai, J.B. Xu, N. Zhao, "Spectroscopic Study of Electron and Hole Polarons in a High-Mobility Donor - Acceptor Conjugated Copolymer", *Journal of Physical Chemistry C*, **2013**, 117, 6835−6841

[4] Y.Q. Li, Y.Z. Zhang, Y. Lei, P.J. Li, H.M. Jian, H.W. Hou, Z. Zheng, *Mater. Sci. Eng. B*, **2012**, 177, 1764-1768.

[5] H.C. Liao, M.C.Wu, M.H. Jao, C.M. Chuang, Y.F. Chen, W.F. Su, *CrystEngComm*, **2012**, 14,3645-3652.

4. PUBLICATION AND AWARDS

[1] H.H. Xu, Y.Q. Jiang, J. Li, B.S. Ong, Z.G. Shuai, J.B. Xu, N. Zhao, "Spectroscopic Study of Electron and Hole Polarons in a High-Mobility Donor - Acceptor Conjugated Copolymer", *Journal of Physical Chemistry C*, **2013**, 117, 6835−6841

Biomedical Engineering Track

Research Reports
In Biomedical Engineering

Newly Funded Projects	
(2014-2016)	* Development of High-speed Laser Scanning Microscope for In Vivo Deep Brain Imaging
	* Mechanism for the transcytosis of targeted nanoparticles across the blood-brain barrier
Continuing Projects	
(2013-2015)	* Development of the Next Generation Neurosurgical Assistant System Based on Functional Brain Mapping
	* Biomimetic scaffold for stem cell based cartilage regeneration and drug delivery
(2012-2014)	* Dielectrophoresis Nano-separator for Precision Manufacturing of Polymeric Nanoparticles for Tumor-Targeted Drug Delivery
Completed Projects	
(2011)	* Viewing Biomolecules at the Right Site by Plasmonic Tweezers and Surface Enhanced Raman Scattering

The following reports are enclosed in "Research Highlights" printed in 2013

Completed Projects	
(2010)	* An inexpensive functional finger prosthesis with rebounded type progressive hinge lock
	* Diffusion Tensor MRI Predictors of Cognitive Impairment in Confluent White Matter Lesion
	* Lanthanide-impregnated molecularly imprinted polymer microspheres as antibody mimics on an optofluidic platform for the detection of disease biomarkers
(2009)	* Terahertz probe for in vivo imaging
	* Signal Processing Strategies on Cochlear Implant Devices for Effective Speech Perception of Tonal Languages
	* Development of A Robotic Endoscope Holder for Nasal Surgery

The following reports are enclosed in "General Report and Research Highlights 2009-2011" printed in October 2011.

Completed Projects	
(2008)	* Development of highly sensitive and large throughput surface enhanced Raman scattering (SERS) substrates for molecular diagnosis
	* Research on Language and Brain Waves
	* Development of an Efficient Locomotion Mechanism for Wireless Active Capsule Endoscope
(2007)	* Bio-electromagnetic Modeling and Experiment Setup for Medical Electronics RF Safety Assessment
	* Medical Applications of Terahertz Imaging
	* Hybrid Assistive Knee Braces with Smart Actuators
(2006)	* RF Radiation Effect and Efficiency of Wireless Medical Devices on Human Body
	* Photonic biosensor micro-arrays for screening of common cancers

The following reports are enclosed in "Research Highlights 2005-2007" printed in January 2008.

Completed Projects	
(2005)	* Cochlear Implants
	* Virtual Anatomy and Dexterous Simulators for Minimal Access Cardiothoracic and Neuro-endoscopic Surgeries * Systematic Synthesis of Nano-informatics Chips by Nano-Robotics Manipulation

Development of High-speed Laser Scanning Microscope for In Vivo Deep Brain Imaging

PI: Professor Shih-Chi CHEN
Department of Mechanical and Automation Engineering, CUHK

Project start date: 1 July 2014

ABSTRACT

This proposal aims to develop new imaging techniques, including tunable frame rate (30 - 17,280 fps) and omnidirectional imaging, for a custom-designed laser scanning confocal and two-photon excitation (TPE) microscope. The new functions will be used for in vivo deep brain imaging on mice.

Current microscopes typically run at a fixed frame rate with a flat imaging plane. However, all biological subjects are "3-dimensional (3-D)" in nature and various biological events, e.g. blood flow or neuron signaling, occur at different time scales. Accordingly, a versatile microscope with capabilities of frame-rate tuning and a 3-D programmable imaging plane is highly desirable. The frame-rate tuning function can be achieved by a new synchronization circuit and related software development. It is worth to note that ultra-high frame rates, i.e. 1000 - 10,000 fps, are achieved by trading off the imaging area, and thus at any frame rate, the "pixel dwell time" of the system remains constant, keeping a low signal-to-noise ratio. 3-D programmable imaging plane is achieved by the introduction of a high-speed piezoelectric objective scanner. During the in-plane raster scan procedure, the objective lens can be moved to any arbitrary position in the Z axis, thus enabling the "omnidirectional scan".

These new functions will be used to investigate deep regions in brain in vivo and enable many new studies that cannot be realized in the past. Specifically, we will follow neuron axons (not in the same plane) in a mouse brain and identify their related neural circuits and simultaneously observe their signaling processes at 1000 fps. We will perform deep brain calcium imaging of visual and motor cortical columns (~800μm deep) and record from multiple hypercolumns in a single scan. Lastly, we will study and image dendritic spines and track the formation and disappearance of individual spines. These results will generate significant impact by elucidating the learning processes involved in visuomotor tasks.

PROJECT OBJECTIVES:

1. Development of the following new functionalities for the confocal and two-photon microscope:
   (a) Tunable frame rate between 30 – 17, 280 frames per second with a constant pixel dwell time.
   (b) A 3-D programmable imaging plane (both flat and curved) that can follow different biological structures in space in vivo, e.g. blood vessels/neurons, and work with different

frame rates.
(c) The microscope can be operated in both fluorescence and reflectance modes and in both upright and inverted configurations.
(d) A microscope system suitable for deep brain high-speed imaging, i.e. 0.8-1.2mm (depth).
(e) The microscope should achieve 0.2/0.6 μm lateral/axial resolution.

2. For in vivo deep brain imaging on mice, we like to achieve the following:
(a) Develop an adaptive algorithm to identify neurons and related neural circuits based on calcium imaging.
(b) Perform deep brain calcium imaging of visual and motor cortical columns to depths of 0.8mm, and record from hypercolumns, 0.5mm across, in a single scan.
(c) Image dendritic spines and track the formation and disappearance of individual spines, as well as overall spine density, as a measure of the plastic changes in neural connectivity.
(d) Correlate the circuit activity and dendritic spine morphological changes to elucidate the learning processes involved in visuomotor tasks.

LONG TERM IMPACT

Most breakthroughs in biology and medicine are driven by the advancement of new diagnostic tools and novel instrumentations. The successful completion of this work will enable scientists to image, discover, and study new biological phenomena that have never been seen before (therefore high impact publications in Nature are expected.); for example, to image and follow neuron axons (not in the same plane) in a mouse brain in vivo and observe their signaling processes at ultra-high frame rate, e.g. 1000 fps, or to image cancer cell trafficking in vivo. We envision our microscope system will be a popular and enabling tool at CUHK, serving university researchers to perform various cutting-edge biological and medical research projects.

For the proposed brain imaging experiments, visuomotor coordination is a central component of human interaction with the environment. It enables an individual to manipulate objects, defend against physical threat and is vital for survival. However, to date little is known about them due to limited instrumentation performance. Our new microscope system enables an unprecedented ability to identify and record neurons/circuits of interest over an arbitrary path/plane and large effective volume, at high temporal and spatial resolution. Elucidation of such circuits and the corresponding neural computation may reveal strategies for visuomotor training, as well as rehabilitation or compensatory therapies in disorders such as brain trauma or visuomotor ataxia. Successful demonstration of this system will have a wider impact in neuroscience research, in which many other higher mammalian functions mediated by other areas of the neocortex can be investigated beyond existing capabilities.

Mechanism for the Transcytosis of Targeted Nanoparticles across the Blood-brain Barrier

PI: Professor CHOI Chung Hang, Jonathan
Department of Electronic Engineering and
Division of Biomedical Engineering, CUHK

Project start date: 1 September 2014

ABSTRACT

In vivo delivery of therapeutics to the brain represents a significant challenge. Unlike small molecules such as nutrients or metabolic wastes, nanoparticles cannot easily penetrate through the blood-brain barrier (BBB), a layer of tightly packed endothelial cells that separates the brain from circulating blood, and accumulate in the brain in clinically relevant amounts. One non-invasive approach to directing intravenously administered nanoparticles across the BBB involves the attachment of ligands on the surface of nanoparticles for engaging receptors on the surface of brain endothelial cells. Such targeted nanoparticles are believed to enter, traverse, and exit the BBB by a process called "receptor-mediated transcytosis". Unfortunately, transcytosis suffers from very limited delivery, typically amounting to less than 1% injected dose per gram of brain tissue (%ID/g). To shed light on this delivery bottleneck, in this proposal, we seek to examine the fundamental interactions between targeted nanoparticles and the BBB *in vivo* at both cellular and subcellular levels. Specifically, we will utilize an array of imaging techniques to elucidate how targeted nanoparticles with different ligand types (e.g., transferrin, DNA oligonucleotides) cross the BBB. Results from the proposed research will guide the design of more effective nanoparticle-based agents to non-invasively treat and image diseases arisen from the central nervous system, such as cancer, stroke, and other neurodegenerative or psychiatric diseases.

PROJECT OBJECTIVES:

A. By applying targeted nanoparticles toa non-contact blood-brain barrier (BBB) model, examine the mechanism fortheir transcytosis across brain endothelial cells *in vitro*. Determine how the choice of targeting ligands dictates a nanoparticle's route of transcytosis, including the intracellular compartments and specific proteins within brain endothelial cells.

B. Using mice that received intravenous injections of targeted nanoparticles, probethe mechanism fortheir transcytosis across brain endothelial cells*in vivo*. Deduce if mechanistic details observed *in vitro*can be translated to animals. For nanoparticles that can traverse across the BBB, identify their distribution inside the brain at the tissue and cellular levels.

LONG TERM IMPACT

A. **Intellectual merit:** Usingnanoparticlesto achieve targeted delivery to the brain via an intravenous injection long suffers from limited rates and amounts of delivery. One cause of this delivery bottleneck is that the biological mechanism that governs how nanoparticles cross the BBB remains poorly understood. The proposed research will create underpinning knowledge that benefits the communities of pharmacology, neuroscience, and nanomaterials.

B. **Technological relevance:** Results will yield materials design principles of more potent second-generation nanoparticle-based agents for treating and imaging brain diseases.

Societal impact: Brain disorders,neurodegenerativeor psychiatric, pose huge economicburden to society, including the cost of therapy and decline in labor productivity. Finding more effective and clinically feasible approaches to delivering therapeutic agents to the brain non-invasively represents high-priority research with profound benefits to society.

DEVELOPMENT OF THE NEXT GENERATION NERUOSURGICAL ASSISTANT SYSTEM BASED ON FUNCTIONAL BRAIN MAPPING

Principle Investigator: Professor Defeng WANG [1,4]
Department of Imaging and Interventional Radiology, CUHK

Co-Investigator: Winnie Chiu-wing CHU [1], Kwok Chu WONG [2], Lin SHI [1, 3]
Research Team Members: LIU Kai, PhD Student [1, 4], SUN Xiaofei, MPhil Student [1, 4]

[1] Department of Imaging and Interventional Radiology, CUHK
[2] Department of Neurosurgery, CUHK
[3] Department of Medicine and Therapeutics, CUHK
[4] Department of Biomedical Engineering and Shun Hing Institute of Advanced Engineering, CUHK

Progress Reporting Period: 1 July 2013 – 30 April 2014

ABSTRACT

Functional magnetic resonance imaging (fMRI) has become a promising approach to accurate function mapping for neurosurgery plan. However, children and patients suffering from developmental brain disorders have difficulties in performing high demand tasks but an alternative approach of resting state fMRI (rsfMRI) without any task required. Several research efforts were dedicated to develop assistant systems based on rsfMRI, which however, still cannot achieve the clinically acceptable efficiency and reliability. Besides, existed methods are developed for adults, which are not suitable for children with the changes of functional connectivity across the developmental age. Our objective is to develop a new generation neurosurgical assistant system based on functional brain mapping. We will propose an efficient and robust approach to determine the correlated functional regions with the advanced sparse representation model. Functional network templates will be constructed for several functions in multiple age stages. The functional mapping result will be integrated to build an efficient navigation system with the electromagnetic tracking device for neurosurgery plan. The developed technology will help to provide optimal plan and precise navigation to improve the efficiency and safety of the clinical neurosurgery, which decrease the risk of functional deficits after neurosurgery.

1. OBJECTIVES AND SIGNIFICANCE

- To identify the functional areas before neurosurgical removal of brain lesion to prevent the risk of functional deficits but the current gold standard approach is in a way of invasive cortical mapping. rsfMRI would be an alternative approach to gather functional information of brain areas;
- The purpose of this proposal is to develop a computational system based on functional brain mapping to guide neurosurgical planning and provide a precise navigation in clinical neurosurgery;
- The proposed navigation system would determine the correlated functional regions with the advanced sparse representation model;
- A functional network templates will be constructed for several functions in multiple age stages;
- The system will be able to perform data acquisition and preprocessing procedure for young children. Detailed data sampling parameters and scanning time will be tested to obtain proper data acquisition procedure;
- The functional correlated regions will be determined from the high dimensional rsfMRI
- The navigation system would provide information for better surgical planning and navigation during the surgery.
- The navigation system would increase the accuracy in removing brain lesion and avoid unnecessary removal to retain the maximum brain function as much as possible.

2. RESEARCH METHODOLOGY

The technology to be developed in this project will enable precise localization of functional areas to aid practical uses in clinical neurosurgical planning and surgical navigation. This novel technology includes data acquisition and preprocessing, detection of correlated regions, network templates construction, automatic identification of functional networks, development of navigation system, system validation and testing.

2.1 Data acquisition and preprocessing

The resting state functional magnetic imaging (rsfMRI) will be acquired at the Shanghai Huashan Hospital and the Prince of Wales Hospital. The optimal parameters will be obtained after several tests of scanning. An effective method will be adopted to preprocess the acquired data for subsequent analysis using the SPM8 tool. Considering the fact that head motion during long acquisition time may cause misalignment across the scans at the different time, images alignment is important for subsequent analysis. In order to enable the subsequent voxel-wise data analysis, the aligned images will be registered to a standard template. Besides, due to the low signal-to-noise ratio of the rsfMRI data, image smoothing will be leveraged to remove the random noises. The strategy of data acquisition and preprocessing will be completed in the first 2 months.

2.2 Detection of functional correlated regions

We will introduce an efficient and robust approach for detection of functional correlated regions from the high dimensional rsfMRI dataset by incorporating the prior knowledge of the brain function of young children. Several detection models have been proposed to identify the correlated regions. Commonly used methods are independent component analysis (ICA) method and seed ROI base approach. The ICA method is time consuming and depends on the number of orders. Therefore, the seed ROI model will be utilized as the basic model.

2.3 Network templates construction

We will construct multiple functional network templates to guide the precise selection of functional areas. To enable automatic identification of functional networks, templates of each function should be first constructed. An effective template construction algorithm will be first advanced to generate templates. Since there are changes of functional connectivity of the young children across the developmental ages, multiple templates will be computed at different ages. The default mode, visual, auditory, language and motor will be investigated for young children in six age stages: 0-2, 3-4, 5-6, 7-8, 9-10 and 11-12 years of age. Initial templates will be chosen with the prior knowledge from the neuroscience research.

2.4 Identification of functional networks

An automatic method will be developed to identify the corresponding functional networks from extracted multiple networks. With a given individual subject, templates will be chosen considering the age and type of function. A similarity measurement method will be developed to compute the similarity values between all the components and the templates. The components with the highest similarity values will be chosen as the function network. This algorithm and its implementation will be accomplished within the 12 months.

2.5 Development of navigation system

The developed components will be integrated to build an efficient navigation system. The electromagnetic tracking device will be utilized to measure the real-time position of surgical tools and fiducials attached to the patient's anatomy. The functional mapping results will be coded with different color and then visualized by overlaying on the high-resolution anatomical T1 MRI data. The diffusion tensor images and magnetic resonance angiography will also be integrated to make more precise location. The key modules of location, tracking, and registering processing will be implemented using the Image-Guided Surgery Toolkit (IGSTK).All the developed modules will be integrated into the framework of the Medical Imaging Interaction Toolkit (MITK) to establish a system with a high degree of interaction. The software will be compatible with commonly used OS of Windows, Macintosh, and Linux. The system will be validated on 200 subjects, including 100 normal and 100 patients.

3. RESULTS ACHIEVED SO FAR

We have published 5 peer-reviewed journal articles and 2 conference articles. In these publications, we have developed a new technique to enhance MR image quality using feature-preserving denoising method, a new technique to perform DTI segmentation, a brain atlas based on Chinese pediatric population and a fractional anisotropy and mean diffusivity analysis on adolescents.

Magnetic resonance imaging (MRI) is an outstanding medical imaging modality. To improve the signal to noise ratio is always a great challenge due to images suffer from noise pollution during image acquisition and transmission. Our publication presents a new technique to enhance image quality using feature-preserving denoising method. Most existing MRI denoising methods have not simultaneously take the global image prior and local image features into account. The denoising method in this publication is implemented based on an assumption of spatially varying Rician noise map. It takes full advantage of the global MR image prior and local image features. Numerous experiments have been conducted on both synthetic and real MR data sets to compare our model with some state-of-the-art denoising methods. The experimental results have demonstrated the superior performance of our proposed model in terms of quantitative and qualitative image quality evaluations [1]. This technique enhances the image quality and completed the task on section 2.1.

DTI scanning is one of the most reliable scanning to reveal the white matter fiber tracks and spinal cord. Results from previous studies demonstrated that some kind of diseases such as adolescent idiopathic scoliosis (AIS) affects the spinal cord, and the connectivity and morphology of the brain included cerebellum. To further study the physiology, morphology, and connectivity of the fiber track in human brain and spinal cord, we have developed a new technique to improve the performance of DTI segmentation. To overcome the disadvantages of requiring adequate prior knowledge and tuning parameters in other techniques, our new method automatically learns an adaptive distance metric by a graph based semi-supervised learning model [2]. Besides DTI segmentation, we have also developed a new technique on GPU-accelerated image registration based on the FLIRT Algorithm [10].

An accurate and representative brain atlas could help in neurosurgery. We have developed a high quality representative brain atlas based on Chinese pediatric population using Intensity and sulci landmark. It is important on medical image analysis and could also be useful for image guide surgeries. The newly constructed atlas can better represent the size and shape of brains of Chinese pediatric population [3]. We have constructed a probabilistic atlas of default mode network (DMN) from resting-state fMRI [5]. We have also developed a brain template based on Chinese children and adolescent [7] and measured the structural network on Chinese Children with Developmental Dyslexia [9]. These works have partially completed tasks in section 2.2 and 2.3.

From our previous studies, we know that the tonsil level in AIS was more negative than that in normal and the somatosensory evoked potentials (SSEP) was disturbed in AIS at above the vertebral C5-6 level. We postulated that the integrity of the spinal cord would have been affected and could be demonstrated by measuring the mean diffusivity (MD) or fractional anisotropy (FA) using DTI. Our recent publication has verified our hypothesis, which we found significantly decreased FA values and increased MD values at the medulla oblongata and C1–2, C2–3, C3–4, and C4–5 segments in patients with AIS compared with healthy subjects [4]. We have also predicted the occurrence of cerebral hyperperfusion syndrome (CHS) using pre- and post-operative change in cerebral blood flow (CBF) on patients with Moyamoya disease after surgery [6, 11], and have mapped the visual functions of dorsal and ventral Stream [8]. These works have partially completed section 2.4.

For section 2.5, we have started to build a navigation system using non-rigid registration to transform preoperative images into intraoperative space for functional data visualization in Image-Guided neurosurgery [12]. We have submitted our preliminary work and it be continued in the next few months to finalize the navigation system.

4. PUBLICATION AND AWARDS

Peer-reviewed journal articles:

[1] Liu RW, Shi L, Huang W, Xu J, Yu SC, Wang D, Generalized total variation-based MRI Rician denoising model with spatially adaptive regularization parameters. *Magnetic Resonance Imaging*, Elsevier Science Inc, Amsterdam, 2014 Mar 18. pii: S0730-725X(14)00086-1. doi: 10.1016/j.mri.2014.03.004. [Epub ahead of print]

[2] Kong Y, Wang D, Shi L, Hui SC, Chu WC, Adaptive distance metric learning for diffusion tensor image segmentation. *PLOS One*, Public Library of Science, San Francisco. 2014 Mar 20;9(3):e92069. doi: 10.1371/journal.pone.0092069. eCollection 2014.

[3] Luo Y, Shi L, Weng J, He H, Chu WC, Chen F, Wang D, Intensity and sulci landmark combined brain atlas construction for Chinese pediatric population. *Human Brain Mapping*, Wiley-Blackwell, New Jersey. 2014 Jan 17. doi: 10.1002/hbm.22444. [Epub ahead of print]

[4] Kong Y, Shi L, Hui SCN, Wang D, Deng M, Chu WCW, Cheng JCY, Variation in Anisotropy and Diffusivity Along Medulla Oblongata and the Whole Spinal Cord in Adolescent Idiopathic Scoliosis: A Pilot Study Using Diffusion Tensor Imaging, *American Journal of Neuroradiology*, American Society of Neuroradiology, Oak Brook. 2014 Aug; vol. 35 (In press)

[5] Defeng Wang, Youyong Kong, Winnie CW Chu, Cindy WC Tam, Linda CW Lam, Yilong Wang, Georg Northoff, Vincent CT Mok, Yongjun Wang, Lin Shi, Generation of the Probabilistic Template of Default Mode Network Derived from Resting-State fMRI, IEEE Transactions on Biomedical Engineering (accepted)

Conference articles:

[6] Defeng Wang, Ka Ming Fung, Lin Shi, Fengping Zhu, Ying Mao. Evaluation of Surgical Outcome of Moyamoya Disease Patients after Revascularization using Atlas-based Magnetic Resonance Brain Perfusion Analysis. European Congress of Radiology. Mar. 6-10, 2014. Vienna Austria. DOI: 10.1594/ecr2014/C-0192

[7] Wong Kok Cheung, Luo Yishan, Shi Lin, Chen Feiyan and Wang Defeng, "Template Building For Chinese Children And Adolescent And Comparison With Western Standard Template", The Conjoint Congress of 18th Convention of Academia Eurasiana Neurochirurgica (AEN) 11th Asia Pacific Multidisciplinary Meeting for Nervous System Diseases (Brain Symposium), Hong Kong, Mar 5-8, 2014

Submitted articles:

[8] Yan-Jia Deng, Lin Shi , Vincent Mok, Winnie Chu, Defeng Wang, Anil T. Ahuja. Mapping the Visual Functions in Dorsal and Ventral Stream using Activation Likelihood Estimation. (Under review at Human Brain Mapping)

[9] Kai Liu, Lin Shi, Feiyan Chen, Mary MY Waye, Vincent CT Mok, Winnie CW Chu, Defeng Wang. Increased Local Segregation of Brain Structural Network in Chinese Children with Developmental Dyslexia (Under review at Cortex)

[10] Defeng Wang, Ping Liu, Lin Shi, Ang Li, Wen-Hua Huang, Jing Qin, Pheng-Ann Heng, Anil T., Ahuja. GPU-accelerated Image Registration based on the FLIRT Algorithm. (Under review at Journal of Medical Systems)

[11] Defeng Wang, Fengping Zhu, Ka Ming Fung, Wei Zhu, Yishan Luo, Winnie CW Chu, Vincent CT Mok, Jinsong Wu, Lin Shi, Ying Mao. Predicting Cerebral Hyperperfusion Syndrome Following Superficial Temporal Artery to Middle Cerebral Artery Bypass based on Intraoperative Perfusion-Weighted Magnetic Resonance Imaging (Under review at Neurosurgery)

[12] Defeng Wang, Yishan Luo, Junfeng Lu, Winnie CW Chu, George KC Wong, Vincent CT Mok, Lin Shi, Jinsong Wu. Non-rigid Registration of Preoperative Images with Intraoperative Images for functional data visualization in Image-Guided Neurosurgery. (Under review at Human Brain Mapping)

BIOMIMETIC SCAFFOLD FOR STEM CELL BASED CARTILAGE REGENERATION AND DRUG DELIVERY

Principal Investigator: Professor BIAN Liming [(1)]
Department of Mechanical and Automation Engineering, CUHK

Co-Investigator: Arthur MAK [(1)]
Research Team Members:
ZHU Meiling, FENG Qian, WEI Kongchang, LI Jinming [(1)]

[(1)] Dept. of Mechanical and automation Engineering

Progress Reporting Period: 1 July 2013 – 30 April 2014

ABSTRACT

Osteoarthritis (OA) is symptomized as progressive degeneration of articular cartilage in human diathrodial joints. A recent study in Hong Kong found that about 10% of the Hong Kong population aged 50 years and older can be diagnosed with knee osteoarthritis [1]. This showed that osteoarthritis is one of the major causes of disability among the Hong Kong population just as in the rest of the world. Current treatments including arthroplasty and mosaicplasty have various major limitations such as limited life span, lack of donor tissue, etc.

hMSCs (human mesenchymal stem cells) have gained increasing popularity as a cell source for cartilage repair, due to their multipotency and easy availability. However, after firstly differentiating (chondrogenesis) into chondrocytes (cartilage cells) like cells, hMSCs continue to differentiate toward a hypertrophic phenotype, resulting in extensive mineralization of the neocartilage formed, which should be free of mineralization. This problem, which motivates this proposed work, is now being recognized as a major obstacle to the widespread adoption of hMSCs as a clinically viable cell source for cartilage repair.

Glycosaminoglycan (GAG) is a key component of the cartilage extracellular matrix (ECM). Sulfated glycosaminoglycans have been shown to maintain the activity of growth factors. Sulfated glycosaminoglycans also attract cations including calcium ions with their negative charges, thereby changing the calcium concentration in the intercellular tissue environment and potentially influencing tissue mineralization. The project proposes to chemically incorporate the sulfate groups into biomaterial scaffold to emulate the biochemical properties of the native cartilage cellular microenvironment. This will allow us to investigate the role of sulfation in regulating hMSC chondrogenesis and subsequent hypertrophic tissue mineralization.

The results of the project will not only help the development of new stem cell therapies for cartilage repair, but will also guide the design of novel scaffold materials for repairing defects in interfacial regions including ligament/tendon to bone insertions and cartilage to bone interfaces.

1. OBJECTIVES AND SIGNIFICANCE

Objective 1: synthesize crosslinkable sulfated glycosaminoglycan biopolymers for the fabrication of hydrogel scaffold.

Objective 2: investigate the effect of sulfated hydrogel scaffolds made of sulfated glycosaminoglycan on the

retention of chondrogenic growth factors.

Objective 3: examine the effect of sulfated hydrogel scaffolds made of sulfated glycosaminoglycan on chondrogenic differentiation of hMSCs.

Objective 4: examine the effect of sulfated hydrogel scaffolds made of sulfated glycosaminoglycan on hypertrophic differentiation of hMSCs and resulting matrix mineralization.

Impact and novelty
The findings from this study will shed light on the influence of scaffold sulfation on drug delivery from biomaterial scaffold. Furthermore, it will also provide guidance on the design of biomaterial scaffold to better control hMSC differentiation and cartilage mineralization. Moreover, mineralization is found in many other connective tissues including bone, menisci and intervertebral discs either as a required developmental process or as a pathological condition. Therefore, the findings from this study will not only enhance hMSC-based cartilage repair but will also be instrumental in developing stem cell based therapies to regenerate or repair other musculoskeletal tissues including bone, menisci and intervertebral discs.

The novelty of this work lies in three aspects. Firstly, the retention and stability of chondrogenic growth factors in sulfated hydrogels has not been thoroughly investigated before; secondly, few previous studies have examined the effects of sulfation of hyaluronic acid on chondrogenesis. Lastly, no prior studies have studied the effect of hydrogel sulfation on hMSC hypertrophy and matrix mineralization following chondrogenesis.

2. RESEARCH METHODOLOGY

Methacrylation of hyaluronic acid (HA)
Methacrylated hyaluronic acid (molecular weight 70kD) (MeHA) will be synthesized as previously reported [23, 34-36] (**Figure 1**). Briefly, methacrylic anhydride (methacrylic anhydride, Sigma) is added to a solution of 1 wt% HA or CS in deionized water, adjusted to a pH of 8 with NaOH, and left to react on ice for 24 hours. The macromer solution will be purified via dialysis (MW cutoff 6–8kD) against deionized water for a minimum of 48 hours with repeated changes of water. The final product will be obtained by lyophilization and stored at -20 ℃ prior to use. The degree of methacrylation of final macromer products will be evaluated by ^{1}H NMR.

Preparation of MeHA Sulfates (S-MeHA)
Since chondroitin sulfate is a sulfated glycosaminoglycan, no additional sulfation of CS is needed. The sulfation of MeHA (HA is a nonsulfated glycosaminoglycan) will be carried out based on an adapted protocol describe previously. Briefly, MeHA will be dissolved in deionized water to produce 1% w/v solution. The solution will be stirred with 3 gram of Dowex-100 ion exchanger added for each gram of MeHA (tetrabutylammonium-form) for 8 hours. After filtration, the polymer solution will be lyophilized and dissolved in DMF at 1% w/v under N_2. Sulfur trioxide/dimethylformamide complex (SO_3-DMF) dissolved in DMF will be added to the TBA-MeHA solution in DMF (molar polymer/SO_3 ratio 1:20) under N_2 at room temperature. The reaction solution will stirred for 60 min. The sulfated products will be purified by precipitation into acetone and neutralized using ethanolic NaOH solution. The formed S-MeHA will be washed several times with acetone and purified by dialysis against distilled water, followed by lyophilization. The degree of sulfation of the S-MeHA will be determined using an automatic elemental analyzer.

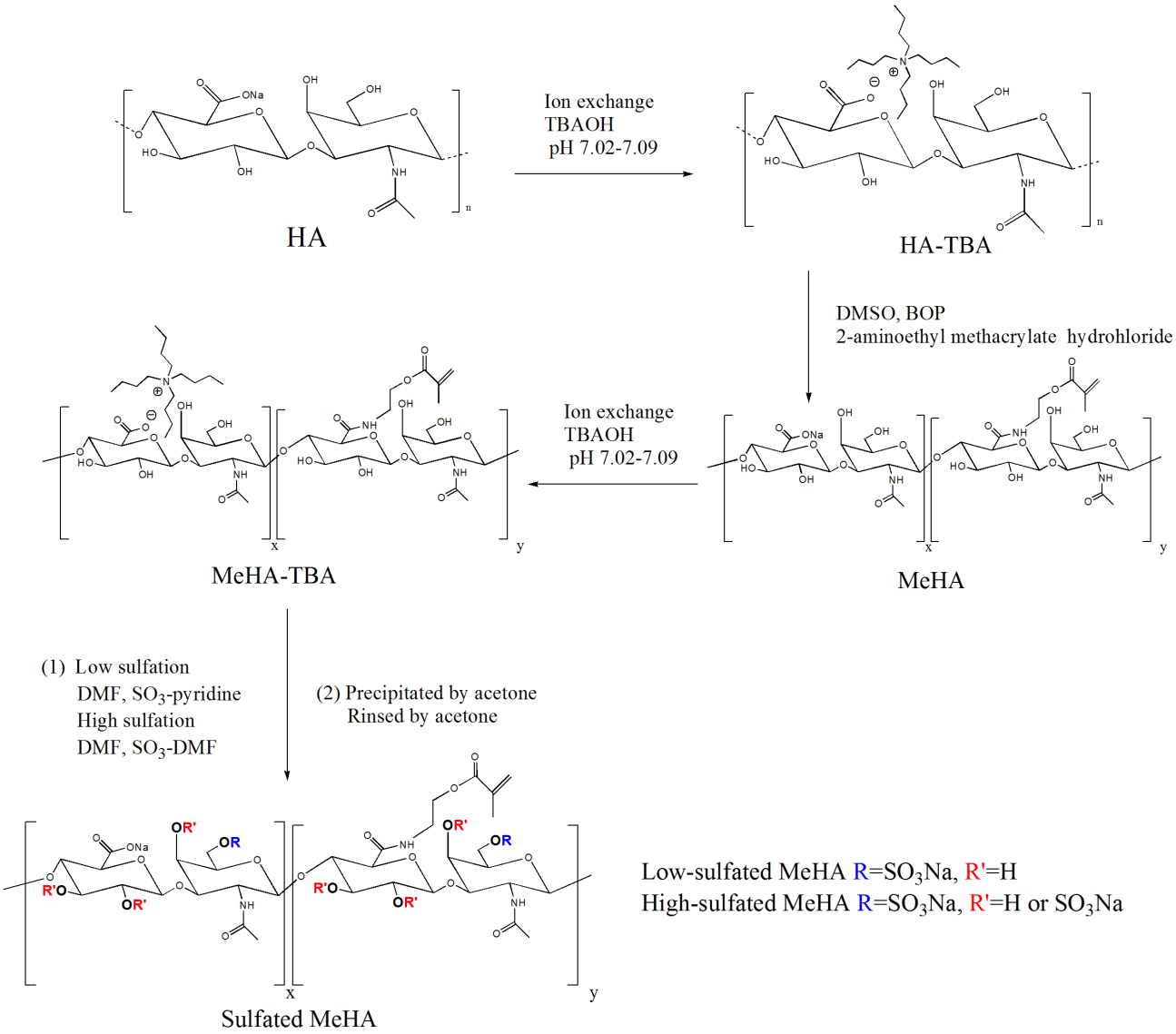

Figure 1. Synthesis of MeHA and S-MeHA

Objective 2

Quantification of the release of encapsulated molecules form hydrogels

Acellular hydrogels will be fabricated by photopolymerization of precursor solutions comprised of MeHA, S-MeHA dissolved in phosphate buffered saline (PBS) containing 0.05 wt% of the photoinitiator I2959 (2-methyl-1-[4-(hydroxyethoxy) phenyl]-2-methyl-1-propanone, Ciba) to allow for UV-mediated polymerization (**Figure 2 A without cells**). The precursor solutions will be exposed to ultra-violet light (UV time: 12 minutes, wavelength: 360nm; intensity: 1.2mW/cm^2) for gelation. Gelation will be assessed by monitoring the storage (G') and loss (G") modulus using a rheometer in a cone and plate geometry. Standard protein molecules used in release studies including bovine serum albumin (BSA, FITC tagged) will be mixed with the precursor solutions and subsequently encapsulated in the hydrogel upon gelation. The hydrogels samples will be incubated in PBS at 37 ° C. The release of the fluorescently tagged BSA will be quantified by a fluorescence microplate reader.

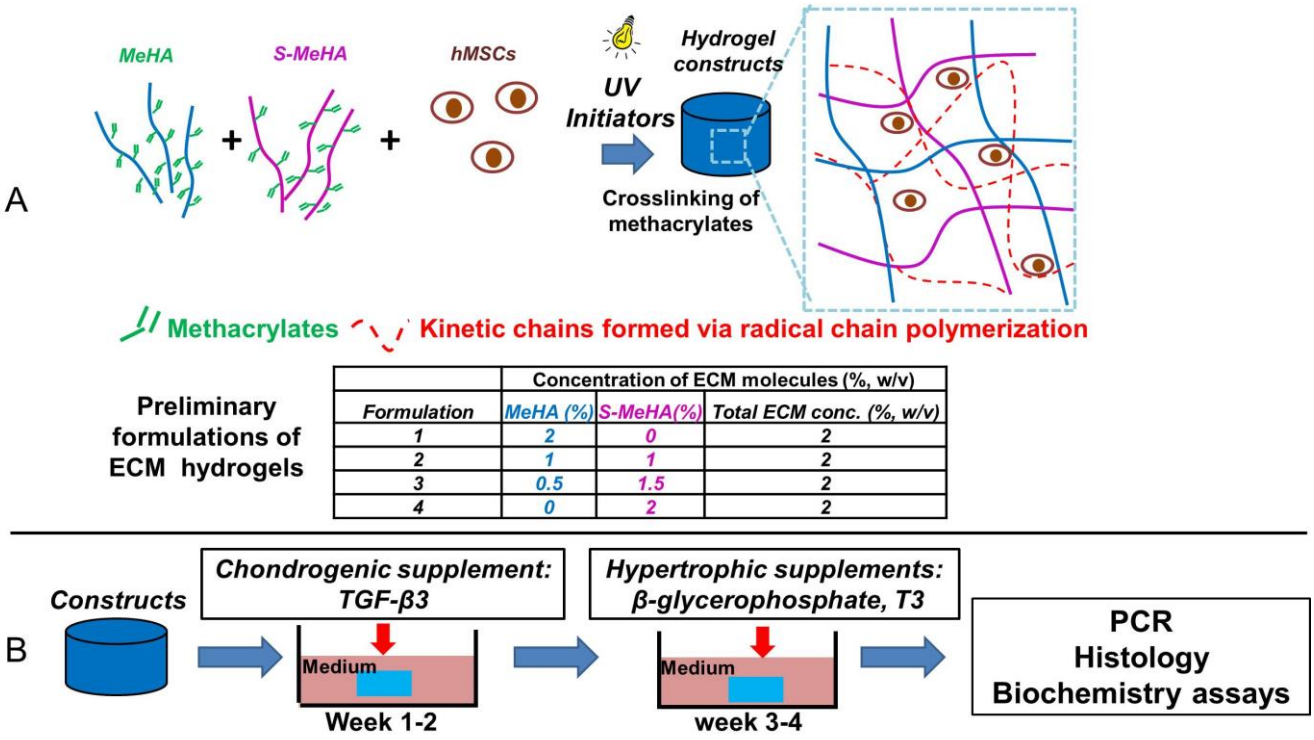

	Concentration of ECM molecules (%, w/v)		
Formulation	MeHA (%)	S-MeHA(%)	Total ECM conc. (%, w/v)
1	2	0	2
2	1	1	2
3	0.5	1.5	2
4	0	2	2

Figure 2. (A) Fabrication of sulfated ECM hydrogels via photocrosslinking. (B) *in vitro* culture of hMSC-seeded hydrogels for chondrogenic and hypertrophic differentiation.

Objective 3 & 4

hMSC encapsulation in hydrogels and chondrogenic and hypertrophic induction

Human MSCs (Lonza) will be expanded to passage 3 in a growth media consisting of α-MEM with 16.7% FBS (fetal bovine serum). MSCs (20 million/ml) will be encapsulated in hydrogel disk constructs as described above (Ø 5mm, 2.6 mm thickness) (**Figure 2 A**). Formed constructs will be cultured in chondrogenic media (DMEM, 1% ITS+Premix, 50 µg/ml L-proline, 0.1 µM dexamethasone, 50µg/ml ascorbate, antibiotics) **supplemented with transforming growth factor (TGF-β3, 10ng/ml)(Figure 2 B)[37]. To evaluate hypertrophy and resulting mineralization by hMSC, a previously established *in vitro* culture model will be employed. Briefly, constructs will be first cultured in chondrogenic media for 2 weeks. Media will be then switched to hypertrophic** induction media (1nM dexamethasone, 1nM triiodothyronine/T3 and 10mM β-glycerophosphate/β-gly) from week 3 through week 4 (**Figure 2 B**)[38] .

Gene expression analysis

Gene expression of chondrogenic (type II collagen, Aggrecan, Sox9) and hypertrophic markers (type X collagen, MMP13, ALP/alkaline phosphatase) at selected time points will be analyzed by real time PCR. Sequences of the primers and probes are listed in a previous publication [31]. The relative gene expression will be calculated using the ΔΔCT method, where the fold difference will be calculated using the expression $2^{\Delta\Delta Ct}$. Each sample will be internally normalized to GAPDH and the expression levels of MSCs at the time of encapsulation.

Biochemical analysis

The PicoGreen assay (Invitrogen) will be used to quantify the DNA content of the constructs. The GAG content will be measured using the dimethylmethylene blue (DMMB) dye-binding assay. The overall collagen content will be assessed by measuring the orthohydroxyproline content via the dimethylaminobenzaldehyde and chloramine T assay. Calcium content will be quantified using a commercial kit (BioVision).

Histological analysis

Constructs will be fixed in 4% formalin, embedded in paraffin, and processed using standard histological

procedures. Immunohistochemical staining will be performed on histological sections (8 µm thick) for targets of interest using the Vectastain ABC kit and the DAB Substrate kit for peroxidase (Vector Labs).

Statistical and power analysis

Statistica (Statsoft) will be used to perform statistical analyses using two-way ANOVA, followed by Tukey's HSD post hoc testing to allow for comparison between groups. Statistical significance will be set at $p < 0.05$. A statistical power analysis indicates that n=8 samples per group should be sufficient for obtaining a study power of 0.85 with significance set at $p<0.05$.

3. RESULTS ACHIEVED SO FAR

Objective 1: we have successfully synthesized sulfated methacrylated hyaluronic acid (HA) with varying degree of sulfation. The synthesis protocols have been established for modifying hyaluronic with both methacrylate groups and sulfate groups sequentially. The synthesis products were evaluated using NMR to confirm and quantify these two modifications on hyaluronic acid. The results show that both methacrylate and sulfate groups were successfully conjugated to hyaluronic acid backbone (Figure 1). For the sulfation, low and high level of sulfation was successfully achieved by controlling the reaction parameters during synthesis (Figure 2).

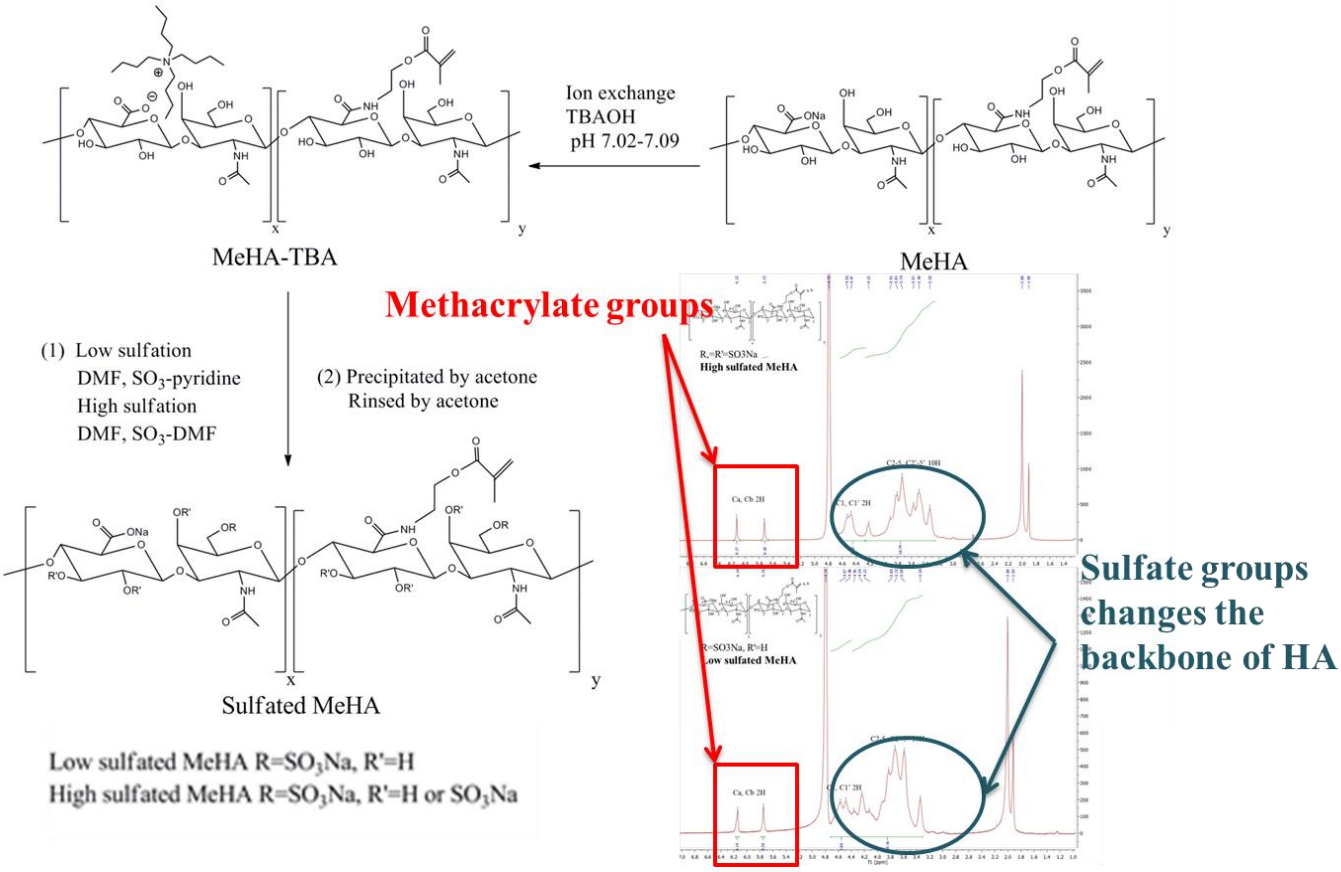

Figure 1. NMR results of the methacrylated HA (MeHA), low-sulfated and high-sulfated MeHA, indicate successful conjugation of methacrylate and sulfate groups to the HA backbone.

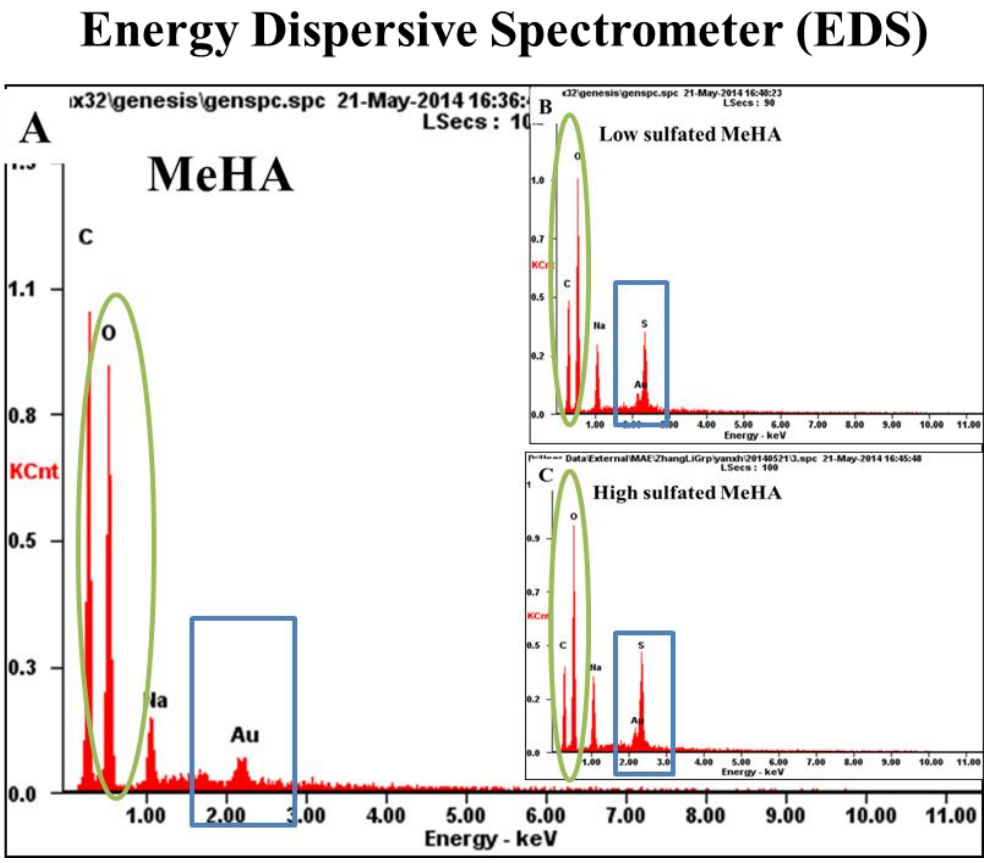

Figure 2. EDS results of the methacrylated HA (MeHA), low-sulfated and high-sulfated MeHA, confirms successful conjugation of different amount of sulfate groups to the HA backbone.

Objective 2: hydrogels have been fabricated using sulfated methacrylated HA (both low and high sulfation MeHA). This demonstrated that the methacrylate groups conjugated are capable of being crosslinked to form hydrogels. DMMB dye staining of the hydrogels confirmed that the different levels of sulfation on the HA molecules are retained in the hydrogels (Figure 3).

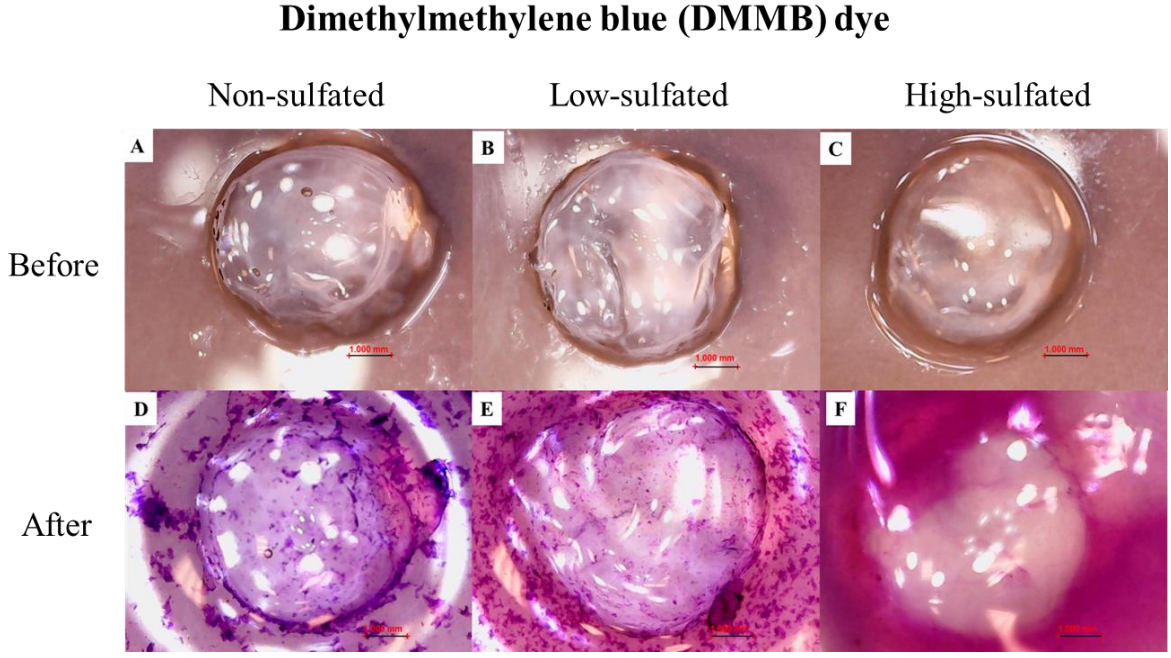

Figure 3. DMMB staining of the fabricated MeHA, low-sulfated and high-sulfated MeHA hydrogels shows more purplish staining in the sulfated hydrogels confirming the presence of sulfate groups.

Objective 3&4: non-sulfated MeHA hydrogels have been evaluated for human mesenchymal stem cells (hMSCs) encapsulation and chondrogenic differentiation. Results show that MeHA hydrogels support chondrogenesis leading to extensive cartilage matrix synthesis by the differentiated stem cells. An in vitro culture model for inducing hypertrophy of the chondrogenically differentiated hMSCs in HA hydrogels has been established (Figure 4). Calcification resulted from stem cell hypertrophy are detected by histology staining. These evaluation and culture protocols will be used to evaluate hMSC differentiation and hypertrophy in the sulfated MeHA hydrogels in the second year.

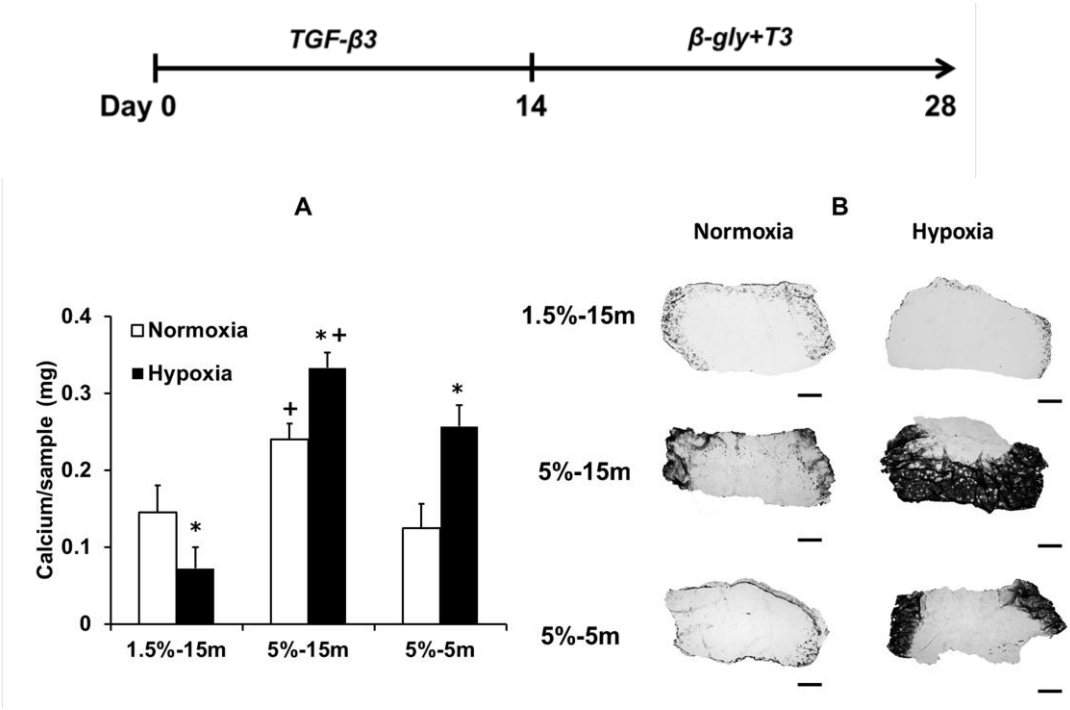

Figure 4. In vitro stem cell hypertrophy protocol has been established and will be used in the next step to investigate the effect of scaffold sulfation on stem cell hypertrophy [1]. Dark staining in the figure shows calcification of the scaffold due to stem cell hypertrophy.

4. PUBLICATION AND AWARDS

(*corresponding author)

[1] Feng, Q.; Zhu, M.; Wei, K.; *Bian, L. Cell-mediated degradation regulates human mesenchymal stem Cell chondrogenesis and hypertrophy in MMP-sensitive hyaluronic acid hydrogels. *PLOS ONE*, accepted for publication, 2014 May *(IF=3.73)*

[2] Zhu, M.; Feng, Q.; *Bian, L. Differential effect of hypoxia on human mesenchymal stem cell chondrogenesis and hypertrophy in hyaluronic acid hydrogels. *Acta Biomaterialia*, 10(3):1333-40. 2014 Mar. *(IF=5.09)*

DIELECTROPHORESIS NANO-SEPARATOR FOR PRECISION MANUFACTURING OF POLYMERIC NANOPARTICLES FOR TUMOR-TARGETED DRUG DELIVERY

Principal Investigator: Professor CHEN Shih-Chi [(1)]
Department of Mechanical and Automation Engineering, CUHK

Co-Investigators:
KUNG Hsiang-Fu [(2)], LIN Marie [(3)], LI Wen Jung[(4)]
Research Team Members:
YANG Shih-Mo [(1)], YAO Hong [(2)], TIAN Yuan [(2)]

[(1)] Dept. of Mechanical and Automation Engineering, CUHK
[(2)] Stanley Ho Centre for Emerging Infectious Diseases, Faculty of Medicine, CUHK
[(3)] Department of Surgery, Prince of Wales Hospital, CUHK
[(4)] Department of Mechanical and Biological Engineering, City University of Hong Kong

Progress Reporting Period: 1 July 2012 – 30 April 2013

ABSTRACT

This research aims to develop a dielectrophoresis (DEP)-based high-throughput nanoparticle separation technology that enables precise separation of polymeric nanoparticles for cancer-targeted drug delivery. Studies suggest that precise control of nanoparticles' sizes and surface charges may (1) further improve the effectiveness of the treatment and (2) reduce the related toxicity level. However, due to the solution-based nanoparticle fabrication procedure, to date there has not been any method reported in literature to precisely control the sizes and surface charges of nanoparticles for cancer-targeted treatment. In this work, we will develop a DEP-based nano-separator that is capable of collecting and separating nanoparticles according to their specific dimensions, e.g. 100nm ± 10nm, and surface charges. PEI-CyD-FA mediated polymeric nanoparticles, a promising new cancer-targeting drug developed by our team, will be used in the DEP device for separation. We will then perform in vivo mouse studies with the separated polymeric nanoparticles in order to investigate and characterize the level of improvements in terms of cancer-targeting sensitivity and toxicity control.

1. OBJECTIVES AND SIGNIFICANCE

The overall goal of the proposed research is the development of four DEP nano-separator devices that can be used to separate and collect polymeric nanoparticles of various sizes. High-throughput nanoparticle separation at the speed of 3 ml/min will be demonstrated via the DEP nano-separators, enabling the precision control of nanoparticles size distribution, ranging from 50 nm to 300 nm. We will perform in vivo studies using an orthotropic hepatocellular carcinoma (HCC) mouse model. Polymeric (H1) nanoparticles will be used to target the somatic tumor in mice. The level of improvements in terms of cancer-targeting sensitivity and toxicity control due to different nanoparticle size distribution will be determined.

Application of the developed DEP-separation technology to nanomedicine and pharmaceutical industry will generate significant impact in the following ways: (1) more precise and specific drug targeting and delivery, (2) reduction in toxicity while improving therapeutic effects, (3) greater control of safety and compatibility, and (4) realization of low cost, high-precision pharmaceutical and medicine manufacturing.

2. RESEARCH METHODOLOGY

1. Model, design and fabricate high-throughput DEP nano-separators optimized for nanoparticle separation.
2. Develop, fabricate and characterize polymer nanoparticle with DEP nano-separator:
   - Prepare the polyplexes of H1/pDNA including H1 synthesis, plasmid expansion and polyplexes formation.
   - DEP separation method: Mix DNA and H1, N(H1) /P(pcDNA)= 20/1 in 2.5% glucose solution, standing for 10 min. Let polyplexes pass through DEP chip under four voltage and frequency conditions for nanoparticle collection. Wash DEP chip without electric field and collect the blocked polyplexes from the outlet.
   - Characterization of the quantity, particle size and zeta potential of both the passed and blocked polyplexes.
   - Determine transfection efficiency of the polyplexes on 293T cells by observing the quantity of EGFP positive result in cells after 24 hours.
3. Perform in vivo mice study to investigate the efficacy of the separated polymeric nanoparticles.
4. Develop new generations of lab-on-a-chip microfluidic devices that integrate various drug fabrication processes into one device and improve overall drug fabrication precision and efficiency.

3. RESULTS ACHIEVED SO FAR

The project has been progressing well and hitting all the milestones. Following, we describe the major results in three sub-sections: **(Section 3.2 – 3.4 contain unpublished results.)**

3.1. Progress on nanomedicine development

We have been optimizing and characterizing the PEI-CyD-FA mediated polymeric nanoparticles for treating tumors. Our recent experiments have proved that coating the adenovirus vector (Adv) with H1 (H1/rAdv) could significantly improve both the efficacy and biosafety of Adv. Enhanced transfection efficiency as well as prolonged duration of gene expression were clearly demonstrated either by intratumoral or systemic injection of a single dose of H1/rAdv in immunocompetent mice. Importantly, repeated injections of H1/rAdv did not reduce the transfection efficiency in immunocompetent mice. Furthermore, H1 transformed the surface charge of the adenovirus capsomers from negative to positive in physiological solution, suggesting that H1 coated the capsid protein of the adenovirus. Figure 1 shows the TEM images of polymeric nanoparticles coated with H1. These promising results were submitted to the Journal of Current Medicinal Chemistry and were accepted for publication in March 2013 [1].

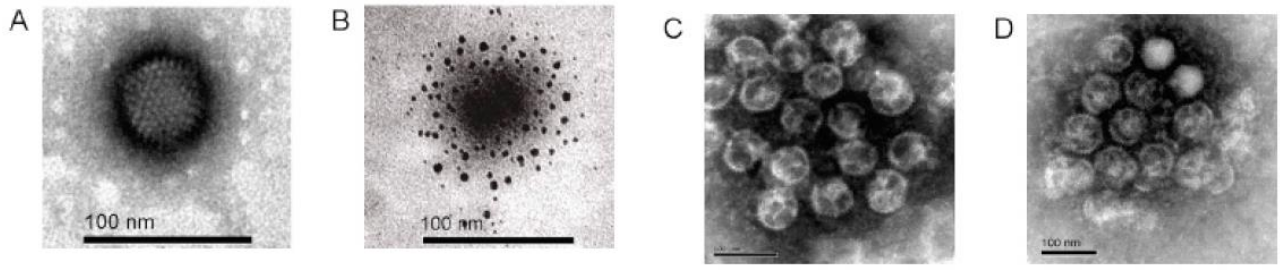

Figure 1: The morphologies of adenovirus and H1/adv particles. Photos were representative photos taken by Transmission Electronic Microscope (TEM). (A) Adenovirus stained by 2% Phosphotungstic Acid (PTA). (B) H1/Adv particles at H1/Adv ratio=4, not stained. (C) Particles at H1/Adv ratio=1. (D) Particles at H1/Adv ratio=2. (C-D) showed aggregation of H1/Adv particles. H1/Adv ratio denotes nmol of amino-group of H1 per 106 rAdv. Standard bar: 100nm.

3.2. Progress on DEP nanoseparator development

We have developed a multi-physics parametric DEP model using COMSO. Important design parameters including flow rate, drag force, flow channel sizes, electrode location, supplied voltage, and frequency were included in this model for device optimization. Figure 2A shows the simulated electric field of the micro-channel which later was used to calculate the DEP force for a given particle size. Based on the parametric model, we designed and fabricated several DEP nano-separators optimized for polymer

nanoparticle (H1/pDNA polyplexes) separation. Figure 2B shows the fabricated DEP electrodes with optimal dimensions; the transparent micro-channels are indicated by the dash-lines, where flows contain nanoparticles come from the right. After passing the electrodes, most particles are trapped by the electrodes, and only particles of desired dimensions are collected.

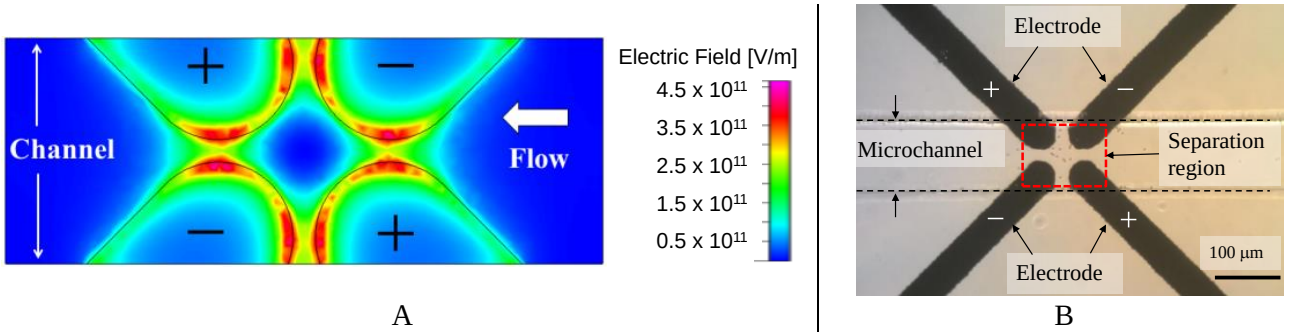

A B

Figure 2: (A) A parametric DEP model developed via COMSOL; (B) Optical image of electrodes and microchannel.

Figure 3A presents the microfabrication processes developed at CUHK for fabricating DEP nanoseparator devices. For steps (a) to (c), the metal electrodes (800 nm titanium) were patterned on a microscope slide by standard photolithography procedure. For steps (d) to (f), PDMS (Sylgard 184, Dow Corning, USA) micro-channels of height of 80µm were defined by using SU-8 negative photoresist. To combine the top and bottom layer of the device, as shown in step (g), surfaces of both the electrode substrate and the PDMS top cover were treated with oxygen plasma; the two parts were subsequently aligned and bonded together. Figure 3B shows an optical image of the completed DEP nanoseparator device.

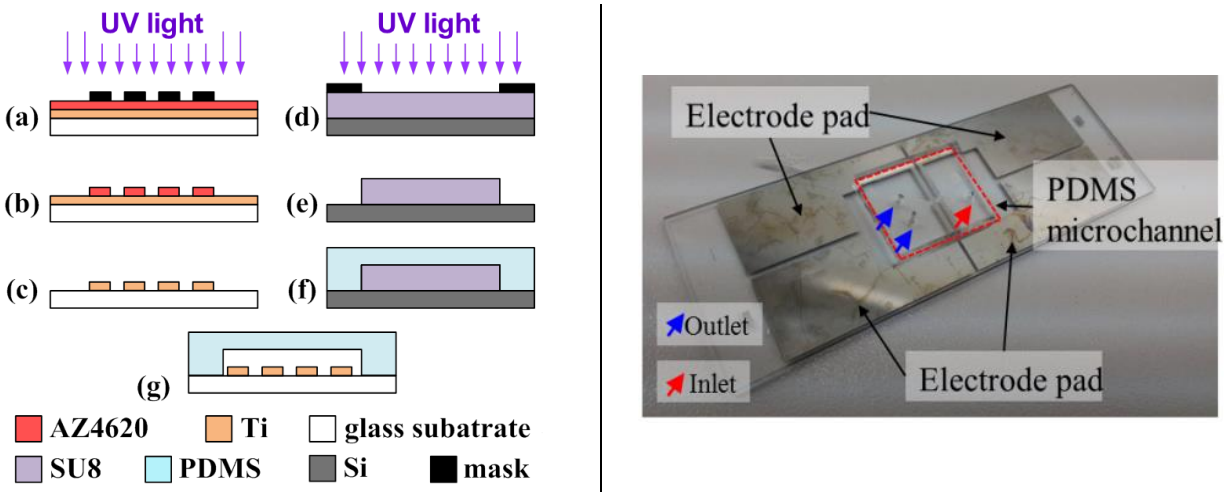

A B

Figure 3: (A) micro-fabrication process of the DEP device; (B) Optical image of the fabricated DEP device.

3.3. Nanoparticle separation experiments

The DEP devices were used to separate H1 coated polymeric nanoparticles (fabricated in Section 3.1). As shown in Fig. 4A, the results of our nanoparticle separation experiments indicate that the size of the separated particles was well controlled with a narrow distribution ($\sigma = 10 \sim 50$ nm); this validates that our physical model is correct and the fabricated DEP devices can effectively block both particles of smaller and larger sizes; this is attributed to the combined effects of the nonuniform electric field distribution on the H1/pDNA polyplexes and its interaction with the nonuniform AC electric field generated by the DEP device. Before the animal experiments, we used the separated polyplexes to treat the cells in vitro in order to verify their effectiveness is not affected by the DEP separation procedure (Transfection dose: 40 µL/well on 293T cells for 24 hours). The results from the cells, shown in Fig 4B, indicate our H1/pDNA polyplexes have better transfection efficiency after passing through the DEP nano-separator. We also expect the separated

polyplexes to have reduced toxicity. This hypothesis will be verified in the coming year when in vivo studies are performed using the orthotropic hepatocellular carcinoma (HCC) mouse model.

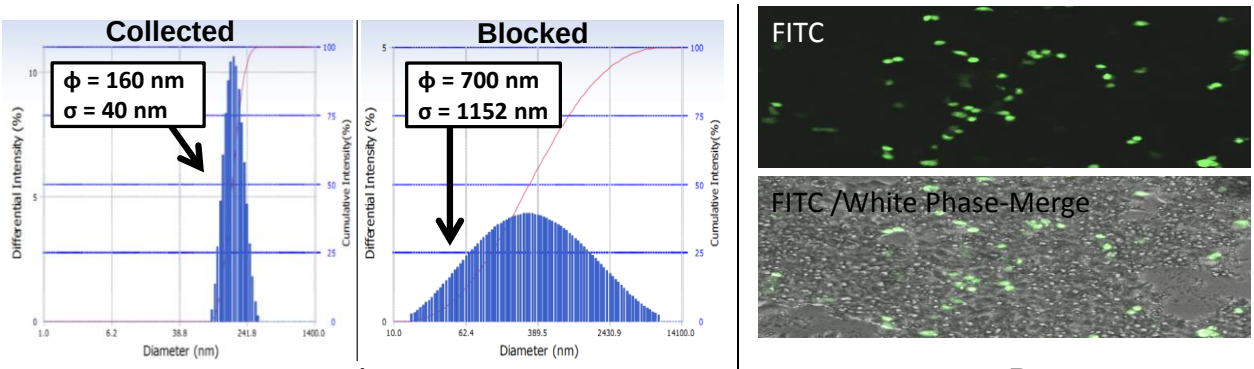

Figure 4: (A) Particle size distribution characterized for both collected and blocked solution; (B) fluorescent image of cells treated with DEP filtered nanoparticle, indicating good transfection efficiency.

3.4. Progress on the development nanomedicine lab-on-a-chip platform

To enhance overall nanomedicine fabrication precision and throughput, we have developed a novel microfluidic device that integrates the nanomedicine preparation process with particle separation procedures. This new device integrates manual operation of DNA and H1 mixing, shaker mixing, particle conjugation, and DEP particle separation into a single device driven by three programmed syringe pumps. The design details and experimental results are shown in Figure 5A and 5B respectively. In Figure 5A, (1) small portions of H1 and DNA are first confined in "droplets", separated by oil; (2-3) the droplets then travel through winding flow channels for mixing and conjugation; (4) the oil and H1/DNA solution are separated in the comb section via surface tension; and (4) lastly passed to the DEP section for particle separation and collection. The images in Figure 5B demonstrate how different sections function. This new device not only greatly simplifies the nanomedicine fabrication process, but also simultaneously improves the precision, quality, and throughput of the drug production.

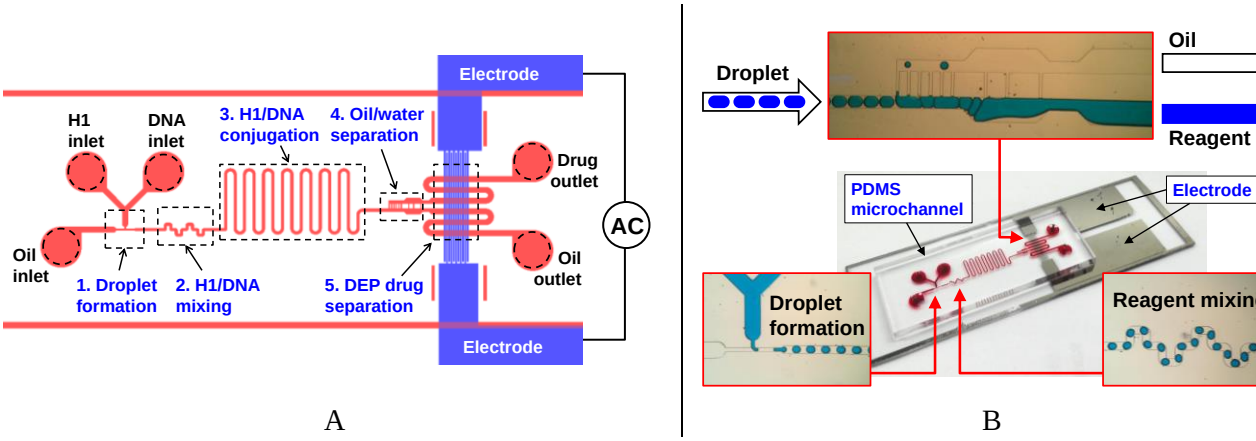

Figure 5: (A) Schematics of the nanomedicine fabrication and separation microfluidic platform; (B) Fabricated microfluidic device and preliminary experimental results.

4. PUBLICATION AND AWARDS

[1] H. Yao, S. Chen, Z. Shen, Y.C. Huang, X. Zhu, X.M. Wang, W. Jiang, Z.F. Wang, X.W. Bian, E.A. Ling, H.F. Kung, M.C. Lin, "Functional Characterization of a PEI-CyD-FA-coated Adenovirus as Delivery Vector for Gene Therapy," *Current Medicinal Chemistry*, March 15, 2013 PMID: 23531212.

VIEWING BIOMOLECULES AT THE RIGHT SITE BY PLASMONIC TWEEZERS AND SURFACE ENHANCED RAMAN SCATTERING

Principal Investigator: Professor Jianbin XU [(1)]
Department of Electronic Engineering, CUHK

Co-Investigators: H.C. ONG [(2)] and Aaron H.P. HO[(1)]
Research Team Members: H.X. ZHANG[(1)]

[(1)] Dept. of Electronic Engineering, [(2)] Dept. of Physics, CUHK

Project Start Date: 1 July 2011
Completion Date: 30 June 2013

ABSTRACT

This project aims at developing high sensitive plasmonic nano-optical tweezers (PNOT) systems for the fields of microfluidics and lab-on-a-chip bio-detection. We have explored new concepts for more efficient and robust multifunctional PNOT. We have analytically investigated the feasibility using two-dimensional metallic arrays of nano-rings or nano-disks for making active PNOT （A-PNOT）. In these structures, multiple trapping locations and very large plasmonic trapping volume are possible by using diffractive coupling resonances. We also have developed approach to maximize the figure-our-merit if nano-hole arrays for surface plasmon resonance sensing. In addition, by incorporating gain medium to these periodic structures, we demonstrate a serious of high quality factor plasmonic resonances with strong electric field strength. Then, we propose by grading the nano-structures, large localized plasmonic field gradient can be created, rendering more efficient PNOT. For example, in the graded nano-disks structure, the optical manipulation of target in nanoscale region is achieved by sequentially switching the wavelength and polarization of the excitation source to enable manipulating-PNOT (M-PNOT), transporting the target molecules in a step-by-step manner to the destination where the sensing is performed. Finally, we also have proposed three multifunctional sensing-PNOT (S-PNOT) platforms for simultaneously performing PNOT and sensing. The first is a coupled plasmonic system based on double-layered metal nano-strip arrays and the second is a hybrid PNOT-microcavity system. In particular, for the second type, nanoparticle (NP) can concurrently acts as a nanoscale sensor and a trap. In fact, we find both the sensing ability and the trapping behavior are improved considerably. For the third platform, we explore low-cost PNOT (L-PNOT) by using gold nano-island substrate for reproducibly trapping and detecting bio-molecules.

1. OBJECTIVES AND SIGNIFICANCE

With surface plasmons, optical trapping and manipulation can go beyond the diffraction limits and down to subwavelength level. In this project, we aim at developing several types of PNOTs. Firstly, we develop gain-assisted or active A-PNOT. Our goal is to efficiently raise the PNOT's active volume and field intensity for trapping the nano-objects within its near field. Secondly, the nano-manipulation issue is very challenging and significant because it not only breaks through the diffraction limit of light, but also realizes a nanoscale controllable domain by using light operation. Up to now, not much has been reported in the literature on NP manipulation using the plasmonic effect. All-optical nano-manipulation of target objects in a predefined pathway still remains very challenging. We expect to propose and realize an M-PNOT for optical manipulations of target really

in nanoscale region. Thirdly, aiming at combining the use of PNOT and surface-enhanced Raman scattering (SERS) or dark-field extinction spectroscopy and demonstrated the possibility for reproducible sensing as S-PNOT. Furthermore, we hope to provide a feasible solution of low-cost PONT, we devoted ourselves to realize the gold nano-island substrate (Au-NIS) that acts as L-PNOT experimentally. All these branches of PNOT provide the advantages of efficiency, fast detection, multifunctional applications, low-cost fabrication and easy for microfluidic lab on a chip integrations.

2. RESEARCH METHODOLOGY

1. Theoretical methods: 2D and 3D finite-difference time-domain (FDTD) modeling are used to achieve the electrodynamics simulations, field patterns, etc. Many initial calculations will be needed to give guidance to the following experiments. Optical force calculation: Maxwell stress tensor (MST) method.
2. Devices fabrication: electron beam lithography, nanoimprint technique, physical vapor deposition (PVD). The superflat gain-doped substrate is realized by doping fluorophore into PMMA, Sol-Gel process and lift-off treatment.
3. Characterization: AFM, SEM, TEM, Hitachi U-3501UV-visible/NIR spectrophotometer. Once all factors have been optimized by analytical method and simulations, molecular species (CV, R6G, DNA, other bio-molecules, etc) that exhibits distinct Raman spectrum will be attached onto Au-NPs for the PNOT trapping and SERS characterizations. Deltanu Examine R modular system and Nikon confocal microscope will be used for measurements.

3. RESULTS ACHIEVED

We list out our achievements as follows:

1. A-PNOT with large active volume and high field:

(i) Until now, PNOTs based on metal dipole antenna, thin film, sharp tip, cavity, holes, and hybrid waveguide have been realized theoretically and/or experimentally. However, to the best of our knowledge, there is no report on optical trapping using metal nano-rings and its two-dimensional arrays. We figured out a design based on nano-rings which provides an effective approach with large active volume for manipulating nano-objects in very low concentration into the high-field region.

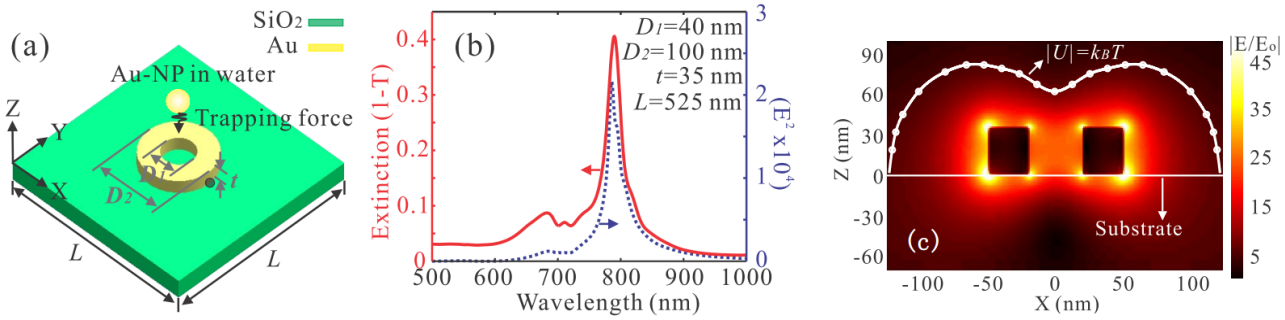

Fig. 1. (a) Schematic of one unit cell of the gold nano-ring arrays. (b) Extinction (solid line) of the nano-ring arrays and the E^2 spectrum (dotted line) of the nano-ring edge as indicated by a black dot in Fig. 1(a). Dimensions of nano-ring: D_1=40 nm, D_2=100 nm, t=35 nm, and L=525 nm. (c) Electric field distribution in the XZ plane and the trapping boundary (white —o—) $|U| = k_B T$. Excitation wavelength and power density are respectively 785 nm and 1 mW/μm^2.

We found that at resonant wavelength of λ=785 nm the nano-ring produces a maximum trapping potential of ~32 $k_B T$ on Au-NPs. The existence of multiple potential wells results in a very large

active volume of ~10^6 nm^3 for trapping the target particles. Figure 1 (a) shows the structure of the proposed gold nano-ring. Figure 1(b) shows typical extinction (solid line) and electric field intensity (E^2, dotted line) spectra at the nano-ring edge as appropriate structural parameters are chosen. Figure 1(c) shows the electric field distribution in the XZ plane, and the calculated trapping boundary (white ─o─). The trapping volume, which takes a symmetric shape for the structure considered, is of the order 10^6 nm^3. This is 10^4 and 10^2 times larger than those of the silver nanoaggregates (~100 nm^3) and dipole antennas (~10^4 nm^3) respectively.

In our calculation, we used Maxwell stress tensor (MST) to calculate the trapping forces experienced by the NP due to enhanced local field. Figure 2 (a) shows the spectra of vertical forces Fz acting on an Au-NP and a polystyrene sphere (PS, n=1.6) as a function of incident wavelength. PS provides a reference case for quantifying the contribution of plasmonic effects. The Au-NP experiences a maximum vertical force Fz as high as 236 pN/W/μm^2, which is ~15 times larger than that seen by the PS because of higher polarizability of gold. We study the trapping force distribution along several directions around the surface of the nano-ring to find the locations where the Au-NP will undergo the strongest trapping potential. The first path is along the axis of (X, 0, 50) nm as indicated by a thick solid arrow in Fig. 2(c). We found that any free Au-NP in the vicinity of the top surface of the nano-ring, the combined effect of Fx and Fz will produce a stable trapping site near the outer corner on the top surface, as indicated by a black dot in the cross-section shown in Fig. 2(c). The other two paths are along the axes of (65, 0, Z) nm and (5, 0, Z) nm as indicated in Fig. 2(d) by the thick solid and dotted arrows.

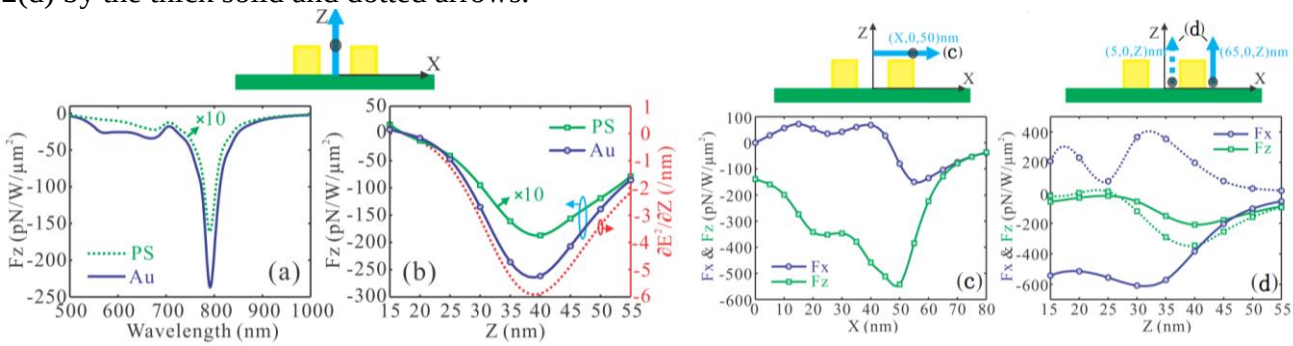

Fig. 2. (a) Fz acting on the Au-NP (solid line) and the PS (dotted line, magnified 10 times) as a function of incident wavelength. Both NPs have a diameter of 20 nm, and are located at coordinate of (0, 0, 35) nm as indicated by a dark dot in cross-section schematic. (b) Spectra of Fz on the Au-NP (─o─) and the PS (─□─, magnified 10 times) as a function of position along the Z axis (X=Y=0), and the electric field intensity gradient along this axis (dotted line), respectively. (c) Spectra of Fx (─o─) and Fz (─□─) as a function of location along the axis of (X, 0, 50) nm (indicated by thick arrow in cross-section schematic). (d) Spectra of Fx and Fz as a function of position along the axes of (65, 0, Z) nm (indicated by thick solid arrow) (─o─ for Fx and ─□─ for Fz), and (5, 0, Z) nm (indicated by thick dotted arrow) (dotted ─o─ for Fx and dotted ─□─ for Fz), respectively.

(ii) Meanwhile, we proposed and analyzed the diffraction coupling of LSP through active surface plasmon polariton (SPP) which would potentially give rise to device realization of the gain-assisted A-PNOT with high field. We demonstrated a significantly strong enhancement of electromagnetic (EM) power for LSPs in the event of diffraction resonance through incorporation of experimentally feasible optical gain to SPPs. Based on such phenomenon, we propose a hybrid plasmonic structure which would potentially give rise to device realization of a gain-assisted PNOT. To the best of our knowledge, there is no report on gain-assisted PNOT. In addition, it is also a promising platform for applications such as SERS, nonlinear optics etc.

A schematic of the proposed hybrid plasmonic structure is shown in Fig. 3 (a). The structure (from bottom to top) consists of an active PMMA substrate in which optical gain is made possible

through doped with dye molecules, a 20 nm silver film and a 15-30 nm SiO_2 spacer. A two-dimensional square lattice of gold nanopillars with periodicity of D=865 nm is deposited on top of the spacer layer. The diameter of the gold nanopillars is 150 nm and their thickness is 40 nm. We used FDTD simulation to calculate the near-field spectral intensity with the monitor placed at the edge of the nanopillar, as shown in Fig. 3 (b). At certain wavelengths, the SPPs can form constructive interference which is just the condition for diffraction resonance. These wavelengths are given by the extended Rayleigh cutoff wavelength $\lambda(i,j)_{m,air,PSP} = (D/m) \times n_{air,PSP} \times (i^2 + j^2)^{1/2}$, where D is the grating constant, m is an integer, $n_{air,PSP}$ is either the refractive index of air or the effective refractive index of PSP medium, and the integers i, j denote the grating diffraction order. This process gives rise to the resonance peaks indicated by the near-field intensity enhancement ($|E|^2$) spectra of the monitor as shown in Fig. 3 (b).

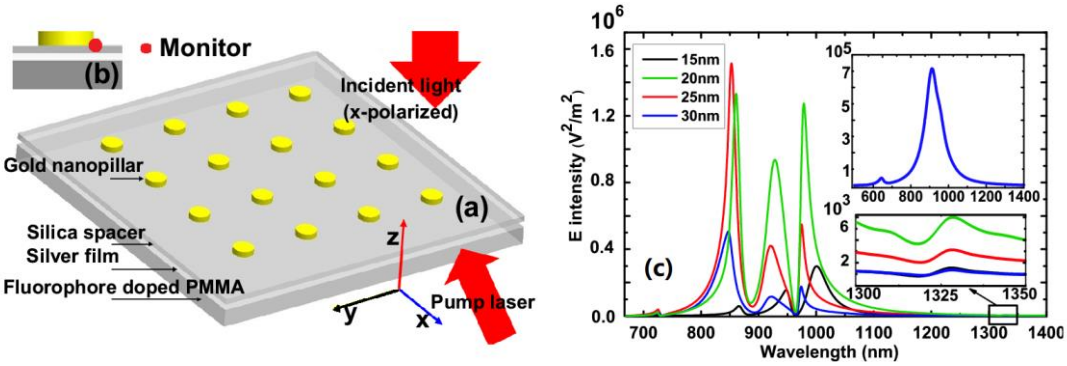

Fig. 3. (a) Schematic of the proposed structure, and (b) the monitor position. (c) Near-field response spectra at the monitor for different SiO_2 spacer thicknesses. Upper inset: near-field response spectrum of an isolated nanopillar with spacer thickness=20 nm. Lower inset: enlarged view of near-field spectra for the range of 1300-1350 nm.

The near-field spectra of the monitor for a 20 nm thick spacer and for different gain levels are shown in Fig. 4 (a). Without optical gain, strong resonance is barely observable. As optical gain is introduced into the system, the near-field intensity at 980 nm increases dramatically. The inset in Fig. 4 (a) reveals more details when the optical gain is $\varepsilon'' = -0.025$, a level that approaches but is still below the lasing threshold at 980 nm. This value corresponds to a gain coefficient of 1068.57 cm^{-1} and the near-field intensity has increased to $2.38 \times 10^7 V^2/m^2$ in this case. The lasing threshold is determined as such because the system will no longer decay but diverge in the time domain if the absolute value of ε'' is bigger than 0.027. Consequently, a SPASER-like phenomenon occurs with the emergence of a very sharp LPR peak. In Fig. 4 (a), the plot produced with $\varepsilon'' = -0.027$ (i.e. the lasering threshold) is a manifestation of the SPASER-like process. Figure 4 (b) shows the electric field intensity pattern when $\varepsilon'' = -0.025$ and $\lambda = 980$ nm, for a unit element of the grating in a XY plane at the nanopillar-spacer interface. In this case, the EM enhancement factor is on the order of 10^7. It is observed that the maximum field intensity focuses on the circumference of the nanopillar rather than some narrow gaps or small spots. Such distribution pattern increases the plasmonic trapping volume which in turn makes the A-PNOT device more feasible. Figure 4 (c) shows the directional pattern of the Poynting vector at the lower surface of the silver film, which clearly reveals the underlying mechanism of the PSP induced diffraction resonance. In Fig. 4 (c), the diagonal in a quaternary unit of the grating contains two entire wave profiles ($m = 2$) that are associated with the (1, 1) order diffraction resonance generated through PSP coupling with (i.e. $\lambda(1,1)_{2,PSP} = 980$nm with n_{PSP}=1.6). We also schematically show in Fig. 4 (d) the charge distribution around a cross-section covering two nanopillars. The laser threshold in terms of gain coefficient in our design is $\sim 10^3\ cm^{-1}$, which is within the limits of semiconductor polymers and laser dyes (highly concentrated).

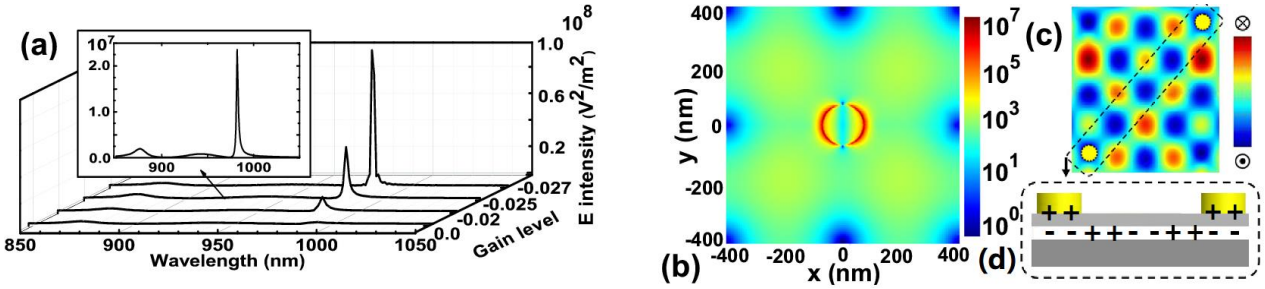

Fig. 4. (a) Near-field spectra for different gain levels. Inset shows an enlarged version of response spectrum when the optical gain approaches a level of $\varepsilon'' = -0.025$. (b) The local-field distribution pattern for a unit element of the grating when we use $\varepsilon'' = -0.025$ and resonant wavelength of 980 nm. It comes from an XY plane located at the nanopillar-spacer interface. (c) Directional pattern of the Poynting vector at the lower surface of the silver film. The dash box represents the two nearest nanopillar (highlighted by dash circle) in a diagonal direction. (d) Schematic of the charge distribution for highlighted region shown in (c).

For the realization of this gain-assisted A-PNOT system, a key component is the superflat substrate that offers optical gain. At this stage, we have figured out a route to achieve such substrate and we are currently in the process of demonstrating the substrate experimentally. The specific process is stated as follows: first, gold film coated silicon wafer is prepared; second, fluorophere doped PMMA solution is deposited uniformly by spin coating onto the gold film; third, after a sol-gel technology, an atomically flat substrate will come into being after lift off, since the opposite surface of the peeled PMMA film is atomic flat silica. Up to now, after grope for optimal conditions, we have successfully fabricated this superflat gain-doped substrate as mass-production with desirable reproducibility and very large area. We plan to utilize the Kretschmann prism configuration to test the performance of its gain level as what is schematically illuminated in Fig. 5 (a). The surface topography from AFM of our gain-doped substrate is shown in Fig. 5 (b), in which one can see that, in a quite large area the planeness is very good. Actually, the RMS roughness is just 0.406 nm, which is quite ideal for the next-step nanofabrication. Our theoretical calculations [in Fig. 5 (c) (d)] show that with 50 nm gold film, 632 nm incidence and a modest gain level ~400 cm^{-1}, a sizable angle shift (about four degrees) already can been observed comparing between passive system and active gain-assisted system. We will use reverse educing method to estimate the gain level from the angle shift.

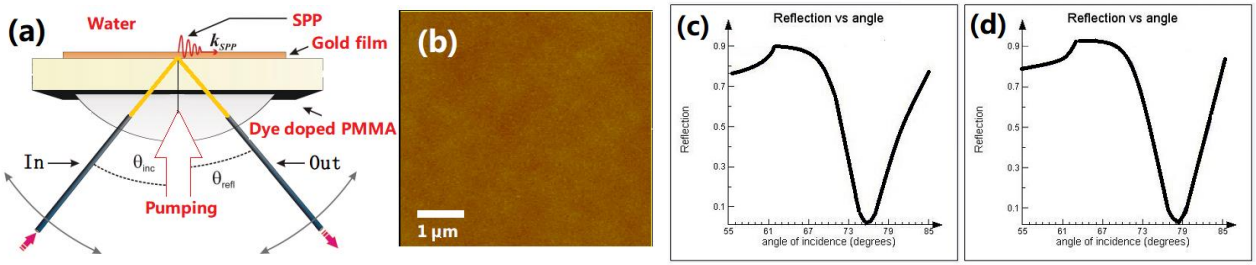

Fig. 5. (a) A typical SPP setup to educe the gain level of our proposed substrate. (b) Surface topography obtained from AFM of the superflat gain-doped substrate. The plasmonic resonance dips for (c) without optical gain, and (d) with gain.

2. M-PNOT for optical manipulations of target in nanoscale region:

We explored an all-optical M-PNOT scheme based on plasmonic nano-disks (NDs) with graded diameters [Fig. 6(a) and (b)]. Our results indicate that the target experiences a trapping potential strength of 5000 kBT/W/μm^2, maximum optical torque of ~336 pN•nm/W/μm^2, and the total active volume reaches ~10^6 nm^3. By switching the wavelength and polarization of the excitation source, target nano-particles trapped by the device can be manipulated from one ND to another one arbitrarily [Fig. 6(a) and (c)].

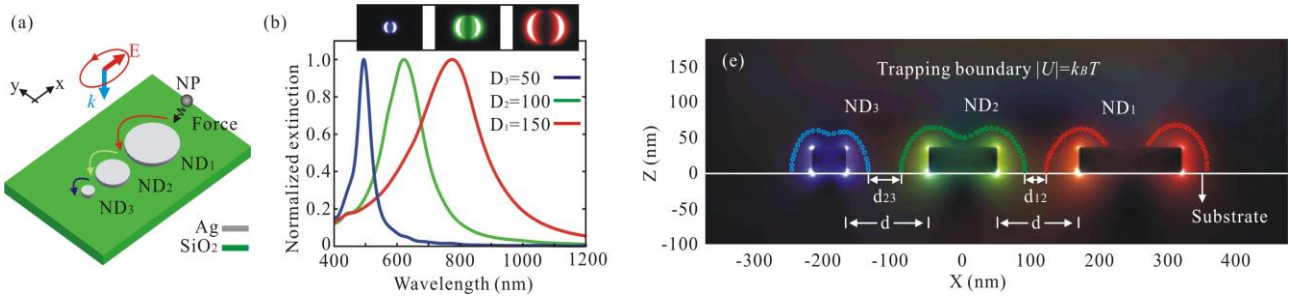

Fig. 6. (a) Schematic of the all-optical nano-manipulation. (b) Normalized extinctions of ND_1, ND_2, and ND_3. The top inset shows $|E|^2$ distributions at resonances for each ND. (c) Trapping boundaries for ND_1, ND_2, and ND_3, respectively, with d=120 nm and incident power density of 1 mW/μm^2.

Figure 7(a) presents the optical gradient force Fx (blue line) experienced by the PS along the X axis (Y=0) at a distance of 5 nm above the NDs for λ=775 nm. The force components Fx (green ○) and Fz (red □) calculated by MST are also shown. One can see that the force Fx obtained from the gradient of $|E|^2$ (blue line) and the MST method (green ○) are in excellent agreement with each other apart from small discrepancies due to the influence of scattering forces. This result implies that the optical trap generated in the current case is dominated by gradient force. Moreover, the normal force component Fz remains negative and reaches a maximum of ~45 pN/W/μm^2 at the edges. Therefore, the resultant force vectors will all point to the edge of ND1 [see Fig. 7(b)]. The gradient forces Fx when the incident wavelengths are switched to λ=622 nm and 495 nm are plotted in Fig. 7(c) and 7(d). Comparing with the results in Fig. 7(a), one can find that the optical force becomes significant around the resonant ND. The non-resonant NDs only contribute to the force disturbance, which are represented as the fluctuations in the force curves above those NDs. Therefore, if we sequentially excite the NDs by varying wavelength and polarization direction of the incident beam, the overall effect of the optical force will always bring the PS to a desired edge of ND where the optical field is most enhanced (i.e., hot-spot).

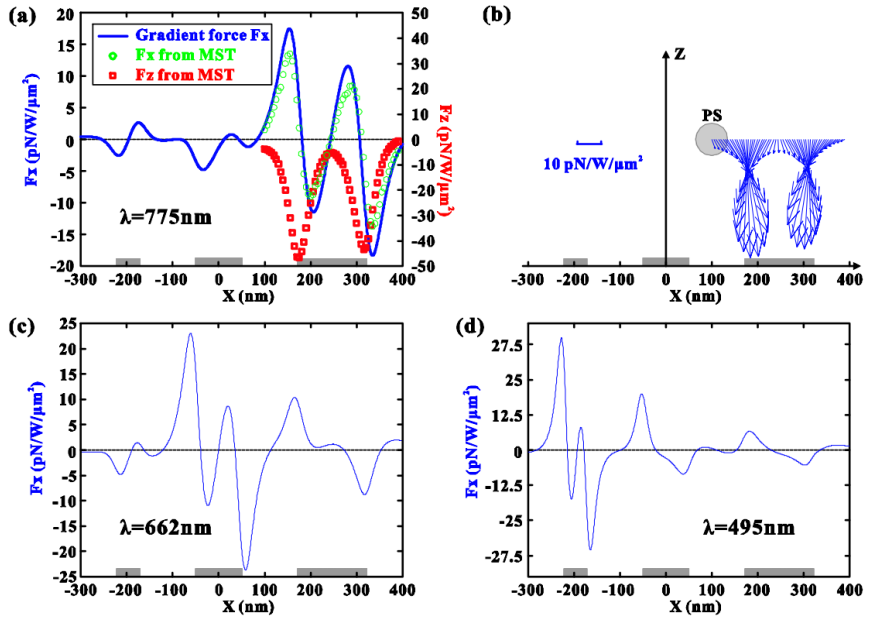

Fig. 7. (Color online) Optical gradient force Fx (blue line) on a PS locating above the NDs with a 5 nm gap as a function of position along the X axis (Y=0) for λ=775 nm (a), 622 nm (c), and 495 nm (d), respectively. The MST calculated force components Fx (green ○) and Fz (red □), and the 2D trapping force vectors for λ=775 nm are also shown in (a) and (b), respectively. The incidences have X-polarization. The three NDs are schematically indicated by grey bars at the bottom. The gap between adjacent NDs is 120 nm.

3. S-PNOT platform for simultaneously trapping and sensing:

(i) An S-PNOT structure which based on double-layered metal nano-strip arrays and SERS-based sensing is also studied by means of mode analysis and two-dimensional FDTD simulations. The nano-strips act as optical antennas through constructive interference of short range SPPs, thus increasing their scattering cross-section and optical field enhancement. Near-field modulation by optical trapped metal NPs is demonstrated. The proposed device shows reasonable figure-of-merit (FoM) and is ready for integration with common optofluidic biosensors. Our results reveal that the device exhibits a refractive index sensitivity of ~200 nm/RIU, and a maximum SERS factor of 10^9-10^{10} from metal NPs trapped in the near-field region. Figure 8 shows the schematic of the coupled system, calculated normalized scattering cross-section as a function of wavelength for the region of interest, and electric field amplitude distributions for excitation of wavelength 514 nm and 633 nm.

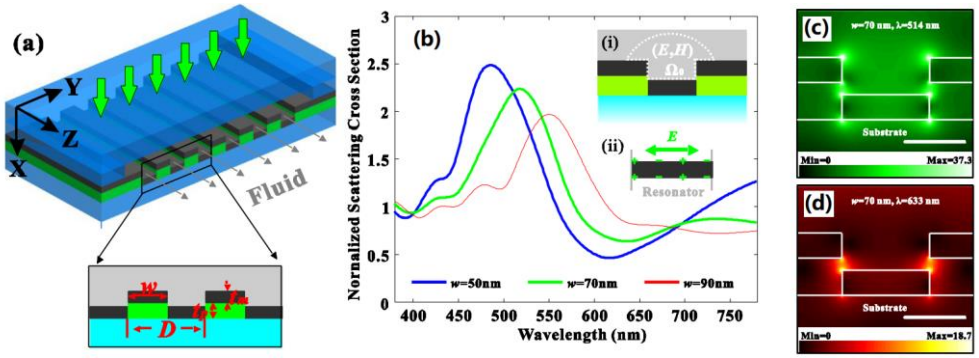

Fig. 8. (a) Schematic of the coupled system including structural parameter symbols. (b) Calculated normalized scattering cross-section as a function of wavelength for the region of interest, denoted as Ω_0 enclosed by the white dashed curve shown in the inset (i). The blue line shows the case for w=50 nm; green line for w=70 nm; and red line for w=90 nm, respectively. Metal nano-strip as an antenna is schematically illustrated in the inset (ii). (c) Electric field amplitude distributions for excitation of λ=514 nm and (d) λ=633 nm. The width of the strip is w=70 nm. The white scale bar denotes a length of 50 nm.

Figures 9 (a) and (b) present the profiles of $\mathbf{E}^2$ (red line) and the corresponding gradients of $\mathbf{E}^2$ (green line) along the transverse [Fig. 9 (a)] and longitudinal [Fig. 9 (b)] lines as the blue arrows denote in the insets respectively.

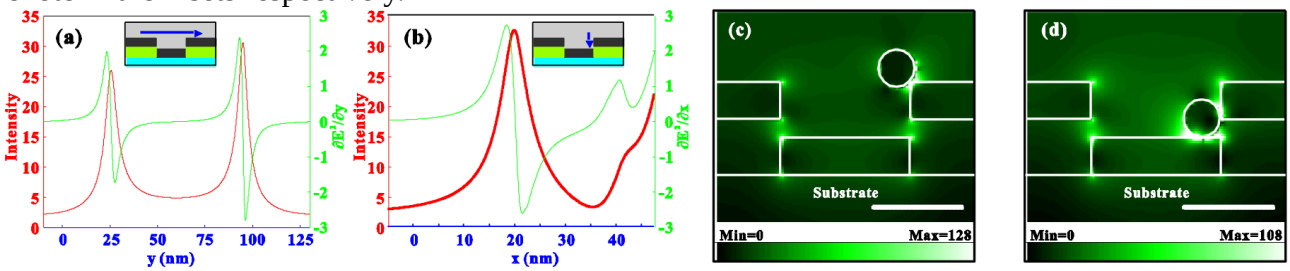

Fig. 9. (a) Profiles of electric field intensity ($\mathbf{E}^2$) (red line) and the corresponding gradients of $\mathbf{E}^2$ (green line) along the transverse (a) and longitudinal (b) lines as denoted by the blue arrows in the insets. Electric field amplitude distributions with an optical trapped 20 nm Ag-NPs at two different sites (c) and (d) for the case of w=70 nm and λ=514 nm. The white scale bar denotes a length of 50 nm.

The negative gradients in the figures imply a trapping force in a direction opposite to that indicated by blue arrows. We demonstrated that stable trapping sites exist at locations where $\mathbf{E}^2$ are strongly localized and the gradients equal to zero, which is consistent with the previous results. Otherwise, for the case of x>35 nm as shown in Fig. 8 (b), the fluctuation of the gradient is resulted from coupling between L1 and L2. The gradient continues its positive value, indicating that the NP will be trapped near the upper surface of L2. Accordingly, we can find the trapping positions for the Ag-NP, as shown in Figures 9(c) and 9(d), using the simulated electric amplitude distributions, respectively. It is clear that the near-field is modulated significantly by the optically trapped NP,

which leads to further field enhancement with the highest level of 128 times. This means that a SERS EF of 10^8 ($1284=2.68\times10^8$) is achievable.

(ii) We also proposed a new S-PNOT scheme based on dark-field extinction spectroscopy. Our design comprising a plasmonic NP placed inside a microcavity. Simultaneously act as nanoscale sensor and PNOT, the NP's sensing ability is improved in a new manner, hence its trapping behavior can become robust. A schematic of the device is illustrated in Fig. 10. An sensing and trapping (ST-NP, silver NP with radius of 25 nm) is placed at the center of a nano-sized detection volume, around which, a dressing ring (with a refractive index of 1.7-2.0) is constructed to serve as cavity. The dark-field spectroscopy of the structure is calculated using FDTD method. A linearly polarized total-field/scattered-field plane wave illuminates the ST-NP and the detection volume from top at normal incidence.

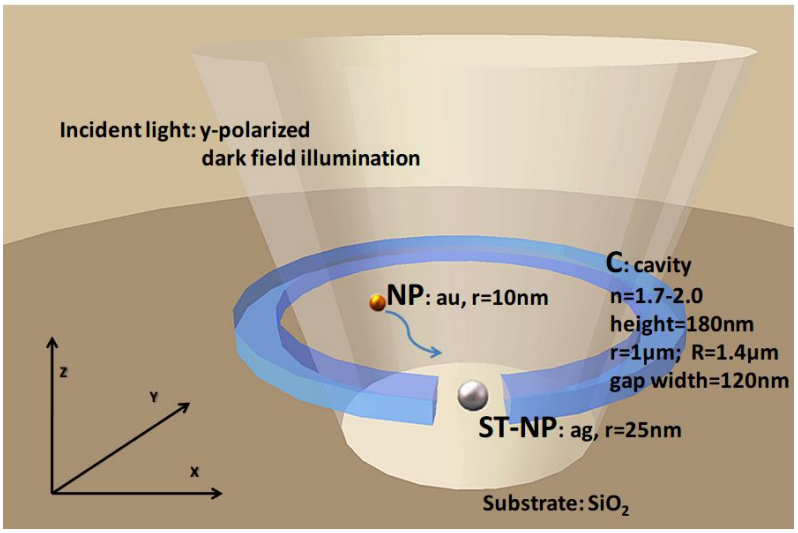

Fig. 10. Schematic of the hybrid ST-NP configuration. The micro-ring has a height of 180 nm, a gap width of 120 nm and an outer and inner radius of $1.4\mu m$ and $1.0\mu m$ respectively. The silver ST-NP has a radius of 25 nm. The incident light locally illuminating the detection volume stands for that used in dark-field spectroscopy.

Figure 11 shows sensing responses from the two configurations: (i) bare ST-NP and (ii) ST-NP with dressing ring cavity (where the ring can be fabricated with Si_3N_4 with a refractive index of 2.0). In both cases, the sensing event involves the trapping of a gold NP with a diameter of 10 nm. For simplicity, we abbreviate (i) the bare ST-NP sensor with a trapped NP as the "ST-NP+NP" and (ii) the ST-NP in dressing ring cavity caseas the "C+ST-NP", so that "C+ST-NP+NP" represents the ultimate case of NP being trapped and sensed by a C+ST-NP system. Figure 11 (b) shows that when a NP is trapped by a simple ST-NP system, the extinction peak increases slightly. However, Fig. 11(a) shows that the C+ST-NP configuration exhibits much larger extinction intensity change (ΔI) caused by the trapped NP. Calculation reveals a FoM of 7.30 for the C+ST-NP+NP system comparing with the bare ST-NP case at the wavelength of 410 nm (normalized to the value of $\Delta I'/I'$ in Fig. 11b). For single-beam operation in the C+ST-NP system, ΔI is much larger. Compared with the case of bare ST-NP (intensity change denoted as $\Delta I'$), C+ST-NP offer 6.83 times higher sensitivity (i.e. $\Delta I/\Delta I'$).

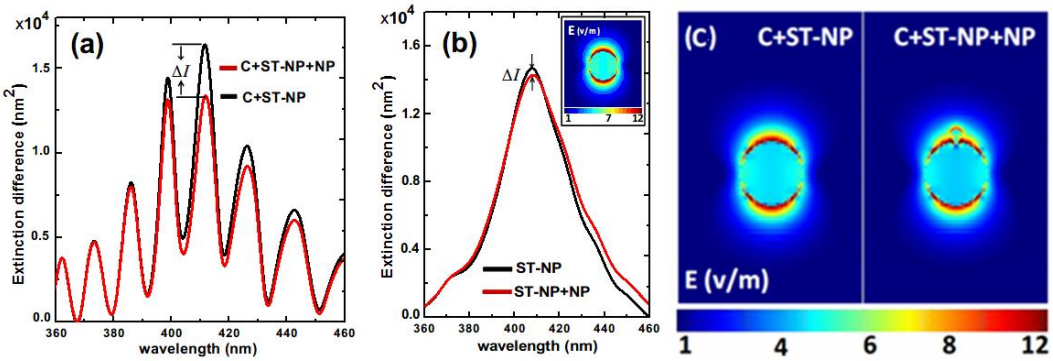

Fig. 11. (a) Extinction spectra of the C+ST-NP+NP and C+ST-NP systems with the dressing ring index n=2. (b) Extinction spectra of the ST-NP and ST-NP+NP systems; inset shows its near-field distribution of ST-NP in the equatorial plane parallel with the substrate. (c) local-field distribution pattern at the middle section of C+ST-NP and C+ST-NP+NP systems.

In our proposed scheme, we amplify ST-NP's sensitivity of far field detection, meanwhile weaken its correlation with ST-NP's near field. This means a trapped NP almost will not affect ST-NP's near-field distribution but can give much impact to C+ST-NP+NP's far field extinction. During trap-and-sense operation, spectral shift can be no longer a required parameter for the proposed C+ST-NP system. With the near-field LPR wavelength almost remains constant, trapping force can be always kept at its strongest level. Inset in Fig. 11 (b) and Fig. 11 (c) show the near-field distributions of the bare ST-NP, C+ST-NP and C+ST-NP+NP systems at the same resonance wavelength (410 nm). To our best knowledge, this proposed S-PNOT is a unique solution so as to avoid unnecessary self-induced back-action effect and to ensure a stable and robust trapping. Besides performing the dual function efficiently, the dressed LPR is also a good candidate for only sensing applications.

4. Low-cost PNOT (L-PNOT) scheme:

We demonstrated the use of PNOT and SERS for reproducible and low concentration of bio-detection.

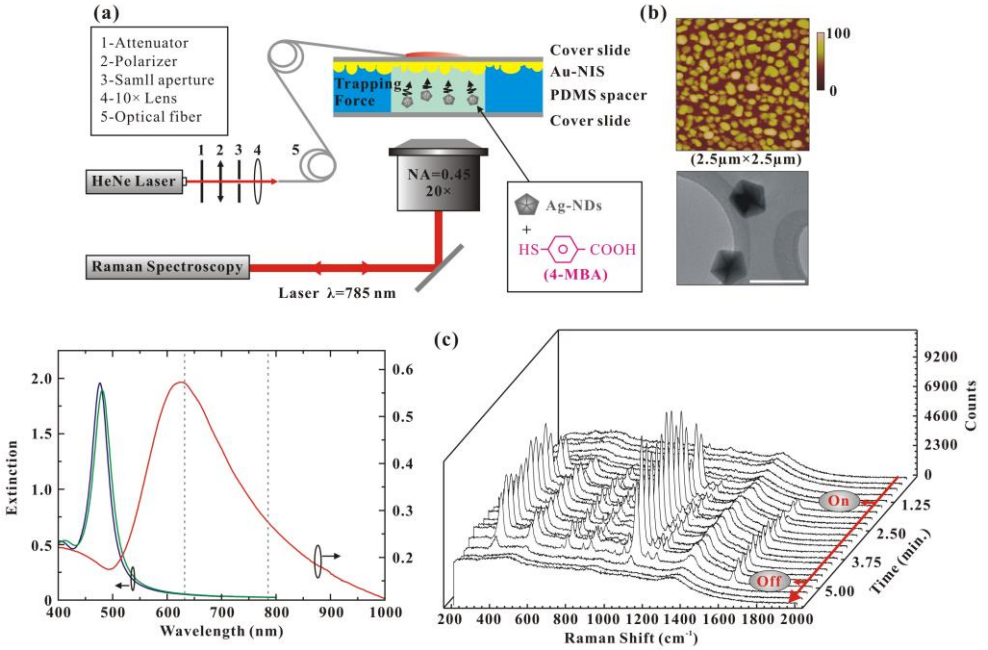

Fig. 12. (a) Schematic of the reproducible bio-detection platform. (b) AFM image of Au-NIS, TEM image of Ag-NDs, and extinctions of them. (c) Temporal Raman spectra showing the trapping and releasing processes.

The effortless gold nano-island substrate (Au-NIS, λ_R=632.8 nm) acts as L-PNOT. The targets are silver nanodecahedrons (Ag-NDs, λ_R=475 nm) that has been bound with bio-molecules [Fig. 12(a) (b)]. As the He-Ne laser is on, the Au-NIS becomes active, thus trap the targets into the hot-region, which can be characterized through the enhanced Raman signals. Turning of the He-Ne laser will lead to the release of target [Fig. 12(c)]. Therefore another round of detection can be conducted when rinse the sample and inject another batch of target. Meanwhile, this L-PNOT with Au-NIS can also trap dielectric NPs. Figure 13 shows the results obtained from trapping experiments. The target is polystyrene sphere (PS) with diameter of 500 nm, which is diluted into DI water. The trapping phenomenon is monitored through a high resolution CCD. The Au-NIS is random distributed after thermal annealing processing of gold thin film (400 ^{o}C and 12 minutes). The incident power density is estimated to be ~0.03 mW/μm^2. The 500 nm PS is trapped and form close pack structure when the trapping laser is on.

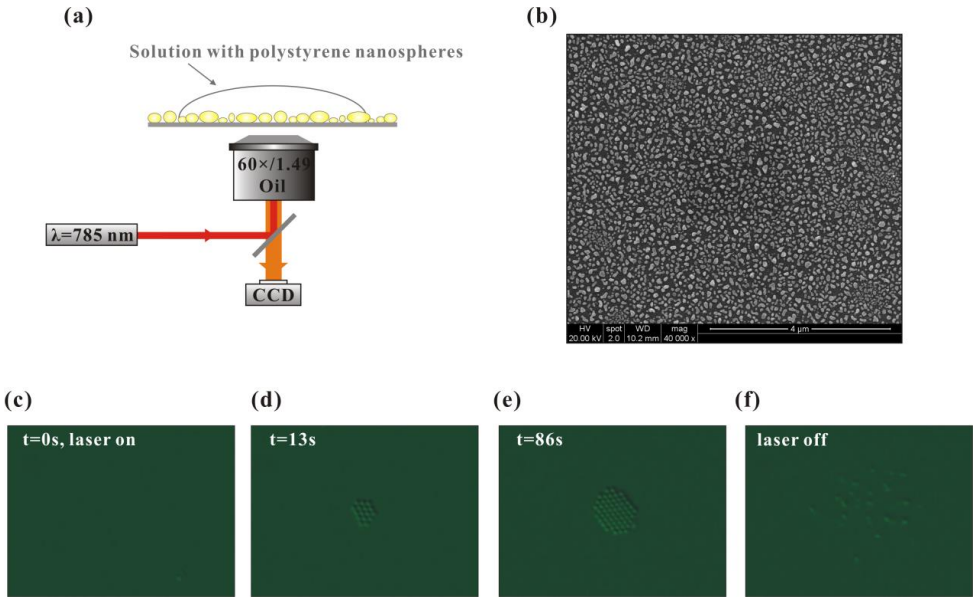

Fig. 13. (a) Setup for plasmonic optical trapping on random distributed gold nano-island substrate. The trapping laser has a wavelength of 785 nm, which is condensed onto the substrate through an oil objective (60×; NA: 1.49). (b) SEM micrograph of substrate. (c-f) Successive images of plasmonic optical trap and release by turning on and off the laser beam respectively.

5. High performing surface plasmon resonance (SPR) sensors

Other than PNOT, we have improved the performance of SPR sensors. We have developed a general scheme to maximize the figure-of-merit (FOM), which is a key performance indicator, of spectral- and phase-based SPR sensors. The FOM is defined as the ratio between sensitivity and linewidth. By using coupled mode theory and Rayleigh scattering formalism, we show for spectral-based SPR, the linewidth can be significantly narrowed by reducing the hole size in periodic nanohole arrays. As a result, FOM higher than 100/RIU has been demonstrated and it is comparable with that of the commercial available prism-based SPR unit. As an example, Fig. 14 shows two 2D Au nanoarrays with different geometries. Both their sensitivities and FOMs are determined to be 754.7 nm/RIU and 105.57/RIU for the first one and 751.18 nm/RIU and 91.05/RIU for the second.

On the other hand, for phase-based SPR, FOM larger than 1000/RIU can be achieved if the radiative decay rate of the resonance matches well the absorption rates. This impedance matching produces a very sharp phase jump at the resonance, enabling a much narrow differential phase profile. As a result, we expect the phase-based SPRs eventually can reach the sensitivity down to single molecular level. As a demonstration, Fig. 15 shows the sensing performance of a 2D Au

nanohole array with period = 750 nm, hole depth and radius = 100 and 80 nm incorporated in a home-built two-channel flow cell. Its absorption and radiative decay rates have been matched with each to yield the sharpest phase jump. Fig. 15(a) shows the differential phase profile $\left|\frac{d\varphi(\lambda)}{d\lambda}\right|$ of (-1,0) SPP mode taken at incident angle = 3.75^{o} in NaCl solutions (from 0 to 8 % by mass) with refractive index n varying from 1.333 to 1.3424. All the peaks are narrow and they show good signal-to-noise ratio. As expected, they gradually red shift to longer wavelength when refractive index increases. The resonance wavelengths are then plotted as a function of refractive index in Fig. 15(b), giving a linear relationship with sensitivity deduced to be 753.06 nm/RIU. The derivative linewidths for different refractive indices are shown in Fig. 15(c) and they are found to vary between 0.36 and 0.73 nm, resulting in the lowest and highest spectral FOM to be 1043 and 2061/RIU, respectively (Figure 5d), and the average FOM to be 1420/RIU at~980-990 nm. Remarkably, these values surpass the performance of not only the commercial available Kretschmann setup (FOM~63/RIU at λ~900 nm) and the nanoparticles (FOM < 7/RIU at λ~600-800 nm) but also the recently reported SPR sensors based on nanorod metamaterials (FOM~330/RIU at λ~1200 nm), Fano resonance from plasmonic crystals (FOM=162/RIU at λ ~ 800 nm) and single slit (FOM = 234/RIU at ~782 nm), and plasmonic Mach-Zehnder interferometer (FOM = 224/RIU at 734 nm).

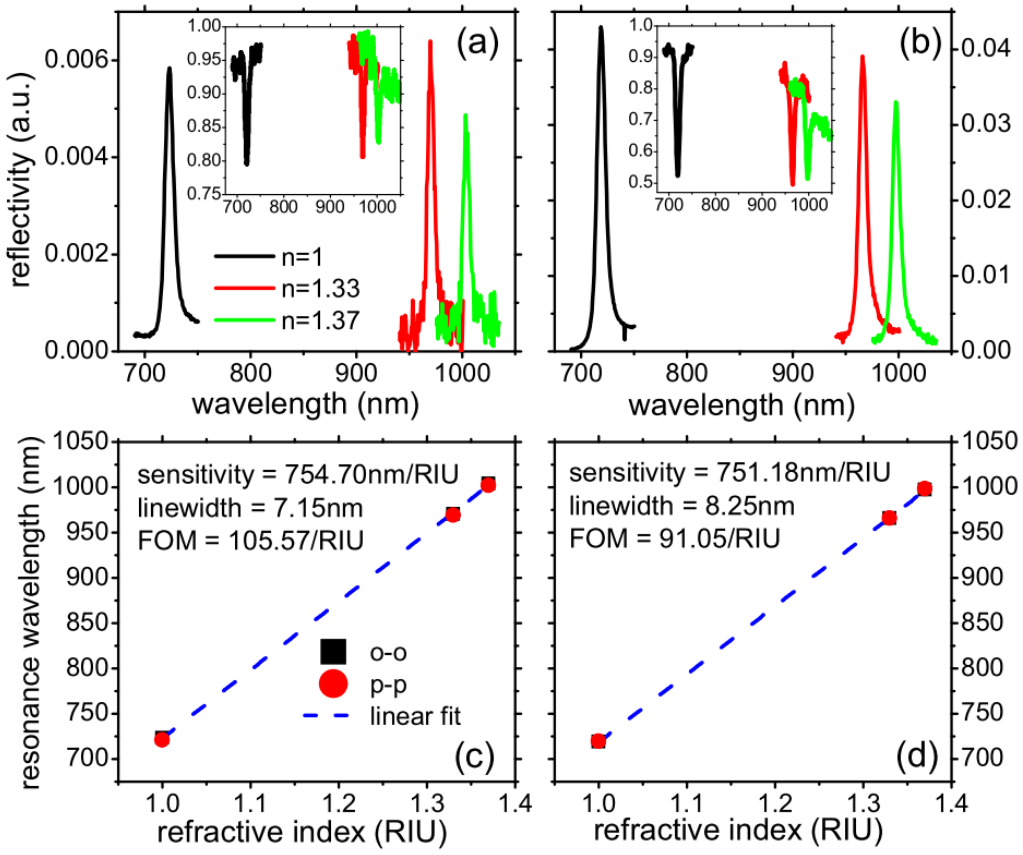

Fig.10. The cross-polarized reflectivity spectra of (1,0) SPP mode taken from two Au arrays with P = 760 nm, d = 70 nm, and (a) r = 35 and (b) 135 nm at θ = 5o in different refractive index media (n = 1, 1.33 and 1.37). The corresponding p-polarized reflectivity spectra are given in the insets for reference. (c) & (d) The corresponding plots of resonance wavelength against refractive index. The back solid squares are determined from cross-polarized reflectivity spectra while the red solid circles are determined from p-polarized reflectivity spectra. The dash lines are linear fits. The sensitivity and FOM are determined to be 754.7 nm/RIU and 105.57/RIU for r = 35 nm and 751.18

nm/RIU and 91.05/RIU for r = 135 nm.

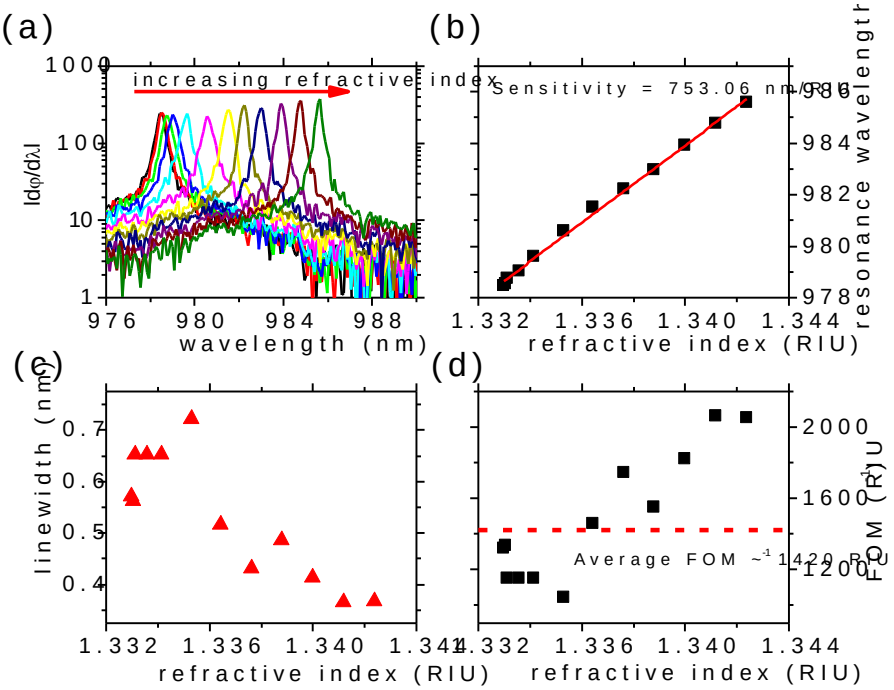

Fig.15. (a) Effect of refractive index on the absolute derivative lineshapes taken from a 2D Au nanohole array with period=750 nm, hole depth and radius=100 and 80 nm. The incident angle is set at 3.75^{o}. (b) Plot of resonant wavelength position with refractive index. The red shift is linear with refractive index, yielding sensitivity = 753.06 nm/RIU. (c) The derivative linewidth is plotted against refractive index. (d) Plot of FOM as a function of refractive index. The dash line indicates the average FOM.

4. PUBLICATION AND AWARDS

1. Z.W. Kang, H.X. Zhang, H.F. Lu, and H.P. Ho, "Double-layered metal nano-strip antennas for sensing applications," Plasmonics DOI 10.1007/s11468-012-9388-7 (2012).

2. Z.W. Kang, H.X. Zhang, H.F. Lu, J.B. Xu, H.C. Ong, P. Shum, and H.P. Ho, "Plasmonic optical trap having very large active volume realized with nano-ring structure," Optics Letters 37, 1748-1750 (2012).

3. H.X. Zhang, H.F. Lu, Y.Y. Zhou, X.Yu, F. Luan and H.P. Ho, "Diffraction resonance with strong optical-field enhancement from gain-assisted hybrid plasmonic structure" Appl. Phys. Lett. 100, 161904 (2012).

4. Z.W. Kang, H.X. Zhang, H.F. Lu, J.J. Chen, and H.P. Ho, "Graded plasmonic nano-disks for near-field nano-manipulation," Optics express (Submission, 2013).

5. H.X. Zhang, Y.Y. Zhou, X. Yu. F. Luan, J.B. Xu, H.C. Ong and H.P. Ho, "Dressing plasmon resonance by particle-microcavity architecture for efficient nano-optical trapping and sensing," Optics Letters (Submission, 2013).

6. L. Zhang, C.Y. Chan, J. Li, and H.C. Ong, "Rational design of high performance surface plasmon resonance sensors based on two-dimensional metallic hole arrays," Opt. Exp. 20, 12610 (2012).

7. S.L. Wong and H.C. Ong, “Phase difference mapping of two-dimensional metallic nanohole arrays,” Appl. Phys. Lett. 100, 233102 (2012).

8. H.Y. Lo and H.C. Ong, “Decay rates modification through coupling of degenerate surface plasmon modes,” Opt. Lett. 37, 2736 (2012).

9. D.Y. Lei, J.T.L. Wan, and H.C. Ong, “Numerical and analytical evaluations of the sensing sensitivity of waveguide mode in one-dimensional metallic gratings,” Nanotechnology, 23, 275501 (2012).

10. H.Y. Lo, C.Y. Chan, and H.C. Ong, “Direct measurement of radiative scattering of surface plasmon polariton resonance from metallic arrays by polarization-resolved reflectivity spectroscopy,” Appl. Phys. Lett. 101, 223108 (2012).

11. Z.L. Cao, H.Y. Lo, and H.C. Ong, “Determination of absorption and radiative decay rates of surface plasmon polaritons from nanohole array,” Opt. Lett. 37 5166 (2012).

12. Z.L. Cao and H.C. Ong, “Direct imaging of radiative decay of surface plasmon polaritons in nanohole arrays by cross-polarization microscopy,” Appl. Phys. Lett. 102, 093108 (2013).

13. C.Y. Chan, Z.L. Cao, and H.C. Ong, “Study of coupling efficiency of molecules to surface plasmon polaritons in surface-enhanced Raman scattering (SERS),” Opt. Exp. 21, 14674 (2013).

14. S.L. Wong, S.Y. Wu, Z.L. Cao, H.P. Ho, and H.C. Ong, “High performing Fano resonance mediated phase-based surface plasmon resonance sensing from plasmonic crystals,” (submitted).

Multimedia Technologies Track

Research Reports
In Multimedia Technologies

Newly Funded Projects (2014 - 2016)	* Managing and Analyzing Big Graph Data
Continuing Projects (2012 - 2014)	* Face Recognition Across Ages Through Binary Tree Learning
Completed Projects (2011)	* Semantic Analysis for Image Resizing
	* Time Critical Applications over a Shared Network
	* Amplify-and-forward Schemes for Wireless Communications

The following reports are enclosed in "Research Highlights" printed in 2013

Completed Projects	
(2010)	* FADE: Secure Cloud Storage with File Assured Deletion
	* Security and Detection Protocols for P2P-Live Streaming Systems
(2009)	* An Opportunistic Approach to Capacity Enhancement in Wireless Multimedia Networks
	* Computer-Aided Second Language Learning through Speech-based Human-Computer Interaction

The following reports are enclosed in "General Report and Research Highlights 2009-2011" printed in October 2011.

Completed Projects	
(2008)	* Pattern Computation for Compression and Performance Garment
(2007)	* Real-time Transmission of High Definition (HD) 3D Video and HD Audio in Gigabit-LAN
	* High Dynamic Range Image Compression and Display
	* Multimedia Content Distribution over Hybrid Satellite-Terrestrial Communication Networks
(2006)	* Automatic Video Segmentation and Tracking for Real Time Multimedia Services
	* Information Retrieval from Mixed-Language Spoken Documents
	* Wireless Networks and Its Potential for Multimedia Applications

The following reports are enclosed in "Research Highlights 2005-2007" printed in January 2008.

Completed Projects	
(2005)	* Mobile Wireless Multimedia Communication
	* An Automatic Multi-layer Video Content Classification Framework
	* Automatic Multimedia Fission, Categorization and Fusion for Personalized Visualization in Multimedia Information Retrieval

Managing and Analyzing Big Graph Data

Principal Investigator: Professor James CHENG
Department of Information Engineering, CUHK

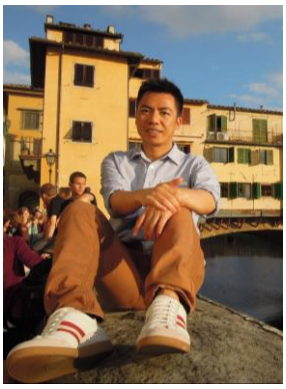

Project start date: 1 July 2014

ABSTRACT

This research proposes to develop effective and scalable techniques for managing and analyzing big graph data, and to apply them for searching and analyzing multimedia data, especially data in online social networks (e.g., Facebook, Twitter, Google+, LinkedIn) and online shopping platforms (e.g., eBay, Amazon, Taobao). Graph is widely used to model online social network structures, as well as many complicated data types such as images and pictures, videos, and other interactivity contents, etc. We propose to study fundamental issues of big graph data research, including the study of elementary substructures and important properties of massive graphs, the modeling of these graphs for prediction and extrapolation studies, and the applications of big graph data in areas that may create impacts in both industry and academia. Currently, we have some initial contacts with engineers from the Alibaba Group, who have shown great interests in our research. In fact, they have already agreed that they would apply our techniques to manage and analyze massive data from their TaoBao online shopping platform, as many of the techniques we propose are exactly the solutions they are looking for. We have planned to visit each other regularly in order to establish a long-term collaboration relationship.

PROJET OBJECTIVES

1. Key issues: The project proposes to develop an efficient and scalable system for managing and analyzing big graph data, with applications in multimedia data in large-scale online social networks and online shopping platforms.

2. Impacts on academia:
   a. The proposed research is a timely study on one of the most important topics in the areas of database and data mining research.
   b. The success of this project can significantly advance research in the field of graph data management and graph mining, and open new directions in effectively and efficiently managing and analyzing rich information embedded in social networks.
   c. Techniques developed in this research will benefit cross-disciplinary research including sociology, physics, biology, ecology, economics, finance, etc., because of the prevalence of graph and network data in their respective domains.

3. Impacts on industry:
   a. The results obtained in this project will provide deeper insights about the patterns of real-world networks and the behaviors of their users including the communications and relationships among them. Such knowledge can be used by industry such as online social

networking companies (e.g., Facebook, Twitter) and telecom operators to better understand user behaviors and their interaction patterns, online auction and shopping platforms (e.g., eBay, Amazon, Taobao) to analyze shopping trends, airlines and other transportation companies for better logistic and itinerary planning, to name but a few.

b. We will actively seek industry collaborators (our current connections include Alibaba, China Mobile, IBM China, MSRA, Huawei) and explore the opportunities of applying our techniques for efficient and effective management and analysis of their data, hence bringing values to their business.

Face Recognition Across Ages Through Binary Tree Learning

Principal Investigator: Professor : Xiaoou TANG[1]
Department of Information Engineering, CUHK

Research Team Member: Zhifeng LI, Associate Prof. [2]

[1] Dept. of Information Engineering, CUHK
[2] Shenzhen Institute of Advanced Technology

Progress Reporting Period: 1 July 2012 – 30 April 2013

ABSTRACT

Children faces change much faster over time than adult faces, making it much more difficult to process by traditional face recognition algorithms. Unfortunately, researches on age invariant face recognition has been sparse and even the state of the art results are poor on children face recognition across different ages. In this project, we focus on this fundamental research problem. We propose a cross modality invariant face recognition approach that reduces age variation gap between two age groups. The algorithms developed here can be applied to a wide range of real world applications, including face verification using ID photos with age gaps, digital family photo-album management with photos ranging from childhood until adult years. More importantly, the algorithms developed in this project are critical in meeting a recent urgent need of finding missing children on the internet.

1. OBJECTIVES AND SIGNIFICANCE

In this project, we focus on a fundamental research topic: age invariant face recognition. It has been shown that the recognition tasks for children faces are much harder than for adult faces. This is mainly because children face profiles undergo larger variations over even a short period of time. The state of the art age invariant recognition algorithms achieve only 40% equal error rate on the FGNET database. To address these challenges, we propose a new identity-preserving face recognition algorithm.

The algorithms developed here can be applied to a wide range of tasks. For example, for face verification using ID photo, usually the ID photo is taken long ago (national ID card in China is valid for 20 years), therefore age variation is a significant factor. For digital family photo-album management application, photos may range from childhood until adult years, thus requires age invariant face recognition algorithms. This project is also inspired by a recent urgent need of finding missing children on the internet. To address this challenge, we try to apply face recognition technology. However, we found that children faces change rapidly over time and there are few existing algorithms that achieve satisfactory performance on cross modality invariant face recognition for children faces. In this project, we propose a new cross modality invariant face recognition algorithms based on new machine learning approaches.

2. RESEARCH METHODOLOGY

Traditional cross modality invariant recognition approaches can be categorized into two groups, cross modality modeling based methods and discriminative learning methods. The modeling methods try to reduce cross modality variation at the preprocessing stage. The discriminative learning methods try to reduce modality gap after the face features are already extracted. Neither approaches work well so far. In this work, unlike the previous works for cross modality face recognition, we propose a novel face representation, the face identity preserved (FIP) feature, which is directly learned from the face images with different ages,

poses, and illuminations. This new representation can significantly remove the cross modality variations of the face images intra-identity, while maintaining the discriminativeness across identities.

Furthermore, unlike the traditional face descriptors, e.g. LBP, Gabor, and LE, where the original image cannot be recovered from the features, FIP features can be used to reconstruct the frontal face image with frontal (natural) illumination of an identity. With this attractive property, the conventional descriptors and learning algorithms can utilize our reconstructed frontal face images as input so as to eliminate the negative effects coming from cross modality variations. Specifically, we propose a new deep network to learn the FIP features, which utilizes both the face images with large poses and illuminations of an identity as input, and reconstructs its frontal face as target.

We also propose a novel approach to address the representation issue and matching issue in age invariant face recognition. In this framework, we first develop a new local descriptor called learning based local binary pattern (LLBP) to encode the micro-structure of the facial images into a set of discrete codes by incorporating a learning based encoding method. The code histogram of the LLBP descriptor is more uniformly distributed than the original LBP descriptor, which means more informative and discriminative. By densely sampling the LLBP descriptor over the entire facial image, sufficient discriminant information can be extracted for further analysis. Since LLBP-based local features span a high-dimensional feature space, to avoid the over fitting problem and improve the recognition performance, we further develop a new subspace learning algorithm called cascade discriminant analysis to refine this feature space.

3. RESULTS ACHIEVED SO FAR

We have developed a new deep learning algorithm to learn the FIP features for cross modality face recognition. Experimental results clearly show the effectiveness of our approach over the state-of-the-art. The paper has been submitted to ICCV and is currently under review.

4. PUBLICATION AND AWARDS

[1] Z. Zhu, P. Luo, X. Wang, and X. Tang, “Deep learning identity preserving face space,” *under review for IEEE Conf. on Computer Vision*, 2013.

SEMANTIC ANALYSIS FOR IMAGE RESIZING

Principal Investigator: Professor WONG, Tien Tsin [1]
Department of Computer Science & Engineering, CUHK

Research Team Members:
YANG Xuan, Postdoc [1], ZHANG Linling, Postdoc [1]
LIU Xueting, PhD student [1] KWAN Kin Chung, PhD student [1]
SHEN Wuyao, PhD student [1] MAO Xiangyu, MPhil student [1]
WONG Ka Wing, MPhil student [1]

[1] Dept. Computer Science & Engineering, CUHK

Project Start Date: 1 July 2011
Completion Date: 30 June 2013

ABSTRACT

With the wide popularity of portable display devices, images are often visualized through small displays of various resolutions and aspect ratios. On the other hand, images are typically captured for large display. Naive image resizing results in over-squeezing of prominent content and loss of details. However, the definition of saliency is usually vague and based on the low-level image features that may not be related to the semantics.

Although high-level semantics analysis (such as automatic recognition of arbitrary objects) is infeasible in the near future, analysis of certain middle-level semantics, such as symmetry and foreshortening, is feasible. In this project, we propose a semantics-aware retargeting framework. Based on the detected semantics, the image can then be retargeted in a more sensible way that preserves the detected semantics. Knowing the semantics not only allows us to resize images and videos more intelligently, but also opens up a new space for retargeting. This new space of cell-by-cell processing provides much flexibility to avoid over-squeezing, over-stretching, and undesirable bending of prominent symmetric structure.

Understanding cells is probably only the first step towards high-level semantic understanding. To further understand the structure these cells form, we plan to approach this challenging semantic analysis problem based on the Gestalt principles of human visual perception. By solving these challenges, we believe the outcome (the knowledge, publications, and algorithms) from the proposed project should motivate further study along the direction of semantics-aware resizing by the community. Besides the developed algorithm should be directly applicable in mobile computing and movie production.

1. OBJECTIVES AND SIGNIFICANCE

The wide availability and popularity of small portable display devices leads to an important display problem, as movies are normally produced in specific resolutions and aspect ratios (4:3 or 16:9). Adaptation is needed for the transition from the legacy 4:3 television to 16:9 HDTV broadcasting, as most legacy videos are not produced for HDTV. Simple scaling for small display may lead to over-squeezing of prominent content and poor visualization. The major challenge of resizing is on how to define the importance. Existing importance metrics rely on low-level image features, which may not correspond to the true semantics.

While computational understanding of general image semantics is infeasible in the near future, detection of middle-level semantics, such as symmetry and foreshortening, is feasible. They can drastically improve the retargeting. For instance, by identifying the symmetry pattern in an image of architectural

buildings, image can be retargeted to a smaller display by removing the repeated windows (cells) of the buildings. This means we can "summarize" the repeated content and avoid the blurry result caused by naive image down sampling. We believe by understanding one more piece of semantics, we can open an extra space for image resizing. The long-term significances and impacts of this project are:

Significance-1: The developed method should be directly applicable to mobile computing and movie production. Legacy images can be automatically retargeted to small display on portable devices as well as HDTV.

Significance-2: As semantics analysis is a novel direction in retargeting, we believe the research publication and algorithms produced will motivate the graphics community and inspire future work.

2. RESEARCH METHODOLOGY

We first tackle one common type of symmetry, the translational symmetry. Existing symmetry analysis methods unfortunately are usually slow for interactive retargeting applications. Instead, we shall propose a real-time and automatic method to detect the symmetry over content with more respect to the semantics. In addition, we can smooth the transformation and intensity of cells across the lattice. So that we can maintain the visual seamlessness over the retargeted lattices, in terms of both geometry (image-space) and illumination.

The first step is to locate the potential cells that form the lattice. Note that we try not to make any assumption on cells and the number of lattices. Our plan is to evaluate the region-based feature detection and identify the most stable one. We may propose a novel region-based feature detection method if none of them is stable enough. The notion of Gestalt (form in German) is very well-known and widely used in various fields. The well-known Gestalt laws by Wertheimer reflect strategies of the human visual system to group objects into forms and create internal representations for them. In this project, we plan to analyze the semantics in the given image by explicitly applying Gestalt grouping laws computationally. We plan to use a subset of these Gestalt laws for grouping subtle image details and hence summarize the image content. We then evaluate the correctness of the proposed method by applying the proposed algorithm on multiple test cases and measuring its correctness comparing to the ground truth. An appropriate evaluation is the user study. The user study shall be conducted in comparing to various state-of-the-art retargeting methods. Another important evaluation is the system throughput.

3. RESULTS ACHIEVED

So far, our work and related algorithms have been published in three *ACM SIGGRAPH* papers (the most prestigious graphics conference, and the venue is so prestigious that all papers are simultaneously published as journal articles in *ACM Transactions on Graphics*), one *IEEE Transactions* paper and two other papers (Section 5). In addition, we have filed a US patent for one of our works (Section 4). Some of our works have also been publicized to the general public via news media (Section 6).

We first developed a prototype image retargeting system. It first extracts the potential cells using MSER, and then constructs the potential lattices. Once lattices are estimated, the system can resize the images using cell-by-cell deletion or insertion. Figure 1 compares our result (e) to existing image retargeting methods. It shows that our method can better preserve the overall structure (of the building in this case) in (a) while achieving the goal of resizing without clipping the building as in (b). The result confirms that understanding more semantics can better (and meaningfully) solve the retargeting problem.

In order to effectively analyze the semantics, the first step is to identify elements/cells. However, a basic element may not be just a simple circle or square, it can be composed of complex components. To help the analysis, we studied the findings in gestalt psychology. Psychologists have theories (some are conflicting) on how humans recognize forms (gestalts) instead of uncorrelated fragments. But these theories are mostly qualitative. We proposed the first computational framework to allow multiple gestalt laws interact with each other in a complex manner [3]. To achieve this goal, we formulate the gestalt formation as a graphcut problem.

Figure 1: Comparison of our result to that of existing image resizing.

As the first attempt, we only applied the semantic analysis on vector graphics. Once the content is analyzed, we can perform abstraction and summarization to reduce the visual content in order to achieve the retargeting goal. Promising results are obtained and published in the prestigious conference *ACM SIGGRAPH Asia 2011* and journal *ACM Transactions on Graphics* [3]. Figure 2 shows our grouping results based on the gestalt laws of regularity and proximity, as well as the shape similarity. With the gestalts (groups), we can perform retargeting by abstraction and summarization.

Figure 2: Reducing the size of Taj Mahal.

However, this is still preliminary if we want to extend to raster images or videos. Real images or videos are noise-contaminated and illumination-interfered, and hence much harder to analyze. For real images, complex texture and details complicate the semantic analysis. Hence, we extend our study to the visual attention study, in particular, the change blindness phenomenon. We believe the human inability to recognize the change of content in two instances of the same view can help us to relieve the image resizing constraint, particularly those visually busy images. We proposed a computational model of change blindness and demonstrated its effectiveness in mimicking human visual perception. The work is published in *IEEE Transactions on Visualization and Computer Graphics* [4]. Figure 3 shows our preliminary results of applying change blindness model to image resizing.

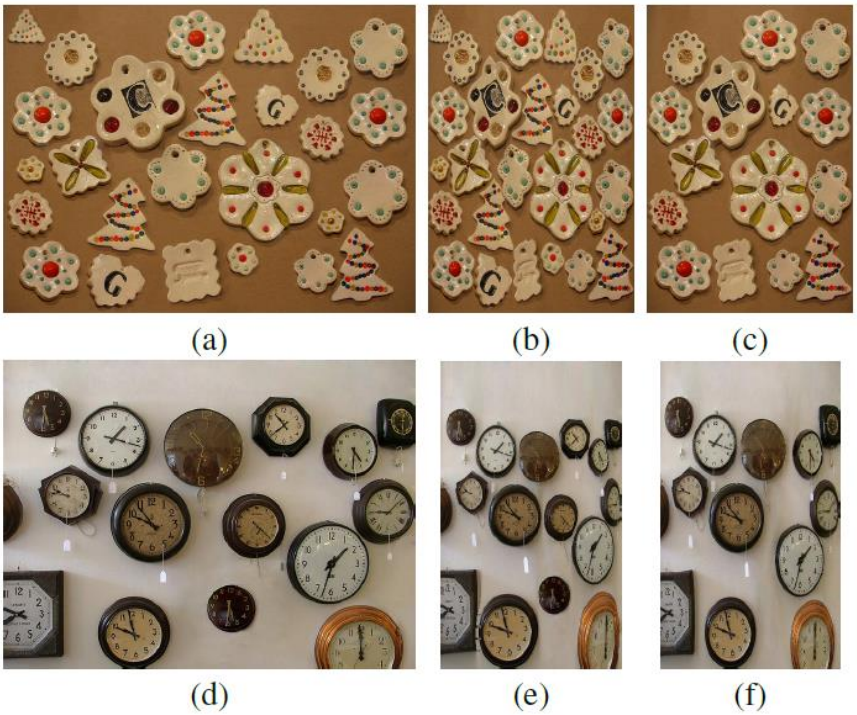

Figure 3: Application of change blindness model in image resizing. (a) & (d) original images; (b) seam carving result; (c) seam carving with our change blindness model; (e) warping result; (f) warping with our change blindness model.

We further studied the image resizing problem of stereo image pairs. When stereo images are retargeted, the consistency or fusibility in terms of color, contrast, and texture, between both views will be a concern. To study the fusibility of two views, we studied various perception models. However, none of the existing works quantitatively studies such fusibility. So we proposed a novel fusibility metric. We also applied the metric to tone mapping and obtained convincing result. The work is published in *ACM SIGGRAPH 2012* (also published in top journal *ACM Transactions on Graphics 2012*) [2]. It has also been publicized to the general public via news media and ICT Expo 2013. The project has drawn the public attention and reported by 11 newspapers and a TV medium. Please refer to Section 6 for the news clips.

4. PATENTS

[A] **T.T. Wong**, X. Yang, L. Zhang, P.A. Heng, "Binocular Visual Experience Enrichment System," *US Provisional Patent Application No. US61/678732*

5. PUBLICATION AND AWARDS

[1] X. Liu, X. Mao, X. Yang, L. Zhang and **T. T. Wong**, "Stereoscopizing Cel Animations," ***ACM Transactions on Graphics (SIGGRAPH Asia 2013 issue)***, Vol. 32, No. , November 2013, to appear.

[2] X. Yang, L. Zhang, **T.T. Wong**, P.A. Heng, "Binocular Tone Mapping," ***ACM Transactions on Graphics (SIGGRAPH 2012 issue)***, Vol. 31, No. 4, July 2012, pp. 93:1-93:10.

[3] L. Nan, A. Sharf, K. Xie, **T.T. Wong**, O. Deussen, D. Cohen-Or, and and B. Chen, "Conjoining Gestalt Rules for Abstraction of Architectural Drawings," ***ACM Transactions on Graphics***

(SIGGRAPH Asia 2011 issue), Vol. 30, No. 6, December 2011, pp. 185:1-185:10.

[4] L. Q. Ma, K. Xu, **T. T. Wong**, B. Y. Jiang and S. M. Hu, "Change Blindness Images," ***IEEE Transactions on Visualization and Computer Graphics***, Vol. 19, No. 11, November 2013, pp. 1808-1819.

[5] W. Feng, L. Wan, Z. Lin, **T.T. Wong** and Z.Q. Liu, "Perceptual Thumbnail Generation," *Perceptual Digital Imaging: Methods and Applications*, Edited by R. Lukac, CRC Press, 2013, pp. 193-221.

[6] H. Wu, **T.T. Wong** and P.A. Heng, "Parallel Structure-aware Halftoning," *Multimedia Tools and Applications*, 2012, to appear.

TIME CRITICAL APPLICATIONS OVER A SHARED NETWORK

Principal Investigator: Professor Wing Shing WONG [1]
Department of Information Engineering, CUHK

Research Team Members:
Yousheng CHEN [2], Qiong YANG, RA[4], Yi CHEN, RA[1], Nan BAO, RA [4]

[1] Dept. of Information Engineering, CUHK
[2] Dept. of Automation, Sun Yat-Sen University
[3] Department of ECE, Boston University
[4] National Mobile Communications Research Lab, Southeast University

Project Start Date: 1 July 2011
Completion Date: 31 July 2013

ABSTRACT

Interest in networked control systems has grown rapidly as many novel applications have been identified such as remotely controlling a network of mobile sensors. These new applications can ultimately lead network applications into a new era. In time-critical networked control applications, feedback and control information to be transmitted necessitates a new type of multimedia data traffic on a network. Different from standard real-time video and audio data, time critical data traffic can tolerate only low bit error probability and bounded delays. Controlling multiple dynamical systems through a shared network can provide significant efficiency improvement and development cost reduction. This project investigates the close relationship between control and communication as exemplified by remote control of time-critical dynamical systems over a shared communication network. For shared networks, one key issue to address is network resource scheduling in order to accomplish various control tasks. In the project, two configurations are considered, namely, the single master multiple slave configuration and the multiple master multiple slave configuration. A time division multiplexing (TDM) scheme was utilized in the case of first configuration. For the more challenging scenario consists of multiple independent controllers, protocol sequence based medium access control (MAC) protocol was deployed. In the controller node, Kalman-based approach was considered to compensate for data packet loss in network transmission. Two platforms were developed to enhance the practicality of the fundamental research. A testbed was developed including three pendulum-cart systems remotely controlled by one or three embedded controllers. To study communication and control issues for networked intelligent agents, we also developed platforms consisting of three micro unmanned aerial vehicles (UAVs) and three unmanned ground vehicles (UGVs).

1. OBJECTIVES AND SIGNIFICANCE

This project aims to investigate the close relationship between control and communication as exemplified by remote control of time critical dynamical systems over a shared communication network. Controlling a group of dynamical systems over a common wireless network involves coupled interaction of communication and control. A fundamental research question is to address the real-time scheduling of network resources for different types of traffic in order to accomplish various control tasks. On the other hand, design of estimation and control strategies for dynamical subsystems over different medium access control protocols is crucial in the control performance of the whole group. To enhance the practicality of the fundamental research, it is essential that experimental platforms be established so that various communication protocols and control strategies can be tested and compared.

2. RESEARCH METHODOLOGY

In the project, the coupled interaction between control and communication is investigated for controlling a group of time critical dynamical systems over a shared communication network. Two configurations are considered, that is, the single master multiple slave configuration and the multiple master multiple slave configuration. A TDM scheme was utilized in the case of first configuration. For the more challenging scenario consists of multiple independent controllers, protocol sequence based MAC protocol was deployed to moderate the access of simultaneous systems in an efficient manner. Efficient data fuse algorithms integrating separate sensors were considered to obtain optimal system states estimation. Kalman-based approach was considered in the control node to compensate for data packet loss in network transmission.

3. RESULTS ACHIEVED SO FAR

(1) The issues of control and communication of multiple plants over a shared wireless network were explored via studying stabilizing and tracking control of multiple pendulum-carts by one or multiple remote controllers. Time division multiple (TDM) based MAC protocols, state estimators and control laws were proposed. A testbed shown in Fig. 1 was developed consisting of three pendulum-cart systems remotely controlled by one or three independent embedded controller. Experimental results validate that the multiple pendulums can be stabilized while the carts accurately track the desired trajectories. The details of the research can be referred to publication [1]. The demo video (MMTP311_Demo[1]) illustrates the remote control of three pendulum-carts over a shared wireless network.

(2) To avoid collisions in a mobile network consisting of Unmanned Aerial Vehicles (UAVs) and/or Unmanned Ground Vehicles (UGVs), safety messages can be broadcast periodically by each of the mobile agent. These safety messages access the same channel and are time sensitive and have stringent delay requirements. Conventional approaches to MAC cannot guarantee real-time performance. In [2], it is proposed that protocol sequences can be used to broadcast safety messages with real-time delay constraints. Details can be found in [2].

(3) The idea of protocol sequence was applied to arbitrate access to the shared wireless network. In particular, the Generalized Prime (GP) sequences based MAC protocol with acknowledgement (ACK) was presented. It is shown that the GP sequence based protocol significantly outperforms the π-persistent random access (RA) MAC scheme with respect to the probability of packet loss. Using the control packets received at the plant as ACK, the performance of the GP sequence and the RA based MAC protocols can be highly improved. A heuristic and computationally efficient estimation and control scheme was considered. Numerical results illustrate that the control performance of the GP sequence based networked control system is much better than that of the π-persistent RA based system. The details of the research can be referred to [3].

(4) For systems employing traditional probabilistic MAC protocols like Carrier Sense Multiple Access (CSMA) and RA protocols, data packets will be lost and the classical separation principle does not hold. Unlike probabilistic protocols, protocol sequences can guarantee that messages are delivered within a bounded delay and hence are suitable choices for time-critical applications. Using protocol sequences and with the aid of a guard time to compensate the variations of processing time in distributed controllers, the data packets can successfully arrive at the actuators once there is no collision at the sensor side. Consequently, the separation principle can still hold for multiple dynamical plants sharing a common wireless network. Using a linear system as prototype, we present suboptimal control algorithms that take advantage of the unique characteristics of the protocol sequence schemes. Numerical results confirm their performance is superior to those based on traditional probabilistic MAC schemes. The details of the research can be referred to [4].

(5) To investigate the interaction between communication and control in networked intelligent agents, the coordination of aerial-ground robots was examined. A visual-based approach is presented to accomplish

cooperation between a micro UAV and a UGV using a single onboard camera. The UAV can autonomously track and land on the moving UGV by detecting and locating the landing target on the UGV. The images captured by the onboard camera are transmitted to the land laptop over a wireless channel. The laptop estimates the relative position from the received images, and transmits the estimated position to the UAV over a wireless channel. Practical experiments show that the UAV can successfully achieve autonomous taking off, tracking and landing on the moving UGV via the proposed vision-based approach. The developed UAV and UGV platforms are shown in Fig. 2 and Fig. 3. Furthermore, autonomous flights for micro UAVs in GSP-denied environments based on onboard sensors are studied in indoor environments. The attitude of an UAV is estimated by fusing the measurements of a 9-DOF inertial measurement unit (IMU). An optical flow sensor provides current velocity and relative positions of the UAV. With the aid of low-cost and lightweight onboard sensors, the proposed control strategy alleviates the restrictions of requiring external and expensive location systems in indoor applications. Experiments demonstrate that the UAVs with onboard sensors can achieve autonomously hovering, trajectory tracking as well as formation flight based on a leader-follower scheme. The details of the research can be referred to [5] [6]. The demo videos (MMTP311_Demo[2], MMTP311_Demo[3]) illustrate autonomous hovering, trajectory tracking and formation flight of UAVs using onboard lightweight and low-cost sensors.

(6) To further study the communication and control issues for networked intelligent agents, an aerial-ground networked system consisting of n UGVs and m UAVs with $n \geq m$ is considered.

- To integrate the advantages of UAVs and UGVs, a hierarchical system structure is considered. With a faster moving speed and wider vision, the UAVs are capable to send high level commands to the UGVs such as acceleration, direction, splitting and merging of the UGVs.
- The leader-follower strategy was considered for decentralized formation control of UGVs. Flexible formations can be achieved by virtue of centroidal voronoi tessellation (CVT) scenario. The CVT scheme can also maximizes the coverage area given sensor ranges. However, the CVT algorithms are computationally expensive in real time control applications. In the project, the desired location of multi-agent is firstly computed by CVT algorithms for any given formation. Subsequently, the leader-follower scheme is considered for the UGVs to achieve and maintain the desired formation. Simulation results based on Stage verify the effectiveness of the proposed formation control scheme.
- The UAV communicates only with the leader of a group of UGVs to alleviate the communication complexities in the cooperation between aerial and ground agents. The UAV estimates its relative position with respect to the UGV leader based on visual methods, and transmits the estimated relative position to the leader of UGVs. The group of UGVs can hence follow the UAV.
- Three wheels omni-directional mobile robots were developed to study the formation control of intelligent agents. The relative position and angular direction can be measured via onboard CCD and ultrasonic sensors. Practical experiments show that the three UGVs can line up as well as form V shapes with various angles based on the leader-follower scheme. The developed UGV platforms are shown in Fig. 4. The demo video (MMTP311_Demo[4]) illustrates the formation control of three UGVs.
- Cooperative control of a group of UGVs and a UAV is in progress. In future work, tracking of a group of UGVs of a UAV based on visual approaches will be considered. Moreover, cooperation between UAVs and UGVs in surveillance applications will be studied.

(7) In the project, we also investigated some related research problems, including the load-balancing problem [7] and cooperative multi-agent systems in which the target objective and the controls exercised by the agents are dependent on the choices they made at initial system time. Optimal control design methodology for linear systems allowing distributed choices is investigated in [8].

4. PUBLICATION AND AWARDS

[1] H. Cheng, Y. S. Chen, W. S. Wong, Q. Yang, L. F. Shen, and J. Baillieul, "Stabilizing and Tracking Control of Multiple Pendulum-Cart Systems over a Shared Wireless Network," in Proc. of 31st Chinese Control Conf., pp. 5849-5854, July 2012, Hefei, China.

[2] Y. Wu, K. W. Shum, W. S. Wong, and L. F. Shen, "Safety-Message Broadcast in Vehicular Ad Hoc Networks Based on Protocol Sequences," accepted for publication in the IEEE Transactions of Vehicular Technology.

[3] H. Cheng, Y. Chen, W. S. Wong, Q. Yang, and L. F. Shen, "Protocol Sequence Based Wireless Media Access Control in Networked Control Systems," in Proc. of 12th Int. Conf. on Automation, Control, Robotics and Vision, pp. 707-712, Dec. 2012, Guangzhou, China.

[4] H. Cheng and W. S. Wong, "Application of Protocol Sequences in Vehicular Ad Hoc Networks," submitted to 2013 IEEE Vehicular Networking Conf., Dec. 2013, USA.

[5] H. Cheng, Y. S. Chen, X. K. Li, and W. S. Wong, "Autonomous Takeoff, Tracking and Landing of a UAV on a Moving UGV Using Onboard Monocular Vision," in Proc. of 32nd Chinese Control Conf., pp. 5895-5901, July 2013, Xian, China. Cheng, Y. S. Chen, and W. S. Wong, "Trajectory Tracking and Formation Flight of Autonomous UAVs in GPS-Denied Environments Using Onboard Sensing," submitted to 2014 IEEE Conf. Robotics & Automation, May 2014, Hong Kong.

[6] Y. Zhang and W. S. Wong, "Distributed Load Balancing in a Multiple Server System by Shift-Invariant Protocol Sequences," *Proceedings of the Wireless Communications and Networking Conference*, April 7-10 2013, Shanghai, China, pp. 1639-1644.

[7] G. Guo, W. S. Wong, and Z. C. Liu, "Cooperative Target Realization in Multi-Agent Systems Allowing Choice-Based Actions," preprint.

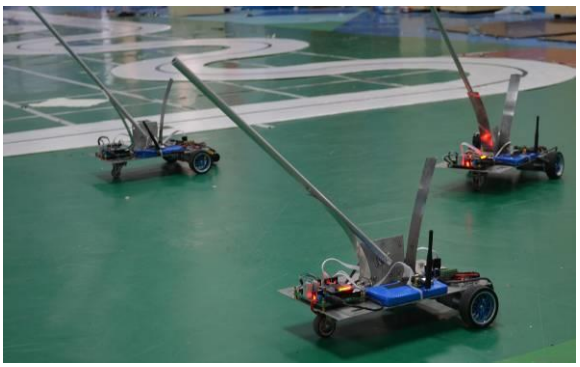

Fig. 1. The remotely controlled pendulum-carts via a shared wireless network.

Fig. 2 (a). The developed micro UAV and UGV platforms.

Fig. 2 (b). The developed micro UAV.

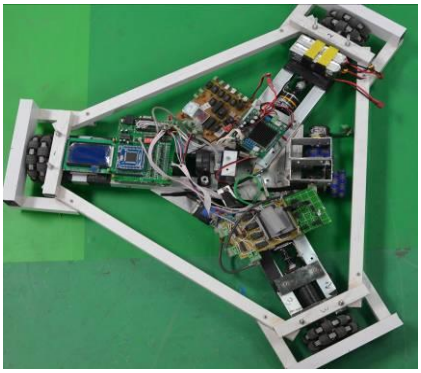

Fig. 2 (c). The developed three wheels omni-directional UGV.

Fig. 2 (d). The UAV autonomously tracks the moving UGV platform via the visual-based approach.

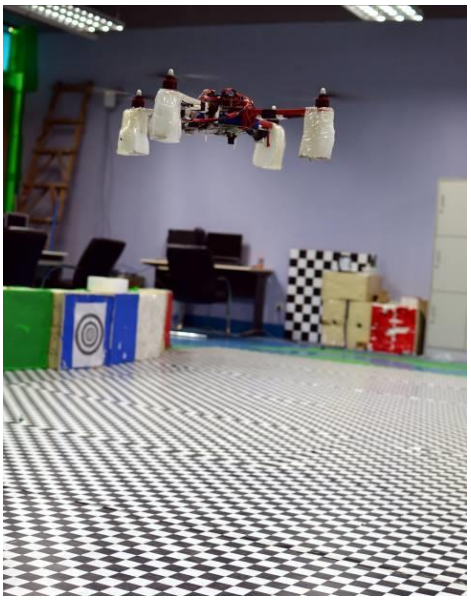

Fig. 3. The UAV autonomously accomplishes hovering and trajectory tracking using onboard sensing.

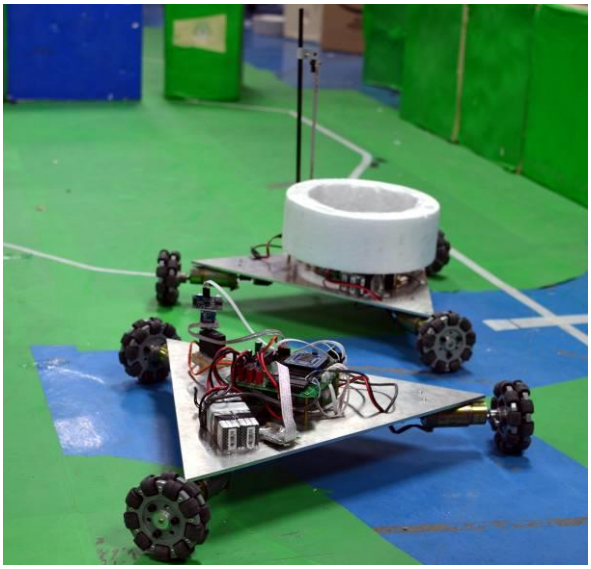

Fig. 4 (a). The developed three wheels omni-directional UGV with the capabilities to measure the relative position and angular direction with respect to the leader.

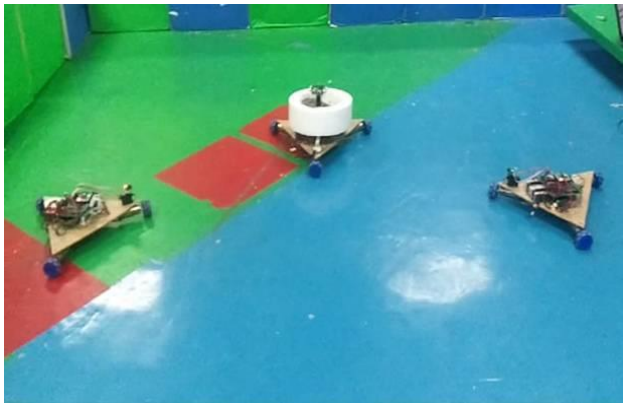

Fig. 4 (b). The formation control platform consists of three omni-directional UGVs, which can line up and form V shapes with various angles.

AMPLIFY-AND-FORWARD SCHEMES FOR WIRELESS COMMUNICATIONS

Principal Investigator: Professor Sidharth Jaggi [(1)]
Department of Information Engineering, CUHK

Research Team Members:
Samar Agnihotri (ex-postdoc, now faculty member at IIT Mandi in India)

Project Start Date: 1 July 2011
Completion Date: 30 June 2013

ABSTRACT

Please state the abstract of the project in this part. The abstract should appear at the top of the report. All manuscripts must be in English.

1. OBJECTIVES AND SIGNIFICANCE

We are increasingly moving into the ``wireless age", where most sensing of the ambient environment (from the homes to the oceans), communication among devices, and the control or change in the environment is mediated through the wireless medium. The technological advances resulting in the advent of smaller, affordable, and computationally powerful devices, and longer-lasting batteries have not only made more and more applications rely on the wireless communication, but also have fueled the demand for still smaller devices, longer untethered access, and more ``bandwidth hungry" online multimedia applications (such as video-on-demand and online gaming). Accommodating such demands and expectations over capacity-limited physical wireless channel has thrown up a daunting research challenge upon us.

Fundamental results on efficiently resolving these often conflicting demands and constraints have been lacking for all but some simple communication scenarios. Even for the case of a single source-destination pair communicating over a wireless network of intermediate relay nodes, we do not yet know the precise nature of these trade-offs. Further, the extant results are mostly of the existential nature, suggesting the existence of good communication schemes achieving certain communication trade-offs, without much consideration to their practical usage.

In this context, we are particularly interested in exploring the performance of a simple communication scheme called *Amplify-and-Forward [1]*, where the intermediate nodes merely forward the scaled version of all the information received at their input terminals. Surprisingly, such a simple scheme turns out to be optimal in some communication scenarios. However, the performance of the amplify-and-forward schemes is often analyzed under various simplifying assumptions on the network size, topology, and received signal. We believe, based on some of our recent work, that without these assumptions better performance guarantees can be given for the amplify-and-forward schemes.

In this project, therefore, we propose to analyze the performance of amplify-and-forward schemes in general wireless relay networks without any of aforementioned assumptions. This way we propose to provide tighter lower bounds to the capacity of the relay networks, and a characterization

of the achievable rates with analog network coding over all signal-to-noise ratios.

2. RESEARCH METHODOLOGY

Background:

A) The capacity of general wireless relay networks is unknown. Towards this end, over the last few years, numerous achievability schemes such as *compress-and-forward* [2], *decode-and-forward* [2], *compute-and-forward* [3], and recently *quantize-map-and-forward* [4] have been proposed. However, these schemes, though really interesting and insightful, only provide existential results: they demonstrate the existence of ``good'' achievable schemes, without any consideration for practical constraints (resource requirements). In [5], an amplify-and-forward scheme has been shown to be a constant gap away from the cutset upper-bound on the capacity of a particular wireless relay network, in the asymptotically high-SNR regime.

In [6-10], an *analog network coding* approach is proposed to exploit the mixing (that the wireless medium offers) of the interfering signals from different sources to achieve better end-to-end throughput. However, the amplify-and-forward scheme is considered in this context under some very restrictive assumptions on network size, topology, synchronization among sources, and high signal-to-noise ratio.

B) In [11], we have considered a general class of wireless relay networks with a single source-destination pair. We established the achievable rate for such a network under any amplify-and-forward scheme without making any assumption on the network size, topology, and received signal-to-noise ratio. Further, we computed the achievable rates for two instances of such general networks under various communication scenarios and showed that these rates are within a factor of half of the cutset upper-bounds asymptotically in network parameters.

Encouraged by our work in [11], we believe that the analysis of the performance of amplify-and-forward schemes in general wireless relay networks will provide not only tighter lower bounds to the capacity of general wireless relay networks, but also the characterization of the achievable rates with analog network coding. In this project, we intend to pursue this direction of research in greater detail.

Research Methodology:

The wireless relay network acts, for all but some simple instances, as an inter-symbol interference channel not only for the source signal but also for the noise introduced at each relay node. The maximum rate of information transfer achievable over such networks with amplify-and-forward, without any assumption on the network or relay operation, is an open problem. *Discrete Fourier Transform* and *Toeplitz forms* based approaches have been proposed by [12] and [13], respectively, among others to characterize the maximum achievable information rates for inter-symbol interference (ISI) channels for source signals. We intend to explore the usefulness of such approaches to characterize the achievable rates for general wireless relay networks with ISI channels for both, the source signal and noise.

Our work in [11] has shown that computing the maximum achievable rate with amplify-and-forward in general wireless relays networks is a computationally hard problem in some instances. However, some results in optimization theory as in [14] suggest that ``good'' heuristic schemes can be developed in such cases that not only approximate the performance well but also allow the distributed implementation of such solutions. In this project, we intend to develop a unified framework for such heuristic schemes to characterize the performance of amplify-and-forward schemes in general wireless relay networks.

[1] J. N. Laneman, D. N. C. Tse, and G. W. Wornell, ``Cooperative diversity in wireless networks: efficient protocols and outage behavior," *IEEE Trans. Inform. Theory*, vol. IT-50, December 2004.

[2] T. Cover and A. E. Gamal, ``Capacity theorems for the relay channel," *IEEE Trans. Inform Theory*, vol. IT-25, September 1979.

[3] B. Nazer and M. Gastpar, ``Compute-and-forward: Harnessing interference through structured codes," *submitted to IEEE Trans. Inform. Theory*, August 2009.

[4] S. Avestimehr, S. N. Diggavi, and D. N. C. Tse, ``Wireless network information flow: A deterministic approach," *submitted to IEEE Trans. Inform. Theory*, December 2010.

[5] M. Gastpar and M. Vetterli, ``On the capacity of large Gaussian relay networks," *IEEE Trans. Inform. Theory*, vol. IT-51, March 2005.

[6] S. Zhang, S. C. Liew, and P. P. Lam, ``Physical-Layer Network Coding," *Proc. ACM MobiCom*, Los Angeles, CA, September 2006.

[7] S. Katti, I. Maric, A. Goldsmith, D. Katabi, and M. Medard, ``Joint relaying and network coding in wireless networks," *Proc. IEEE ISIT 2007*, Nice, France, June 2007.

[8] S. Katti, S. Gollakotta, and D. Katabi, ``Embracing wireless interference: analog network coding," *Proc. ACM SIGCOMM*, Kyoto, Japan, August, 2007.

[9] I. Maric, A. Goldsmith, and M. Medard, ``Analog network coding in the high-SNR regime *Proc. IEEE WiNC 2010*, Boston, MA, June 2010.

[10] A. Argyriou and A. Pandharipande, ``Cooperative protocol for analog network coding in distributed wireless networks," *EEE Trans. Wireless. Comm.*, vol. TWC-9, October 2010.

[11] S. Agnihotri, S. Jaggi, and M. Chen, ``Amplify-and-Forward in General Wireless Relay Networks," *submitted to IEEE ISIT*, February 2011.

[12] W. Hirt and J. L. Massey, ``Capacity of the discrete-time Gaussian channel with intersymbol interference," *IEEE Trans. Inform. Theory*, vol. IT-34, May 1988.

[13] S. Shamai, L. H. Ozarow, and A. D. Wyner, ``Information rates for a discrete-time Gaussian channel with intersymbol interference and stationary inputs," *IEEE Trans. Inform. Theory*, vol. IT-37, November 1991.

[14] M. Chiang, ``Geometric Programming for Communication Systems," Foundations and Trends in Communications and Information Theory, vol. 2, August 2005.

3. RESULTS ACHIEVED

A quite successful line of work was carried out by my postdoc Samar Agnihotri (see [3], [4], and [5] below), building on his earlier work ([11] above). Specifically, Samar was able to recast the

wireless analog network coding problem in terms of a "network ISI" channel (where noise at each of the links shows up at the receiver in the form of Inter-Symbol Interference, due to coding operations performed by each node, and also potentially different delays along different paths to the receiver). Samar was able to characterize, for large classes of physical layer network coding problems, what the structure of optimal amplifications would be at intermediate nodes (surprisingly, nodes should not always amplify up to the maximum allowed power gain – sometimes this amplifies some types of noise too much!), and give computationally efficient algorithms to compute this vector of gains.

In other parallel lines of work, in [1] my student was able to characterize the optimal throughput for communication in the presence of a power limited "blind" jammer – someone who wishes to stop to from communicating, and perhaps even knows what you want to say, but not how you're going to say it (stochastic encoding). The power of stochastic encoding for continuous alphabet channels had not been investigated before.

In [2], we were able to give *very* computationally efficient communication schemes for some classes of communication problems, specifically when only a few out of potentially a large set of users is attempting to communicate in a distributed manner with a single receiver (for instance when many cell-phone users wish to communicate with a cellphone base-station, without necessarily knowing how many other users there are and their identities and not having to worry about not interfering with their transmissions). We were able to demonstrate connections with the compressive sensing problem, and obtain communication schemes that are both near optimal in a throughput sense, while at the same time having only linear decoding complexity.

Finally, in [6] we were able to demonstrate network error-correcting codes that are able to effectively interface with algebraic network codes and are able to correct worst-case binary errors in networks (this is in contrast to prior models, wherein usually worst-case packet errors were considered).

Together, these works provide significant progress in understanding the impact of noise in wireless communication settings, and the interaction with network coding.

4. PUBLICATION AND AWARDS

[1] F. Haddadpour, M. J. Siavoshani, M. Bakshi, S. Jaggi, "On AVCs with Quadratic Constraints," *ISIT 2013*,

[2] M. Bakshi, S. Jaggi, S. Cai, M. Chen, "SHO-FA: Robust compressive sensing with order-optimal complexity, measurements, and bits," *presented at Allerton 2012*, Oct. 2012.

[3] S. Agnihotri, S. Jaggi, and M. Chen, "Analog Network Coding in General SNR Regime: Performance of Network Simplification" *presented at ITW 2012*.

[4] S. Agnihotri, S. Jaggi, and M. Chen, "Analog Network Coding in General SNR Regime: Performance of A Greedy Scheme", *presented at the Network Coding Workshop (NetCod)*, Boston, 2012.

[5] S. Agnihotri, S. Jaggi, and M. Chen, "Analog Network Coding in General SNR Regime", *International Symposium on Information Theory (ISIT)*, Boston, 2012.

[6] Q. Wang, S. Jaggi, S.-Y. Li, "Binary Error Correcting Network Codes", *presented at ITW 2011, Paraty, Brazil*

Shun Hing Distinguished Lecture Series

To achieve the Institute's mission to promote appreciation of engineering in society through education programs, the Institute has organized a Shun Hing Distinguished Lecture Series. So far, **thirty-seven** distinguished lectures have been presented by renowned scholars. These lectures all were very well received and we will continue to line up and invite outstanding researchers to visit CUHK and to deliver distinguished lectures for the Institute. Here to show the five distinguished lectures between 2013 and June 2014.

Interference Mitigation in Heterogeneous and Small Cell Networks

by Professor Li-Chun WANG

Dept. of Electrical and Computer Engineering
National Chiao Tung University
Taiwan

Date: 31 March 2014, Monday

Abstracts

Heterogeneous and small cell networks (HetSNets), utilizing a mix of macrocells, remote radio heads (RRH), picocells, femtocells, and relays, have gained the attentions of wireless industry and research community. Even with many accomplishments in HetSNets recently, many technical challenges still remain.

In this talk, we focus on the inter-cell interference issues in HetSNet. First, we introduce a time-division duplex (TDD) and the frequency-division duplex (FDD) coexisting system, in which TDD small cells reuse the uplink spectrum of the FDD macrocellular system. A joint beamforming and scheduling technique is proposed to mitigate the inter-cell interference between TDD small cells and the FDD macrocell. Secondly, an interference-aware cluster technique for the cloud-based radio access network (C-RAN) is discussed, which can effectively reduce the inter-cell interference and inter-cluster interference. Thirdly, we discuss the cell density issue from the both aspects of throughput and energy efficiency. Based on stochastic geometry analysis, we find the optimal cell size for small cells in the interference-limited environment. To conclude this talk, we highlight some potential research issues for HetSNet in the next generation mobile network.

Blind Interference Alignment with Diversity

by Professor Wei ZHANG

Associate Professor
School of Electrical Engineering & Telecommunications
The University of New South Wales, Sydney,
Australia

Date: 27 November 2013, Wednesday

Abstracts

Interference alignment has been recently studied as an effective tool to achieve degree of freedom (DoF) of wireless interference channels. DoF is also known as multiplexing gain or capacity pre-log scaling factor and provides a capacity approximation of wireless network in the high signal-to-noise ratio region. However, the interference alignment technique requires channel state information at transmitters (CSIT) for the design of precoder so that the interferences can be aligned at receivers. Blind interference alignment can overcome the limitation of CSIT by adopting pattern reconfigurable antennas at receivers. In this work, the wireless interference channel is investigated from a different perspective and the diversity benefits of wireless interference channels are explored. A space-time coding approach is designed to achieve high diversity gain and high rate for MISO interference channels with reconfigurable receiver antennas. A family of space-time codes is proposed with blind interference alignment to accommodate various needs of diversity-rate tradeoff.

Stochastic Geometry in Dynamic State Estimation

by Professor Ba-Ngu VO

Dept of Electrical & Computer Engineering
Curtin University
Australia

Date: 19 November 2013, Tuesday

Abstracts

The last decade has witnessed exciting developments in multi-target state estimation with the introduction of stochastic geometry to the field. Stochastic geometry--the marriage between geometry and probability--is a mathematical discipline that deals with random spatial patterns. The history of stochastic geometry traces back to the problem of Buffon's needle and has long been used by statisticians in many diverse applications including astronomy, atomic physics, biology, sampling theory, stereology, etc. Since 2003, Mahler's seminal work on the random finite set approach to multi-target filtering, which culminated in the probability hypothesis density (PHD) filter, has continued to attract substantial interests from academia and industry alike. The PHD filters have been used in oil pipeline tracking by British Petrolium, ground target tracking in the September 2007 NATO 'Bold Avenger' defence exercise and the US space fence program by Lockheed Martin. This seminar presents an overview of the random finite set paradigm to dynamic state estimation and outlines recent developments beyond the PHD filters as well as applications in areas such as sensor scheduling, computer vision, and field robotics.

Co-sponsored by:
IEEE Signal Processing Society Hong Kong Chapter

An Information Extraction Approach to Next-Generation Speech Processing

by Professor Chin-Hui LEE

Professor
School of Electrical and Computer Engineering
Georgia Institute of Technology

Date: 5 August 2013, Monday

Abstracts

The field of automatic speech recognition (ASR) has enjoyed more than 30 years of technology advancement due to the extensive utilization of the hidden Markov model (HMM) framework and a concentrated effort by the community to make available a vast amount of language resources. However the ASR problem is still far from being solved because not all information available in the speech knowledge hierarchy can be directly and effectively integrated into state-of-the-art systems to improve ASR performance and enhance system robustness. It is believed that some of the current knowledge insufficiency issues can be partially addressed by processing techniques that can take advantage of the full set of acoustic and language information in speech. On the other hand in human speech recognition (HSR) and spectrogram reading we often determine the linguistic identity of a sound based on detected cues and evidences that exist at various levels of the speech knowledge hierarchy, ranging from acoustic phonetics to syntax and semantics. This calls for a bottom-up knowledge integration framework that links speech processing with information e xtraction, by spotting speech cues with a bank of attribute detectors, weighing and combining acoustic evidences to form cognitive hypotheses, and verifying these theories until a consistent recognition decision can be reached. The recently proposed ASAT (automatic speech attribute transcription) framework is an attempt to mimic some HSR capabilities with asynchronous speech event detection followed by bottom-up speech knowledge integration and verification. In the last few years it has demonstrated potentials and offered insights in detection-based speech processing and information extraction. This presentation is intended to illustrate new possibilities of speech research via linking analysis and processing of raw speech signals with extracting multiple layers of useful speech information. By organizing these probabilistic evidences from the speech knowledge hierarchy, and integrating them into the already-powerful, top-down HMM framework we can facilitate a knowledge rich, bottom-up and data-driven framework that will lower the entry barriers to ASR research and further enhance the capabilities and reduce some of the limitations in the state-of-the-art ASR systems. Everyone in and out of the current ASR community will be able to contribute to this worthwhile effort to building a collaborative ASR community of the 21st Century.

Co-organized by:
CUHK MoE-Microsoft Key Laboratory of Human-Centric Computing and Interface Technologies

Space-Time Coding for MIMO Wireless Network

by Professor Wei ZHANG

Associate Professor
School of Electrical Engineering & Telecommunications
The University of New South Wales, Sydney,
Australia

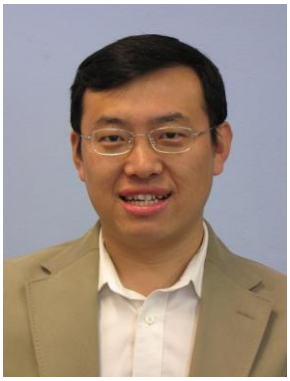

Date: 20 February 2013 Wednesday

Abstracts

For point-to-point MIMO wireless communications, space-time coding has been developed in the last decade to achieve the full diversity and high code rate, such as Alamouti code, Golden Code, Silver Code, Perfect space-time code, etc. In this talk, I will present our recent work on space-time code designs for MIMO wireless networks, including interference channels and X channels, where multiple users each with M antennas communicate with multiple receivers each with N antennas simultaneously. A group interference cancellation algorithm is applied at each receiver to eliminate the interference from all undesired transmitters. A systematic design of space-time codes is proposed for each user to achieve full diversity, i.e., MN, for interference channels and X channels, respectively.

Shun Hing Institute of Advanced Engineering (SHIAE)
The Chinese University of Hong Kong
Shatin, N.T., Hong Kong

Office : Room 702, William M.W. Mong Engineering Building
Tel : (852) 3943 4351
Fax : (852) 3943 4354
Email : info@shiae.cuhk.edu.hk
Website : http://www.shiae.cuhk.edu.hk